Mathematical modelling of crack problems in bi-material structures containing imperfect interfaces using the weight function technique

Adam Vellender

Aberystwyth University

2013

THESIS
submitted to Aberystwyth University
by
Adam Stephen Vellender, MMath (Wales)
In Candidature for the Degree of
PHILOSOPHIAE DOCTOR

Declaration

This work has not previously been accepted in substance for any degree and is not being concurrently submitted in candidature for any degree.

Signed ..... (candidate)

Date .....

Statement 1

This thesis is the result of my own investigations, except where otherwise stated. Other sources are acknowledged by footnotes giving explicit references. A bibliography is appended.

Signed ..... (candidate)

Date .....

Statement 2

I hereby give consent for my thesis, if accepted, to be available for photocopying and for inter-library loan, and for the title and summary to be made available to outside organisations.

Signed ..... (candidate)

Date .....

Acknowledgements

Firstly, I would like to express my sincere gratitude to my supervisor Prof. Gennady Mishuris for his encouragement and support. It has been a privilege to experience his mathematical guidance and his boundless, unerring enthusiasm and drive for research in mathematics. His mathematical wisdom and ingenuity is truly inspiring and the time he has spent to impart his knowledge is most gratefully appreciated.

Thanks to the mathematics department within the Institute of Mathematics and Physics at Aberystwyth University for being such a fantastic place to study. Since the moment I arrived in Aberystwyth as an undergraduate student in 2005, so many staff have helped nurture my love of mathematics. Throughout my PhD studies, the Mathematical Modelling of Structures, Solids and Fluids research group have offered superb comments and I would like to give special thanks to Dr. Robert Douglas as my second supervisor, who has been a valuable source of advice and encouragement throughout.

I also acknowledge the Aberystwyth Postgraduate Research Studentship (APRS) without which, it would have been impossible to write this thesis. Moreover, I thank Prof. Alexander Movchan and Dr. Andrea Piccolroaz who were coauthors of the journal papers corresponding to the work in chapters 3 and 5 respectively.

I thank my many officemates throughout my three years for their camaraderie and friendship. Sebastian Wildfeuer, Doris Stingl, Andreas Dürmeier, Lewis Pryce, Piotr Kusmierczyk and Jen Wheatley have all been a great support both in and out of the office and have played a huge role in making my PhD years highly enjoyable.

None of this would have been possible without the love and encouragement of those closest to me. Mum, Arthur, Dad and Dan have always been

there for me and have been an unstintingly supportive family. Finally, the belief shown in me by Trish has driven me on and her support and affection has been especially appreciated. Thank you.

Abstract

The main aim of this thesis is to generalise weight function techniques to tackle crack problems in bi-material linearly elastic and isotropic solids with imperfect interfaces.

Our approach makes extensive use of weight functions which are special solutions to homogeneous boundary value problems that aid in the evaluation of constants in asymptotic expressions describing the behaviour of physical fields near crack tips.

We use newly derived weight functions and respective techniques to tackle various aspects of a number of problems. The first major application is the use of the new weight functions to aid in the analysis of Bloch–Floquet waves; results include the derivation of a low dimensional model including junction conditions and the evaluation of a fracture criterion in the form of a constant in the asymptotic expansion of physical fields near crack tips. The second major application uses the new weight functions to assist in perturbation analysis. In particular, Betti's formula is applied in an imperfect interface setting, which introduces new conditions and asymptotic behaviour in comparison to previously studied perfect interface cases.

We first derive a weight function by employing the Wiener-Hopf technique in a bi-material strip containing a semi-infinite crack and an imperfect interface. We then present an asymptotic algorithm that uses the new weight function to evaluate coefficients in the asymptotics of solutions to problems of wave propagation in a thin bi-material strip containing a periodic array of

finite-length cracks situated along an imperfect interface between two materials. We introduce and solve a low dimensional model and give relationships between its solution's behaviour at junction points and the behaviour of physical fields near the crack tip in the full original model problem.

The low dimensional model is then used to estimate eigenfrequencies of the periodic structure. We will find via comparisons against finite element simulations that the model gives excellent estimates in most cases for the frequencies of waves propagating through the strip; however, a small discrepancy is found for standing wave eigenfrequencies.

We address this discrepancy by suggesting an improvement to the asymptotic model and perform computations which demonstrate a greatly improved accuracy for standing wave eigenfrequencies in both the imperfect and ideal interface problems.

We then move on to consider our second major problem which concerns out-of-plane shear in an infinite domain containing a semi-infinite crack situated on an imperfect interface. We derive a weight function for this geometry and use Betti's identity to relate the behaviour of physical fields near the crack tip to that of the weight function and prescribed loadings on the crack faces. In particular, the method presented allows for the prescribed tractions to be point forces, as well as continuous loadings.

Having obtained the weight function, we then conduct perturbation analysis to determine how small linear defects such as elliptic inclusions influence the forces near the crack tip. Computations are performed which demonstrate how the unperturbed solution depends upon the parameter of interface imperfection, and how the location of defects may shield or amplify the stresses near the crack tip.

Contents

Chapter 1

Bibliographical review and structure of the thesis

In this thesis, we will analyse a number of problems whose common theme is the interaction of cracks with imperfect interfaces in linearly elastic and isotropic solids. A main element of our analysis will be the derivation and application of new weight functions – special solutions to homogeonous boundary value problems which aid in the evaluation of asymptotic constants describing the behaviour of physical fields near crack tips.

We begin this opening chapter by outlining where the work comprising this thesis has been published and disseminated, before presenting a review of the literature, making mention of important concepts and advances in elasticity theory and fracture mechanics. The remainder of this present chapter will then outline the structure of the remainder of the thesis.

1.1 Publications and dissemination

Chapters 3, 4 and 5 of this thesis correspond to three papers, two of which at the time of writing are published in academic journals with the third having been submitted for publication. The details of these papers appear in the bibliography on page 162 as references [62, 63, 64].

I have presented the work at the following conferences and workshops:

- WIMCS Wales Mathematics Colloquium 2010, Gregynog, May 2010.
- First LMS-WIMCS Workshop on the Wiener-Hopf Method and Applications, Aberystwyth, May 2010.
- WIMCS Wales Mathematics Colloquium 2011, Gregynog, May 2011.
- Metamaterial Structures and Dynamic Localisation of Defects Workshop, Liverpool, December 2011.
- British Applied Mathematics Colloquium, Leeds, April 2013.
- CERMODEL2013, Trento, July 2013.

1.2 Bibliographical review

The roots of elasticity theory can be traced back through many centuries. Hooke's Law for instance finds its genesis in the second half of the 17th century. In the intervening centuries, many of the great names of mathematics have considered problems of elasticity. Euler [17] considered stationary configurations of an elastic rod in 1744, and Daniel Bernoulli derived in 1751 the differential equation governing the vibration of beams and found the solution in the case of small deformations.

Despite advances in the field of elasticity between these early discoveries and the start of the 20th century, the pioneering work in the field of fracture

mechanics did not begin until 1913, when British civil engineer Charles Inglis [25] studied an elliptical hole in glass under tensile load applied in a perpendicular direction to the ellipse. He found that the stress concentration was greatest at the ellipse's vertices. In 1920, Griffith [22] (who was motivated by a discrepancy between theoretical estimates and experimental data for the stress required to fracture glass) extended the work of Inglis by stretching the ellipse out into a crack, and realised that Inglis' result implied that a body containing a crack could not sustain an applied load. He discovered that the macroscopic potential energy of the system depended on the size of the crack, and since extending the crack creates some new crack surface, a certain amount of work per unit area of crack surface must be released at a microscopic level. Griffith described this work as a *surface energy* Ω_S in addition to the potential energy Ω, and applied the equilibrium principle of minimum potential energy

$$\frac{\partial}{\partial l}(\Omega + \Omega_S) = 0. \tag{1.1}$$

Irwin [26] added the elastic *stress-intensity factor*, K, as an important parameter by which a crack tip field can be characterised. This quantity (which depends upon the geometry of the domain, the size and location of the crack and the magnitude and distribution of loading on the material) gives a criterion for the crack to propagate; if K exceeds a quantity called the *fracture toughness* of the cracked body's material, then the crack will begin to grow. Irwin also demonstrated that for Mode I loading (see Section 2.3.1 for the definitions of fracture modes) under plane stress conditions, the energy release rate G, which quantifies the energy 'leaving' the material through the crack tip, is related to the stress intensity factor via the formula

$$G = -\frac{\partial \Omega}{\partial l} = \frac{K^2}{E}, \tag{1.2}$$

where E is the Young's modulus of the material.

The first crack tip contour integral expression to compute the elastodynamic energy release rate was proposed by Atkinson and Eshelby [3]. They argued that the form for dynamic growth should be the same as for quasistatic growth with the elastic energy density replaced by the total mehanical energy density (the sum of the elastic and kinetic energy). These ideas were extended by Rice [57] and Cherepanov [13], independently, through the introduction of the path-independent J-integral. In the case of quasistatic linear elastic conditions, J and G coincide.

The calculation of the stress-intensity factor K is not always straightforward. In irregular-shaped domains, it is often not possible to find analytic expressions for K, and so finite element and boundary element approaches may be resorted to; many such treatments can be found in the literature, for example the approach of Gifford and Hilton [19]. The paper of Maz'ya *et al.* [37] gave a very general method to find asymptotic forms of solutions to Dirichlet or Neumann problems close to the vertices of cones, and in doing so established the theoretical foundation required for so-called *weight functions*.

For more regular domains, weight functions are an especially powerful tool in aiding the evaluation of stress intensity factors. The concept of weight functions was introduced into electrostatics by Bueckner [11]. These provide weights for the loads applied to the crack surfaces, such that their weighted integrals over the crack surfaces provide the stress intensity factors at a chosen point. Weight functions have been found for a variety of different geometries; Bueckner [12] found weight functions for several types of crack including penny-shaped and half-plane cracks in homogeneous elastic media in both two-dimensional and three-dimensional settings. Rice [56] derived

the weight functions corresponding to a crack of finite length. Zheng, Glinka and Dubey [72] obtained weight functions for a corner crack in a finite thickness plate and Kassir and Sih [30] found the elastostatic weight functions for a 3D semi-infinite crack in an infinite body. A number of handbooks were published in the 1970s and 80s (for instance [47]) which collected together stress intensity factors for many types of specific configurations; while these were useful resources, any minor change in loading or geometry to those listed in the handbook would cause difficulties.

Rice further developed the theory for three dimensional crack problems in the work [60]. Willis and Movchan [71] used the Wiener-Hopf method to construct dynamic weight functions for arbitrary time-dependent loading of a plane semi-infinite crack extending at constant speed in an infinite isotropic elastic body. Lazarus and Leblond [33] used Bueckner's method to find the expression for the variation of the stress intensity factors for a wavy crack and Piccolroaz *et al.* [51] later employed the Wiener-Hopf technique to find analytic expressions for the so-called 'Lazarus-Leblond' constants which were not found in the original paper [33]. More recently and of particular relevance to this thesis, weight functions for a thin bi-material strip containing a periodic array of interfacial cracks have been derived using the Wiener-Hopf method by Mishuris *et al.* [44]; we review this paper in detail in Chapter 2. We also give mention to the book of Noble citeNoble as a rich resource on Wiener-Hopf analysis.

An important development in fracture mechanics was the study of cracks which sit along the interface between different materials. A pioneering work was that of Williams [66]. Inspired by geophysical problems, he considered two separate isotropic homogeneous regions separated by a crack and found

that the singularity near the crack tip has the sharp oscillatory character of the type $r^{-1/2}\sin(b\log r)$, $r \to 0$. While this oscillatory behaviour appears to be unphysical, Rice and Sih [55] showed that the obtained stress intensity factors can be used together with G and J integrals to obtain useful information from the fracture mechanics point of view. Willis examined three dimensional interfacial crack problems in a series of papers [68], [69] and [70]; the first of these considers the stress field around a crack on the plane interface between two bonded dissimilar anisotropic elastic half-spaces. Rice [59] considered the validity of the two dimensional complex stress intensity factor K for an interfacial crack between dissimilar solids and found that similar values of K for two cracked bodies imply similar states at the crack tip.

The concept of an *imperfect interface* is of particular importance to this thesis. Two major advances were made towards this concept in the 1970s: one by Atkinson and the other by Comninou. Atkinson [4] recognised that the interface between two different materials is almost never sharp. He suggested two models, both of which replace the interface by a thin strip of finite thickness. In one model, the thin strip (which contains a crack) is homogeneous with elastic modulus different to those of the two main materials. The other provides a gradual transition with the crack placed along the interface between the first main solid and the thin interface layer; this avoids the oscillatory behaviour and retains the usual square root singularity at the crack tip. Comninou [14] approached the interface crack problem from a contact mechanics viewpoint by accepting the presence of inequalities and allowing for partial closure at the tips.

Klarbring and Movchan [31] presented an asymptotic model of adhesive

joints in a layered structure. Mishuris [40] found the asymptotic behaviour of displacements and stresses in a vicinity of the interface crack tip situated on a non-ideal[1] interface between two different elastic materials, where the non-ideal interface is replaced by non-ideal transmission conditions. Mishuris and Kuhn [41] then reduced the corresponding modelling boundary value problem to a system of singular integral equations with moving and fixed point singularities. The existence and uniqueness of the system's solution were proved and asymptotic expansions of displacements and stresses near the crack tip found. Benveniste and Miloh [9] considered a thin curved isotropic layer of constant thickness between two elastic isotropic media in a two dimensional plane-strain setting and derived seven distinct types of interface conditions depending on the softness or stiffness of the layer. Benveniste [8] later presented a general interface model for a three-dimensional arbitrarily curved thin anistoropic interphase between two anisotropic solids.

For imperfect interfaces, there is no square-root singularity at the crack tip and so the stress intensity factor concept is not applicable. Instead there exist a number of analogues to the stress intensity factor which act as fracture criteria. The *crack tip opening displacement* (CTOD) was proposed independently by Wells [65] and Cottrell [15] as a fracture criterion where significant plastic deformation precedes fracture. Later works by Rice and Sorensen [58], Shih *et al.* [61] and Kanninen *et al.* [27] for Mode I crack extension justified the use of CTOD as a plausible fracture parameter to capture local yielding. Neuber [48] and Novozhilov [49] considered a fracture criterion based

[1]When we refer to a 'non-ideal interface', unless otherwise stated we mean a soft imperfect interface. Similarly, we use the terms 'perfect interface' and 'ideal interface' interchangably. Different types of imperfect interface exist (stiff and soft for instance); we discuss these in Section 2.3.2 on page 24.

on *average stress* over a characteristic length. Barenblatt [7] and Dugdale [16] independently proposed *cohesive zone models* for studying plasticity at the crack tip. These models take non-linear material behaviour at the crack tip into account and introduce cohesive forces directly to the crack surfaces. Willis [67] discussed the relationship between these Barenblatt-Dugdale models and found a relationship between Griffith's suface energy and Barenblatt's modulus of cohesion, provided the forces act over a short range, which is true in practice. In classical geometries these criteria can all be used; they give similar values for critical load and so can all be considered useful indicators for crack growth. In more complex situations, different criteria may give slightly different quantitative results (e.g. critical load, direction of crack propagation) but usually provide good qualitative results from a fracture mechanics point of view.

1.2.1 Conclusions and motivation

While the literature contains well-established models of interfacial cracks in bi-materials for a range of geometries, the weight function technique has not been applied previously in cases where cracks lie on an imperfect interface. As discussed above, the presence of an imperfect interface fundamentally changes the behaviour of displacement and stress distributions in the vicinity of the crack tip. This creates new challenges in adapting the ideas behind the weight function approach to find expressions for important asymptotic constants which can act as fracture criteria. For instance, the weight function will possess different behaviour near the tip and identities that relate the weight function to the physical solution will be different to those previously used in perfect interface settings. By considering differently config-

ured problems concerned with stresses near crack tips, spectral properties of thin waveguides and perturbation analysis, this thesis aims to demonstrate that the weight function technique can be extended to imperfect interface problems and in such cases gives an efficient method by which important asymptotic information can be computed.

1.3 Thesis structure

In Chapter 2, we will give a summary of background material that serves to introduce a number of key concepts and techniques that will be used extensively throughout the remainder of the thesis. The chapter begins by summarising important results from the theory of analytic functions and then shows how they are elegantly and powerfully combined to form the Wiener-Hopf technique. We will also make a précis of the derivation of transmisson conditions for soft and stiff imperfect interfaces.

We begin the new work in Chapter 3, which considers a problem inspired by Mishuris *et al.* (2007) [44]. We consider a similar geometry of a thin bi-material strip containing an array of finite-length interfacial cracks, but with the crucial new feature of an *imperfect interface* between the cracks which is characterised by an imperfection parameter κ. This change in formulation fundamentally changes many aspects of the problem. The problem is singularly perturbed, and so taking even very small values of κ (corresponding to an 'almost-perfect' interface) gives a qualitatively significantly different weight function than that derived by Mishuris *et al.* [44] for the perfect interface case. Further, the well-known square root singularity phenomenon at the crack tip which is found in crack problems incorporating perfect interfaces is no longer present, and so the new weight function is used to derive

constants which take the place of stress intensity factors.

The plan of work in Chapter 3 can be summarised as follows:

1. We first formulate the weight function problem and use Fourier transform and Wiener-Hopf techniques to obtain its solution. While problems regarding cracks in domains including imperfect interfaces have been previously studied (for example in [1]), no corresponding weight functions have been hitherto constructed.[2]

2. Asymptotic analysis enables us to find analytic expressions for all important constants which describe the weight function's behaviour near to, and far from, the crack tip.

3. We then present an application of the newly derived weight function to the analysis of Bloch-Floquet waves in a thin structure containing a periodic array of cracks and imperfect interfaces. We follow a similar asymptotic algorithm to that of Mishuris *et al.* [44] but the presence of the imperfect interface requires different analysis to be conducted.

4. Computations are conducted which show how various aspects of the solution are influenced by the extent of imperfection of the interface κ.

Chapter 4 will focus heavily on the low dimensional model which forms part of the asymptotic algorithm detailed in Chapter 3. Mishuris *et al.* [44] found for the perfect interface that the low dimensional model is very accurate when predicting eigenfrequencies of waves that propagate through the thin strip, but a small discrepancy exists in the prediction of standing wave eigenfrequencies. We will discover that the same is true of our model

[2]Some factorisation has been conducted; however it is not convenient for the purpose of performing numerical computations and so we present a different factorisation.

for the imperfect interface case, so will devote this chapter to addressing this discrepancy. Our approach is to amend the existing model by also expanding the square of the frequency ω^2 as an asymptotic series of the form $\omega^2 = \omega_0^2 + \varepsilon\omega_1^2 + O(\varepsilon^2)$. While it is not immediately apparent *a priori* that this amendment will lead to a significant and useful correction in standing wave eigenfrequencies while leaving the accuracy of propagating eigenfrequency estimates intact, computations (which are performed for both perfect and imperfect interface cases) demonstrate that typically an improvement in accuracy of around an order of magnitude is obtained through this amended approach. We will adopt the following outline structure for the chapter:

1. We formulate the problem and summarise our proposed approach.

2. The improved low dimensional model is derived and we discuss the impact of the extra assumption on the junction conditions.

3. We solve the corrected zero order and first order low dimensional models, including the computation of the correction term ω_1.

4. Numerical computations are performed for both perfect and imperfect interface cases, with various mechanical and geometric parameters. We present dispersion diagrams and investigate the effectiveness of the eigenfrequency correction. This includes discussions of limitations of the asymptotic model.

We will then progress to consider a different problem, which is formulated in the whole plane rather than the strip heretofore considered. In Chapter 5, we will formulate and solve a weight function problem in a bi-material plane containing a semi-infinite crack on an imperfect interface. Mode III problems in similar domains containing an imperfect interface have been

studied by Antipov *et al.* [1], but no corresponding weight function has been previously derived. The analogous perfect interface weight functions have been found by Piccolroaz *et al.* [52], but the addition of the imperfect interface to the problem fundamentally and significantly alters many aspects of the sought weight function. We will then present an application of this new weight function. Inspired by the work of Piccolroaz *et al.* [54] and Mishuris *et al.* [45], using Betti's identity we will derive constants which describe the behaviour of the physical solution near the crack tip and will then investigate via the dipole matrix method how the presence of small linear defects shield or amplify the propagation of the main crack. An outline of the plan of work is as follows:

1. We formulate the physical and weight function problems. The Wiener-Hopf technique allows us to solve the weight function problem and find asymptotic expansions for important quantities.

2. We apply the Betti identity in the imperfect interface case and draw comparisons against the equivalent procedure for the perfect interface case.

3. The unperturbed solution u_0 is derived by employing Wiener-Hopf analysis. We then conduct perturbation analysis using the dipole matrix method and arrive at an expression for the change in an important constant from an asymptotic expansion (denoted a_0) describing the leading term of the traction near the crack tip induced by the presence of the small defect.

4. Computation methods are discussed and performed to give plots of how the extent of interface imperfection κ affects the magnitude of tractions

near the crack tip a_0. We also show how the location of the small defect relative to the crack tip can increase or decrease the stresses near the crack tip, thus shielding or amplifying the propagation of the main crack.

We conclude the thesis in Chapter 6 by summarising the main results and discussing their applicability to related problems, before suggesting some areas in which future work could extend the ideas and techniques used in the previous chapters.

Chapter 2

Background

2.1 Theoretical background

In this section we will outline the main mathematical tools which will be used extensively throughout the remainder of this thesis. We begin with results concerning properties of analytic functions of complex variables before presenting some important properties of Fourier transforms. We conclude this section by summarising the Wiener-Hopf technique.

2.1.1 Analytic functions of complex variables

Consider a function $f : \Omega \subset \mathbb{C} \to \mathbb{C}$ of the complex variable $z = x + iy$ defined in a neighbourhood Ω of a particular point.

Definition 1. *f is analytic at z if f is differentiable with respect to z at that point. Similarly, f is analytic on the set Ω if f is analytic at every point in Ω.*

Definition 2. *f is entire if it is defined on the whole complex plane $\mathbb{C}$ and is analytic everywhere.*

The property of analyticity is a very far-reaching one. Some immediate consequences include

- **The Cauchy-Riemann Equations.** If f is analytic in $\Omega \subset \mathbb{C}$, then writing $f(z) = u(x, y) + iv(x, y)$, it follows that

$$\frac{\partial u}{\partial x} = \frac{\partial v}{\partial y}, \qquad \frac{\partial u}{\partial y} = -\frac{\partial v}{\partial x}. \tag{2.1}$$

- **Existence of all derivatives.** Analyticity of f implies that derivatives of all orders exist. In particular, this allows a Taylor series to be constructed at any point within the domain of analyticity of f.

- **Harmonic nature of real and imaginary parts.** If $f = u + iv$ is analytic in Ω, then u and v are harmonic in Ω. That is, $\nabla^2 u = 0$ and $\nabla^2 v = 0$ in Ω. This result is an immediate consequence of the Cauchy-Riemann equations.

Theorem 1 (Cauchy integral theorem)**.** *If $f(z)$ is analytic on and inside a simple closed curve Γ in the complex plane, then*

$$\int_{\Gamma} f(z)dz = 0. \tag{2.2}$$

Theorem 2 (Generalised Cauchy integral formula)**.** *Suppose $f(z)$ is analytic on and inside a simple closed curve Γ which encloses a region of the complex plane. Then if a is a point inside Γ,*

$$f^{(n)}(a) = \frac{n!}{2\pi i} \int_{\Gamma} \frac{f(z)}{(z-a)^{n+1}} \mathrm{d}z, \tag{2.3}$$

where $f^{(n)}$ denotes the n-th derivative of f.

The special case of $n = 0$ is often referred to as the Cauchy integral formula. This can then be used to obtain Liouville's theorem which we shall use extensively, since it is a key part of the Wiener-Hopf technique.

Theorem 3 (Liouville's theorem)**.** *A bounded entire function of a complex variable is constant.*

The Wiener-Hopf technique more generally employs the generalised version of this theorem, which is stated below.

Theorem 4 (Generalised Liouville theorem)**.** *If f is entire and if, for some integer $k \geq 0$, there exist positive constants A and B such that*

$$|f(z)| \leq A + B|z|^k, \tag{2.4}$$

then f is a polynomial of degree at most k.

Wiener-Hopf problems also make use of analytic continuation, which can be stated as follows.

Theorem 5 (Analytic continuation)**.** *Let f_1, f_2 be analytic functions in respective open subsets of the complex plane Ω_1 and Ω_2, coinciding in an open domain $\Omega_1 \cap \Omega_2$. Define f by*

$$f(z) = \begin{cases} f_1(z) & \text{if } z \in \Omega_1, \\ f_2(z) & \text{if } z \in \Omega_2. \end{cases} \tag{2.5}$$

Then f is analytic in $\Omega_1 \cup \Omega_2$.

2.1.2 Fourier transforms

Fourier transforms will be used extensively throughout this thesis as a tool to solve boundary value problems. Here we define our notation for Fourier transforms and present key analyticity properties.

Definition 3. *Let $f(x)$ and defined for $x \in \mathbb{R}$ and integrable over any finite interval of x. The Fourier transform of f is denoted $\bar{f}$ and defined by*

$$\bar{f}(\xi) = \int_{-\infty}^{\infty} f(x) e^{i\xi x} \mathrm{d}x; \tag{2.6}$$

with $\xi \in \mathbb{C}$.

We will often encounter cases where f is identically zero on a half-line. Such cases lead to Fourier transforms with useful analyticity properties. In particular, suppose $f(x)$ is zero for all $x < 0$. If f has only a finite number of finite discontinuities on $\mathbb{C}$, is bounded except at a finite number of points, and $|f(x)| = O(e^{-\gamma^- x})$ where γ^- is some real positive constant as $x \to +\infty$ then

$$\bar{f}(\xi) = \int_{0}^{\infty} f(x) e^{i\xi x} \mathrm{d}x \tag{2.7}$$

is analytic in the upper half-plane $\mathrm{Im}(\xi) > -\gamma^-$. Similarly, suppose $g(x)$ is zero for all $x > 0$, has a finite number of finite discontinuities on $\mathbb{R}$, is bounded except at a finite number of points, and $g(x) = O(e^{\gamma^+ x})$ as $x \to -\infty$ for some real positive constant γ^+. Then

$$\bar{g}(\xi) = \int_{-\infty}^{0} g(x) e^{i\xi x} \mathrm{d}x \tag{2.8}$$

defines an analytic function in the lower half-plane $\mathrm{Im}(\xi) < \gamma^+$. We say that $\bar{f}$ in (2.7) is a *plus function* and $\bar{g}$ in (2.8) is a *minus function* and will often denote functions with these properties with a minus or plus superscript in the following chapters.

Definition 4 (Inverse Fourier transform)**.** *Let $f(x)$ be integrable over any*

finite interval of x *and*

$$|f(x)| = \begin{cases} O(e^{-\gamma^- x}) & \text{as } x \to +\infty \\ O(e^{\gamma^+ x}) & \text{as } x \to -\infty. \end{cases} \tag{2.9}$$

where $\gamma^{\pm} > 0$ *are constants. The inverse Fourier transform of the function* $\bar{f}(\xi)$ *as defined in Definition 3 is given by*

$$f(x) = \frac{1}{2\pi} \int_{-\infty+i\beta}^{\infty+i\beta} \bar{f}(\xi) e^{-i\xi x} \mathrm{d}\xi, \tag{2.10}$$

where $\beta \in \mathbb{R}$ *satisfies* $-\gamma^- < \beta < \gamma^+$.

A particularly useful result is the following

Theorem 6. *Let* $f : \mathbb{R} \to \mathbb{R}$ *be differentiable and define* $g(x) = \frac{\mathrm{d}f}{\mathrm{d}x}$. *Then*

$$\int_{-\infty}^{\infty} g(x) e^{i\xi x} \mathrm{d}x = -i\xi \bar{f}(\xi). \tag{2.11}$$

It is this property that makes the Fourier transform a classic method with which to solve linear differential equations, since differentiation in the original variable becomes algebraic multiplication after applying the transform.

Another useful result concerns Fourier transforms and convolutions.

Theorem 7 (Convolution theorem)**.** *Let* $\bar{f}(\xi)$ *be a Fourier transform which can be factorised into a product of transforms*

$$\bar{f}(\xi) = \bar{f}_1(\xi) \bar{f}_2(\xi). \tag{2.12}$$

Then the function $f(x)$ *is the convolution of* $f_1(x)$ *and* $f_2(x)$*, that is,*

$$f(x) = (f_1 * f_2)(x) = \int_0^x f_1(x - \tau) f_2(\tau) \mathrm{d}\tau. \tag{2.13}$$

The Fourier transform pair possesses asymptotic properties that allow certain aspects of the asymptotic behaviour of a function to be determined from its transform and vice versa. Theorems that give an asymptotic property of one member of the transform pair from a known asymptotic property of the other are called *Abelian-type theorems* (some authors make a distinction between Tauber and Abel theorems depending on which member of the pair yields information about the other but we shall refer to both as Abelian-type theorems). Abelian-type theorems can be used, for example, to deduce the behaviour of a transform for large values of its argument from the asymptotic behaviour of the physical solution near the crack tip. We will later state and prove a particularly useful Abelian-type theorem which is stated as Theorem 10 on page 44.

2.2 The Wiener-Hopf method

The Wiener-Hopf technique elegantly combines the powerful theorems relating to analytic functions of complex variables to solve certain types of partial differential equations.

A Wiener-Hopf equation is a functional equation that holds in a strip of the complex plane of the form

$$A(z) + \Phi^+(z) = \Xi(z)\Phi^-(z) \tag{2.14}$$

for all z in a strip of the complex plane parallel to the real axis, say $-\gamma^- < \mathrm{Im}(z) < \gamma^+$ with $\gamma^\pm > 0$. Here, $A(z)$ (zero in the homogeonous case) and $\Xi(z)$ are analytic in the strip and are defined for all $z \in \mathbb{C}$. The functions $\Phi^+(z)$ and $\Phi^-(z)$ are unknowns to be found and are analytic in overlapping half-planes $\mathrm{Im}(z) > -\gamma^-$ and $\mathrm{Im}(z) < \gamma^+$ respectively.

The Wiener-Hopf technique hinges upon the factorisation of the function $\Xi(z)$ into the product of functions

$$\Xi(z) = \Xi^+(z)\Xi^-(z), \tag{2.15}$$

where $\Xi^+(z)$ and $\Xi^-(z)$ are analytic and nonzero in respective half-planes $\mathrm{Im}(z) > -\gamma^-$ and $\mathrm{Im}(z) < \gamma^+$. Assuming such a factorisation is admitted, (2.14) can be rearranged to give

$$\frac{A(z)}{\Xi^+(z)} + \frac{\Phi^+(z)}{\Xi^+(z)} = \Xi^-(z)\Phi^-(z). \tag{2.16}$$

The function $\frac{A(z)}{\Xi^+(z)}$ is then decomposed as

$$\frac{A(z)}{\Xi^+(z)} = Q^+(z) + Q^-(z), \tag{2.17}$$

where $Q^+(z)$ and $Q^-(z)$ are analytic in the half-planes $\mathrm{Im}(z) > -\gamma^-$ and $\mathrm{Im}(z) < \gamma^+$ respectively. This decomposition is unique up to an additive entire function. Substitution of this additive decomposition into (2.16) yields the fully factorised Wiener-Hopf equation

$$Q^+(z) + \frac{\Phi^+(z)}{\Xi^+(z)} = \Xi^-(z)\Phi^-(z) - Q^-(z), \tag{2.18}$$

which is valid in the strip $-\gamma^- < \mathrm{Im}(z) < \gamma^+$. Both sides of (2.18) represent functions analytic in their respective half-planes and coincide within the common strip of analyticity. It follows from the identity theorem for analytic functions that either side is the analytic continuation of the other and so together they represent the entire function $E(z)$.

We will often find that the left and right hand sides of (2.18) behave algebraically at infinity, that is

$$\left| Q^+(z) + \frac{\Phi^+(z)}{\Xi^+(z)} \right| = O(|z|^{c_+}),\ \mathrm{Im}(z) > -\gamma^-,\ |z| \to \infty, \tag{2.19}$$

$$|\Xi^-(z)\Phi^-(z) - Q^-(z)| = O(|z|^{c_-}),\ \mathrm{Im}(z) < \gamma^+,\ |z| \to \infty. \tag{2.20}$$

Liouville's theorem in such cases, providing that there are no essential singularities, yields that the entire function $E(z)$ is a polynomial of degree at most m, where $m = \max\{n \in \mathbb{Z} : n \leq \min\{c_+, c_-\}\}$. Thus the functions $\Phi^+(z)$ and $\Phi^-(z)$ are now known up to a finite number of constants, the polynomial coefficients.

Of course, this technique relies upon the ability to factorise functions of complex variables into the sum or product of functions which are analytic in overlapping half-planes. In the scalar case, the additive decomposition used in (2.17) makes use of the following theorem (Noble, p.13).

Theorem 8. *Let $f(z)$ be an analytic function in the strip $\tau^- < \mathrm{Im}(z) < \tau^+$, such that $|f(z)| < C|\mathrm{Re}(z)|^{-p}$, $p > 0$ for $|\mathrm{Re}(z)| \to \infty$, the inequality holding uniformly for all z in the strip $\tau^- + \varepsilon \leq \mathrm{Im}(z) \leq \tau^+ - \varepsilon$, $\varepsilon > 0$. Then for $\tau^- < c < \mathrm{Im}(z) < d < \tau^+$,*

$$f(z) = f^+(z) + f^-(z), \tag{2.21}$$

where

$$f^+(z) = \frac{1}{2\pi i}\int_{-\infty+ic}^{\infty+ic} \frac{f(\xi)}{\xi - z}\mathrm{d}\xi, \qquad f^-(z) = -\frac{1}{2\pi i}\int_{-\infty+id}^{\infty+id} \frac{f(\xi)}{\xi - z}\mathrm{d}\xi, \tag{2.22}$$

where $f^+(z)$ is analytic for all $\mathrm{Im}(z) > \tau^-$, and $f^-(z)$ is analytic for all $\mathrm{Im}(z) < \tau^+$.

The proof of this theorem follows from Cauchy's integral theorem. Theorem 8 is also useful for the multiplicative factorisation required in (2.15). Taking logarithms of (2.15) gives

$$\log \Xi(z) = \log \Xi_+(z) + \log \Xi_-(z), \tag{2.23}$$

and so

$$\Xi^{\pm}(z) = \exp\left\{ \frac{\pm 1}{2\pi i} \int_{-\infty \mp i\varepsilon}^{\infty \mp i\varepsilon} \frac{\log \Xi(\xi)}{\xi - z} \mathrm{d}\xi \right\}, \tag{2.24}$$

where $\varepsilon > 0$ is chosen to be sufficiently small so the contours of integration lie within the strip of analyticity of $\Xi(z)$.

It will often be important for us to describe the asymptotic behaviour of the functions $\Xi^{\pm}(z)$ defined in (2.24) as $z \to 0$ and as $z \to \infty$ for particular functions $\Xi(\xi)$. Commonly we will apply this procedure to functions which have purposely been chosen to tend to a constant value (often chosen to be 1) near zero and infinity. We will state the asymptotics in this case of $\Xi^{\pm}(z)$ as a theorem in Section 3.1.5.

2.3 Cracks and interfaces

We describe in this section some models of fracture and interfaces, which will introduce concepts that are of importance to this thesis. We first discuss asymptotics near crack tips before showing the derivation of transmission conditions for important types of interface.

2.3.1 Mathematical models of cracks

Let us consider the geometry of an unbounded body with a crack occupying the (x, y)-plane and take the crack front to be parallel to the y-axis. The crack is defined to be the surface across which the displacement field $\mathbf{u}$ is discontinuous. Irwin [26] noted that the upper and lower crack surfaces can be moved with respect to each other in three independent ways. These three types of deformation are called *modes*: Mode I, Mode II and Mode III. Mode I describes in-plane opening (a tensile stress acting normal to the plane of

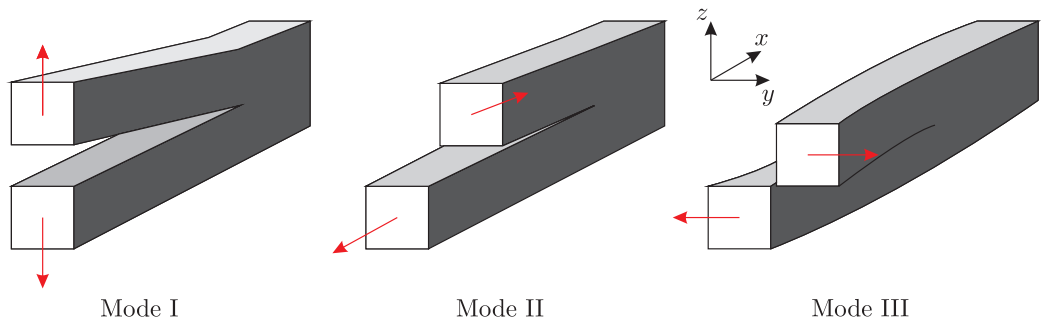

Figure 2.1: The three fracture modes.

the crack), Mode II describes in-plane shearing (a shear stress acting parallel to the plane of the crack and perpendicular to the crack front) and Mode III describes out-of-plane shearing (a shear stress acting parallel to the plane of the crack and parallel to the crack front). These are indicated on Figure 2.1.

Each of the three modes has an associated stress field near the crack tip. Let us arrange our co-ordinate system as in Figure 2.1 so that the x direction is normal to the crack edge, the y direction is parallel to the crack edge and the z direction is perpendicular to crack plane. The origin $\mathbf{0}$ sits along the crack edge. Then defining the distance from the crack as r, the three stress components σ_{zz}, σ_{xz} and σ_{yz} have asymptotics as $r \to 0$ near the tip of the form

$$\sigma_{zz} = \frac{K_I}{(2\pi r)^{1/2}} + O(1), \ \sigma_{xz} = \frac{K_{II}}{(2\pi r)^{1/2}} + O(1), \ \sigma_{yz} = \frac{K_{III}}{(2\pi r)^{1/2}} + O(1). \quad (2.25)$$

The stress intensity factors K_I, K_{II} and K_{III} depend on the geometry of the cracked body and the applied loading. They characterise the intensity of the local stresses and as discussed in the bibliographical review in Chapter 1, act in fracture criteria. That is, given two bodies with differently sized cracks and different loadings, if the stress intensity factors are equal, then in the vicinity of the crack tip, the stress and displacement fields will be the

same. Thus if crack extension begins in one body at a certain critical stress intensity factor called the fracture toughness, then the crack in the second body can be expected to also begin to grow as the stress intensity factor exceeds that body's fracture toughness.

2.3.2 Imperfect interfaces and transmission conditions

The presence of an imperfect interface in a bi-material structure is a crucial feature of many of the problems discussed in this thesis. Throughout, when we write 'imperfect interface' we shall be referring to a *soft imperfect interface*. Such interfaces model a thin layer of a soft adhesive material between the two main materials. If instead the two main materials have a stiff thin layer between them, the interface is referred to as a *stiff imperfect interface*. Typically these very thin layers are replaced in problem formulations by transmission conditions. In this subsection we show the derivation of transmission conditions for a Mode III crack that model two different types of imperfect interface.

Perfect interface

Before presenting the derivation of transmission conditions for soft and stiff imperfect interfaces, let us state the interface conditions for a perfect interface. A perfect or ideal interface is characterised by continuity of both displacement and traction across the interface. For instance, a perfect interface along a line $y = 0$ joining two bodies of shear moduli μ_1 and μ_2 respectively occupying $y > 0$ and $y < 0$ is described by the conditions

$$u_1\big|_{y=0+} = u_2\big|_{y=0-}, \qquad \mu_1 \frac{\partial u_1}{\partial y}\bigg|_{y=0+} = \mu_2 \frac{\partial u_2}{\partial y}\bigg|_{y=0-} \tag{2.26}$$

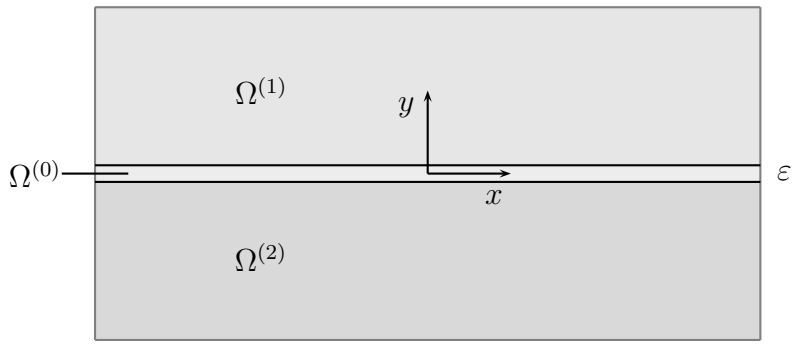

Figure 2.2: Thin layer of thickness ε occupying $\Omega^{(0)}$.

where $u_j = u_j(x, y)$ is the displacement field in the domain

$$\{(x, y) \in \mathbb{R}^2 : (-1)^{j+1} y > 0\}. \tag{2.27}$$

Soft imperfect interface

We follow the approach employed for example by Antipov [1]. We consider two bodies $\Omega^{(1)}$ and $\Omega^{(2)}$ connected through a thin interface layer $\Omega^{(0)}$ of thickness ε. $\Omega^{(1)}$ and $\Omega^{(2)}$ are occupied by materials with respective shear moduli μ_1 and μ_2, while $\Omega^{(0)}$ houses a softer adhesive material of shear modulus $\mu_0 = \varepsilon\mu$, where μ is of the same order as μ_1 and μ_2.

For out-of-plane shear we consider the displacement field $(0, 0, u(x, y))$ with the only non-zero component being the z-component which depends solely upon x and y. The displacements u_1, u_2 and u_0 in domains indicated by their subscripts satisfy the equations

$$\nabla^2 u_j = 0 \quad \text{in } \Omega^{(j)}, \quad j = 0, 1, 2. \tag{2.28}$$

Across the interfacial boundaries, displacement and tractions are assumed

continuous, that is

$$u_1|_{y=\varepsilon/2} = u_0|_{y=\varepsilon/2}, \qquad \mu_1 \frac{\partial u_1}{\partial y}\bigg|_{y=\varepsilon/2} = \mu_0 \frac{\partial u_0}{\partial y}\bigg|_{y=\varepsilon/2}, \tag{2.29}$$

$$u_2|_{y=-\varepsilon/2} = u_0|_{y=-\varepsilon/2}, \qquad \mu_2 \frac{\partial u_2}{\partial y}\bigg|_{y=-\varepsilon/2} = \mu_0 \frac{\partial u_0}{\partial y}\bigg|_{y=-\varepsilon/2}. \tag{2.30}$$

Let $\chi = y/\varepsilon$, so that within the thin adhesive layer $\Omega^{(0)}$, $|\chi| < 1/2$. Now, in terms of x and χ we see that

$$\nabla^2 u_0 = \frac{1}{\varepsilon^2}\frac{\partial^2 u_0}{\partial \chi^2} + \frac{\partial^2 u_0}{\partial x^2} = 0. \tag{2.31}$$

Letting $u_0^{(0)}$ denote the leading term of u_0, we see that

$$\frac{\partial^2 u_0^{(0)}}{\partial \chi^2} = 0, \quad \text{in } \Omega^{(0)}, \tag{2.32}$$

and therefore

$$u_0^{(0)} = A_1^{(0)}(x) + \chi A_2^{(0)}(x), \tag{2.33}$$

where $A_1^{(0)}$ and $A_2^{(0)}$ are functions solely of x. Continuity of displacement (equations (2.29) and (2.30)) imply that

$$A_1^{(0)}(x) = \frac{1}{2}(u_1(x,0) + u_2(x,0)), \tag{2.34}$$

$$A_2^{(0)}(x) = u_1(x,0) - u_2(x,0), \tag{2.35}$$

and then applying the condition for continuity of tractions we obtain

$$\mu_1 \frac{\partial u_1}{\partial y}\bigg|_{y=0+} = \mu_2 \frac{\partial u_2}{\partial y}\bigg|_{y=0-} = \mu_0 \frac{\partial u_0^{(0)}}{\partial \chi} = \mu_0(u_1(x,0^+) - u_2(x,0^-)) \tag{2.36}$$

to leading order. Thus we have shown that for an imperfect interface the leading order term of tractions is continuous across the interface layer and is proportional to the displacement jump across the interface.

Stiff imperfect interface

For the stiff imperfect interface we follow the approach given by Mishuris *et al.* [43]. We again consider two bodies $\Omega^{(1)}$ and $\Omega^{(2)}$, but with a thin layer $\Omega^{(0)}$ between them which is highly rigid. That is, we assume that

$$\mu_0 = \frac{1}{\varepsilon}\mu, \tag{2.37}$$

where μ is of the same order of magnitude as μ_j for $j = 1, 2$. As in the soft interface case, displacement and traction are assumed continuous across the interfacial boundaries, that is conditions (2.29) and (2.30) hold. We write asymptotic expansions for the displacement fields u_j $(j = 1, 2)$ and u_0 as

$$u_j(x, y, \varepsilon) = u_j^{(0)}(x, y, \varepsilon) + \varepsilon u_j^{(1)}(x, y, \varepsilon) + \varepsilon^2 u_j^{(2)}(x, y, \varepsilon), \quad j = 1, 2, \tag{2.38}$$

$$u_0(x, \chi, \varepsilon) = u_0^{(0)}(x, \chi, \varepsilon) + \varepsilon u_0^{(1)}(x, \chi, \varepsilon) + \varepsilon^2 u_0^{(2)}(x, \chi, \varepsilon), \tag{2.39}$$

where $\chi = y/\varepsilon$. Taking the second conditions (continuity of tractions) in each of (2.29) and (2.30), we see that

$$\frac{\mu}{\varepsilon^2}\left(\frac{\partial u_0^{(0)}}{\partial \chi} + \varepsilon\frac{\partial u_0^{(1)}}{\partial \chi} + \varepsilon^2\frac{\partial u_0^{(2)}}{\partial \chi}\right)\Bigg|_{\chi=\pm 1/2} = \mu_j \left.\frac{\partial u_j^{(0)}}{\partial y}\right|_{y=0\pm} + \ldots = O(1), \tag{2.40}$$

and so it follows that

$$\left.\frac{\partial u_0^{(0)}}{\partial \chi}\right|_{\chi=\pm 1/2} = 0. \tag{2.41}$$

Therefore $u_0^{(0)}$ is χ-independent, which implies continuity of leading order displacements across the interface for $u_j^{(0)}$:

$$u_1^{(0)}(x, 0^+) = u_2^{(0)}(x, 0^-). \tag{2.42}$$

Comparing coefficients of ε we see that inside the thin layer,

$$\frac{\partial^2 u_0^{(2)}}{\partial \chi^2} = -\frac{\partial^2 u_0^{(0)}}{\partial x^2}. \tag{2.43}$$

The right hand side of (2.43) does not depend on χ and so

$$\left.\frac{\partial u_0^{(2)}}{\partial \chi}\right|_{\chi=1/2} - \left.\frac{\partial u_0^{(2)}}{\partial \chi}\right|_{\chi=-1/2} = -\frac{\partial^2 u_0^{(0)}}{\partial x^2}. \tag{2.44}$$

Finally, (2.40) yields the following transmission condition:

$$\mu_1 \left.\frac{\partial u_1^{(0)}}{\partial y}\right|_{y=0+} - \mu_2 \left.\frac{\partial u_2^{(0)}}{\partial y}\right|_{y=0-} = -\mu \left.\frac{\partial^2 u_1^{(0)}}{\partial x^2}\right|_{y=0+}. \tag{2.45}$$

Thus for a stiff interface, there is no displacement jump across the interface but there is an interfacial jump in traction proportional to the second partial derivative of the displacement with respect to x.

Slightly curved imperfect interfaces

The derivations presented above have been generalised by Mishuris [42] for a thin, slightly curved, nonhomogeneous and weakly anisotropic elastic interface in both stiff and soft cases. For the soft slightly curved interface, transmission conditions take the form

$$\left[\!\left[\mu \frac{\partial u^{(0)}}{\partial y}\right]\!\right](x) = 0, \quad [\![u^{(0)}]\!](x) - \tau_*(x)\mu_j \frac{\partial u_j^{(0)}}{\partial y}(x,0) = 0. \tag{2.46}$$

while for the stiff slightly curved interface,

$$[\![u^{(0)}]\!](x) = 0, \quad \left[\!\left[\mu \frac{\partial u^{(0)}}{\partial y}\right]\!\right](x) + \frac{\partial}{\partial x}(\tau^*(x)\frac{\partial}{\partial x})u_j^{(0)}(x,0) = 0. \tag{2.47}$$

Here, the notation $[\![\cdot]\!]$ denotes the jump of the argument across the imperface from the positive to the negative side (that is, $[\![u^{(0)}]\!](x) = u^{(0)}(x,0^+) - u^{(0)}(x,0^-)$); we will use this notation extensively throughout the thesis. The functions $\tau_*(x)$ and $\tau^*(x)$ are defined by the equations

$$\tau_*(x) = H(x) \int_{-1/2}^{1/2} \nu_2^{-1}(x,\xi)\mathrm{d}\xi, \qquad \tau^*(x) = H(x) \int_{-1/2}^{1/2} \nu_1(x,\xi)\mathrm{d}\xi, \tag{2.48}$$

where $\varepsilon H(x)$ is the thickness of the interfacial layer (which depends on x), ν_j are rescalings of μ_j (which varies in the interfacial layer) and ξ is a rescaling of y.

Chapter 3

Bloch-Floquet waves in a thin bi-material strip containing a periodic array of cracks and imperfect interfaces

We begin to cover the new ground by addressing the problem of determining a weight function in a domain representing a bi-material strip containing a semi-infinite interfacial crack. Where the crack is not present the interface is considered *imperfect*, modelling a thin layer of adhesive between the materials.

We consider in this chapter Mode III deformation and describe the extent of the interface's imperfection by a positive parameter denoted κ. The problem we study here is a singular perturbation problem; taking very small values for κ gives a qualitatively significantly different weight function from that derived for the perfect interface case in [44] which corresponds to the

formulation with $\kappa = 0$. Moreover, large values of κ can lead to interesting effects where the boundary layers surrounding different crack tips decay slowly so they can no longer be considered as having no influence on the Bloch-Floquet conditions. This effect is discussed in [5]; for the analysis presented in the present chapter we assume that κ is not large enough for these effects to come into play and later find a condition for this to be the case. As mentioned in the previous chapter, problems regarding cracks in domains including imperfect interfaces have been studied for instance in [1] and [43], but no corresponding weight function has previously been constructed.

Aside from the presence of imperfect interfaces, another critical characteristic of the problem is that the strip considered is very thin. In addition to the strip itself being very thin, imperfect interfaces are typically replaced with an extremely thin layer of a softer bonding material in finite element computations (see for example [9, 23, 43]). This makes FEM modelling for particularly thin strips extremely difficult or even impossible and motivate the need for the asymptotic approach. In this chapter we compare the asymptotic model with finite element simulations only in cases when the strip is not too thin, but stress that the finite element methods are unsuitable for the limiting case whereas the asymptotics remain valid. The asymptotic method also obtains crucial constants which describe the solution's behaviour at the crack tips which are vital for determining whether fracture may occur. These important constants would not be attained by finite element methods.

The plan of the work is as follows. We first formulate the weight function problem and use Fourier transform and Wiener-Hopf techniques to obtain the solution. Asymptotic analysis enables us to find analytic expressions for all important constants. We then present an application of the weight

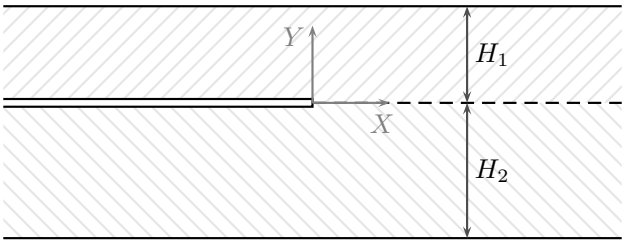

Figure 3.1: Geometry for the weight function.

function to the analysis of Bloch-Floquet waves in a structure containing a periodic array of cracks and imperfect interfaces. This application involves the derivation of junction conditions. Asymptotic theories for structures like rods and plates have received much attention throughout the history of elasticity theory. For multi-structures however, conditions in engineering practice are often formulated on the basis of intuitive physical assumptions. For example, the zero order junction conditions for the problem addressed fit with physical intuition. It is important to give these conditions a rigorous mathematical footing; moreover, higher order junction conditions do not follow such intuition [32].

We conclude by presenting a comparison between the perfect interface case studied in [44] and the imperfect interface case presented here.

3.1 Weight Function

3.1.1 Formulation of the Problem

The geometry of the strip in which we construct the weight function is shown in Figure 3.1. We define our domain Π_B to be the union of $\Pi_B^{(1)}$ and $\Pi_B^{(2)}$,

where

$$\Pi_B^{(j)} = \{(X,Y) : X \in \mathbb{R}, \quad (-1)^{j+1}Y \in (0, H_j)\}, \quad j = 1, 2.$$

$\Pi_B^{(1)}$ corresponds to the material above the cut with shear modulus μ_1, while $\Pi_B^{(2)}$ corresponds to the material below the cut with shear modulus μ_2. The materials have respective thicknesses H_1 and H_2. A semi-infinite crack with its tip placed at the origin occupies $X < 0$, while the rest of the interface is assumed to be imperfect.

The functions w_1 and w_2 are defined in domains $\Pi_B^{(1)}$ and $\Pi_B^{(2)}$ respectively as solutions to the Laplace equation

$$\nabla^2 w_j(X,Y) = 0, \quad (X,Y) \in \Pi_B^{(j)}. \tag{3.1}$$

We impose boundary conditions along the horizontal parts of the boundary of Π_B and on the crack face itself and denote the components of stress in the out-of-plane direction by

$$\sigma_{nz}^{(j)}(X,Y) := \mu_j \frac{\partial w_j}{\partial n}, \quad j = 1, 2. \tag{3.2}$$

We further assume a zero stress component in the out-of-plane direction along the top and bottom of the strip, as well as along the face of the crack itself:

$$\sigma_{YZ}^{(1)}(X, H_1) = 0, \quad \sigma_{YZ}^{(2)}(X, -H_2) = 0, \quad X \in \mathbb{R}, \tag{3.3}$$

$$\sigma_{YZ}^{(1)}(X, 0^+) = 0, \quad \sigma_{YZ}^{(2)}(X, 0^-) = 0, \quad X < 0. \tag{3.4}$$

Ahead of the cut we impose the imperfect transmission conditions

$$\sigma_{YZ}^{(1)}(X, 0^+) = \sigma_{YZ}^{(2)}(X, 0^-), \quad X > 0, \tag{3.5}$$

$$w_1|_{Y=0^+} - w_2|_{Y=0^-} = \kappa \sigma_{YZ}^{(1)}(X, 0^+), \quad X > 0, \tag{3.6}$$

where $\kappa > 0$ is a parameter describing the extent of imperfection of the interface.

We seek solutions in the class of functions that decay exponentially as $X \to +\infty$ and are bounded as $X \to -\infty$:

$$w_j = O(e^{-\gamma^+ X}), \quad X \to +\infty; \qquad w_j = C_j + O(e^{\gamma^- X}), \quad X \to -\infty, \quad (3.7)$$

where $\gamma^\pm > 0$ and C_j are constants to be sought from the analysis. At the vertex of the crack, the solution w_j is assumed to be weakly singular, with

$$w_1, w_2 = O(\ln |X|), \quad X \to 0. \quad (3.8)$$

Formally, conditions (3.1)-(3.7) are similar to those in [44] (which considers the perfect interface) if we take $\kappa = 0$. However, with $\kappa > 0$ the problem is a singular perturbation problem and the behaviour described in (3.8) is entirely different.

3.1.2 An auxiliary problem

We now introduce an auxiliary solution $\mathcal{Y}$ defined as

$$\mathcal{Y}(X,Y) = \begin{cases} \mathcal{Y}_1(X,Y), & (X,Y) \in \Pi_B^{(1)}, \\ \mathcal{Y}_2(X,Y), & (X,Y) \in \Pi_B^{(2)}, \end{cases} \quad (3.9)$$

which satisfies the Laplace equation (3.1) along with the boundary and transmission conditions (3.3)-(3.5), but the conditions at infinity and at the vertex of the crack are modified as follows:

$$\mathcal{Y}_j = O(e^{-\gamma^+ X}), \quad X \to +\infty, \quad (3.10)$$

$$\mathcal{Y}_j = C_j X + D_j + O(e^{\gamma^- X}), \quad X \to -\infty, \quad (3.11)$$

$$\mathcal{Y}_j = \mathcal{Y}_j(0^+, 0) + O(X \ln |X|), \quad X \to 0. \quad (3.12)$$

The functions w and $\mathcal{Y}$ are related via the formula

$$w(X,Y) = \frac{\partial}{\partial X}\mathcal{Y}(X,Y), \quad (3.13)$$

where $w(X,Y)$ takes the value of $w_1(X,Y)$ above the crack line and $w_2(X,Y)$ below it, analogously to (3.9).

Bearing this relationship in mind, we often later refer to $\mathcal{Y}$ as a 'weight function' as well as w. It is also shown in [40] that

$$\mathcal{Y}_j(R,\theta) \sim \frac{(-1)^j a_0^{(\mathcal{Y})}}{\pi\mu_j}\left\{\frac{\mu_1\mu_2\kappa\pi}{\mu_1+\mu_2} + \left[1-\ln\left(\frac{R}{b_0^{(\mathcal{Y})}}\right)\right]R\cos\theta \right. \\ \left. + (-1)^{j+1}(\pi+(-1)^j\theta)R\sin\theta\right\}, \quad R\to 0, \quad (3.14)$$

where the co-ordinates (R,θ) describe the polar co-ordinate system centred at the origin with $\theta\in[0,\pi]$ for $\mathcal{Y}_1$ and $\theta\in[-\pi,0]$ for $\mathcal{Y}_2$.

3.1.3 Derivation of Wiener-Hopf equation

We define the Fourier transforms with respect to X of $\mathcal{Y}_j$ by

$$\bar{\mathcal{Y}}_j(\xi,Y) = \int_{-\infty}^{\infty} e^{i\xi X}\mathcal{Y}_j(X,Y)\mathrm{d}X. \quad (3.15)$$

The functions $\bar{\mathcal{Y}}_j$ are analytic in the strip $S=\{\xi\in\mathbb{C}: -\gamma^+ < \mathrm{Im}(\xi) < 0\}$, and have a double pole only at the point $\xi=0$ (this follows from the linear behaviour of $\mathcal{Y}_j$ near minus infinity), so

$$\bar{\mathcal{Y}}_j(\xi,Y) \sim \frac{1}{\xi^2}C_j - i\frac{D_j}{\xi} + O(1), \quad \xi\to 0. \quad (3.16)$$

Note that the functions $\bar{\mathcal{Y}}_j(\xi,Y)$ can be analytically extended to the strip

$$\tilde{S} = \{\xi\in\mathbb{C}: -\gamma^+ < \mathrm{Im}(\xi) < \gamma^-\}.$$

Let us now introduce $[\![\mathcal{Y}]\!]$, the jump in $\mathcal{Y}$, defined by

$$[\![\mathcal{Y}]\!] = \mathcal{Y}_1|_{Y=0+} - \mathcal{Y}_2|_{Y=0-}. \quad (3.17)$$

We see from (3.16) that the Fourier transform of the jump $[\![\mathcal{Y}]\!](X)$ in general has a double pole at the point $\xi = 0$.

We introduce the following notation:

$$\Phi^-(\xi) = \overline{[\![\mathcal{Y}]\!] - \mu_1\kappa\frac{\partial\mathcal{Y}_1}{\partial Y}\bigg|_{Y=0+}} = \int_{-\infty}^{0}\left([\![\mathcal{Y}]\!](X) - \mu_1\kappa\frac{\partial\mathcal{Y}_1}{\partial Y}\bigg|_{Y=0+}\right)e^{i\xi X}\mathrm{d}X, \tag{3.18}$$

where we have taken into account the imperfect transmission conditions $[\![\mathcal{Y}]\!] - \mu_1\kappa\frac{\partial\mathcal{Y}_1}{\partial Y}\big|_{Y=0+} = 0$ for $X > 0$. The function $\Phi^-(\xi)$ is analytic in the half-plane $\mathrm{Im}(\xi) < 0$ and has a double pole at $\xi = 0$. Thus it can be analytically extended into the half-plane $\mathbb{C}^- = \{\xi \in \mathbb{C} : \mathrm{Im}(\xi) < \gamma^-\}$. We further define the function

$$\Phi^+(\xi) = \mu_1\int_0^{\infty}\frac{\partial\mathcal{Y}_1}{\partial Y}\bigg|_{Y=0+}e^{i\xi X}\mathrm{d}X, \tag{3.19}$$

and so according to the condition (3.4) of zero traction on the crack faces, $\Phi^+(\xi)$ is analytic in the half-plane $\mathbb{C}^+ = \{\xi \in \mathbb{C} : \mathrm{Im}(\xi) > -\gamma^+\}$.

We expect the asymptotic behaviours of the functions $\Phi^\pm$ to be of the form

$$\Phi^\pm(\xi) = \frac{E_1^\pm}{\xi} + \frac{E_2^\pm\ln(\mp i\xi)}{\xi} + O\left(\frac{1}{\xi^2}\right), \quad \xi \to \infty, \tag{3.20}$$

in the respective domain according to (3.12); we later confirm this to be true.

Taking Fourier transforms of the Laplace equation in X gives that

$$\frac{\partial^2\bar{\mathcal{Y}}_j}{\partial Y^2} - \xi^2\bar{\mathcal{Y}}_j = 0, \tag{3.21}$$

whence the Fourier transforms of the functions $\mathcal{Y}_j$ are of the form

$$\bar{\mathcal{Y}}_j(\xi, Y) = A_j(\xi)\cosh(\xi Y) + B_j(\xi)\sinh(\xi Y). \tag{3.22}$$

Upon the application of boundary and interfacial conditions expressions re-

lating $A_j(\xi)$ and $B_j(\xi)$ are found:

$$B_j(\xi) = (-1)^j A_j(\xi)\tanh(\xi H_j), \quad j = 1, 2; \qquad \mu_1 B_1(\xi) - \mu_2 B_2(\xi) = 0. \tag{3.23}$$

Moreover, $\Phi^{\pm}(\xi)$ can be expressed in terms of $A_j(\xi), B_j(\xi)$:

$$\Phi^-(\xi) = A_1(\xi) - A_2(\xi) - \mu_1\kappa\xi B_1(\xi), \quad \Phi^+(\xi) = \mu_1\xi B_1(\xi). \tag{3.24}$$

It follows that the functions $\Phi^+(\xi)$ and $\Phi^-(\xi)$ satisfy the functional equation of the Wiener-Hopf type

$$\Phi^-(\xi) = -\Xi(\xi)\Phi^+(\xi), \tag{3.25}$$

in the strip $-\gamma^+ < \mathrm{Im}(\xi) < 0$, where

$$\Xi(\xi) = \frac{1}{\xi}\left(\frac{1}{\mu_1}\coth(\xi H_1) + \frac{1}{\mu_2}\coth(\xi H_2) + \kappa\xi\right), \tag{3.26}$$

and $-\gamma^+$ is equal to the size of the imaginary part of the first zero of $\Xi(\xi)$ lying below the real axis. We stress here that the form of the Wiener-Hopf kernel $\Xi(\xi)$ demonstrates that the weight function problem is a singular perturbation problem as $\kappa \to 0$; the presence of the term involving κ fundamentally alters the asymptotic behaviour of $\Xi(\xi)$ as $\xi \to \infty$. This asymptotic behaviour influences our choice of factorisation of $\Xi(\xi)$ which we perform in the following subsection.

3.1.4 Factorisation of the Wiener-Hopf kernel

Before we factorise the Wiener-Hopf kernel $\Xi(\xi)$, we must determine its behaviour near $\xi = 0$ and also for $\xi \to \infty$. We find that near $\xi = 0$, the kernel has a double pole, in particular

$$\Xi(\xi) = \frac{\eta}{\xi^2} + O(1), \qquad \eta = \frac{1}{\mu_1 H_1} + \frac{1}{\mu_2 H_2}. \tag{3.27}$$

It is readily seen that as $\xi \to \infty$, the function $\Xi(\xi)$ tends toward the constant value κ. With this behaviour in mind, our aim is to factorise $\Xi(\xi)$ into the product of functions that are analytic in overlapping half-planes, with one such function (which we shall denote $\Xi_*(\xi)$) being well-behaved in a strip containing the real axis, non-zero and tending towards a constant (for convenience and without loss of generality this constant will be 1) both as $\xi \to 0$ and as $\xi \to \pm\infty$.

We note that the kernel function $\Xi(\xi)$ as defined in (3.26) can be written in the form

$$\Xi(\xi) = \kappa \frac{(\lambda + i\xi)(\lambda - i\xi)}{\xi^2} \Xi_*(\xi), \tag{3.28}$$

where

$$\Xi_*(\xi) = \frac{\xi(\mu_1 \coth(\xi H_2) + \mu_2 \coth(\xi H_1) + \mu_1\mu_2\kappa\xi)}{\mu_1\mu_2\kappa(\lambda^2 + \xi^2)}, \tag{3.29}$$

and

$$\lambda = \sqrt{\frac{\mu_1 H_1 + \mu_2 H_2}{\mu_1\mu_2 H_1 H_2 \kappa}}. \tag{3.30}$$

Now, $\Xi_*(\xi)$ is analytic in a strip containing the real axis, clearly positive, even and smooth for all $\xi \in \mathbb{R}$ and has been chosen in such a way so that $\Xi_*(\xi)$ tends towards 1 as $\xi \to \pm\infty$ and as $\xi \to 0$. Furthermore, it can be factorised in the form

$$\Xi_*(\xi) = \Xi_*^+(\xi)\Xi_*^-(\xi), \tag{3.31}$$

where

$$\Xi_*^\pm(\xi) = \exp\left\{ \frac{\pm 1}{2\pi i} \int_{-\infty \mp i\beta}^{\infty \mp i\beta} \frac{\ln \Xi_*(t)}{t - \xi} \mathrm{d}t \right\}, \tag{3.32}$$

and $\beta > 0$ is chosen to be sufficiently small so the contours of integration lie within the strip of analyticity of $\Xi_*(\xi)$. The functions $\Xi_*^\pm$ are analytic in their respective half-planes.

To conclude this subsection, we have factorised $\Xi(\xi)$ in the form given in (3.28) and (3.31), where $\Xi_*^{\pm}$ are analytic in the half-planes denoted by their superscripts. Note that in the specific case $H_1 = H_2$, a different factorisation has been obtained in [1].

3.1.5 Asymptotic behaviour of Ξ_* and Ξ_*^+

We now seek asymptotic estimates of $\Xi_*^+(\xi)$. We first note that for ξ within the strip of analyticity,

$$\Xi_*(\xi) = 1 + O(|\xi|^2), \quad \xi \to 0. \tag{3.33}$$

Let us now consider more accurately the behaviour of $\Xi_*(\xi)$ for $\xi \in \mathbb{R}$ as $\xi \to \infty$. Noting that $\Xi_*(\xi)$ is an even function, it follows from (3.26) that

$$\Xi_*(\xi) = 1 + \frac{\mu_1 + \mu_2}{\mu_1\mu_2\kappa|\xi|} - \frac{\lambda^2}{\xi^2} + O\left(\frac{1}{|\xi|^3}\right), \quad \xi \to \pm\infty. \tag{3.34}$$

The same estimate is true for any ξ lying in the strip of analyticity. In order to calculate asymptotic estimates for the function $\Xi_*^+(\xi)$ from the expressions we have calculated from $\Xi_*(\xi)$, we introduce the following theorem.

Theorem 9. *Let*

$$\Xi_*^+(\xi) = \exp\left\{\frac{1}{2\pi i}\int_{-\infty-i\beta}^{\infty-i\beta} \frac{\ln \Xi_*(t)}{t-\xi}\mathrm{d}t\right\}, \tag{3.35}$$

where $\Xi_*(t)$ is analytic in a strip containing the real axis, positive, even, smooth for all $t \in \mathbb{R}$ and satisfies the asymptotic estimates

$$\Xi_*(t) = 1 + O(|t|^2), \quad t \to 0, \tag{3.36}$$

$$\Xi_*(t) = 1 + \frac{c}{|t|} + O(t^{-2}), \quad t \to \pm\infty, \tag{3.37}$$

and $\beta > 0$ is sufficiently small to ensure that the contour of integration lies within the strip of analyticity. Then $\Xi_*^+(\xi)$ satisfies the following asymptotic estimates:

$$\Xi_*^+(\xi) = 1 + \frac{\alpha\xi}{\pi i} + O(|\xi|^2), \quad \xi \to 0, \tag{3.38}$$

$$\Xi_*^+(\xi) = 1 + \frac{c}{\pi i}\frac{\ln(-i\xi)}{\xi} + O\left(\frac{1}{|\xi|}\right), \quad \mathrm{Im}(\xi) \to +\infty, \tag{3.39}$$

where α is defined by

$$\alpha = \int_0^\infty \frac{\ln \Xi_*(t)}{t^2}\mathrm{d}t. \tag{3.40}$$

Proof. Introduce the auxiliary function

$$\Theta_*^+(\xi) = \int_{-\infty-i\beta}^{\infty-i\beta} \frac{\ln \Xi_*(t)}{t-\xi}\mathrm{d}t, \tag{3.41}$$

so that $\Xi_*^+(\xi) = \exp((1/2\pi i)\Theta_*^+(\xi))$. We first note that $\Theta_*^+(0) = 0$ since the integrand is odd and estimate (3.36) demonstrates integrability of Ξ_* at the zero point, allowing us to take $\beta = 0$. Thus

$$\Theta_*^+(\xi) = \int_{-\infty-i\beta}^{\infty-i\beta} \left[\frac{\ln \Xi_*(t)}{t-\xi} - \frac{\ln \Xi_*(t)}{t}\right]\mathrm{d}t = \xi \int_{-\infty-i\beta}^{\infty-i\beta} \frac{\ln \Xi_*(t)}{t(t-\xi)}\mathrm{d}t \to 0, \quad \xi \to 0,$$

since the integral is bounded. Also, we have that

$$\int_{-\infty-i\beta}^{\infty-i\beta} \frac{\ln \Xi_*(t)}{t^2}\mathrm{d}t = \int_{-\infty}^{\infty} \frac{\ln \Xi_*(t)}{t^2}\mathrm{d}t = 2\int_0^\infty \frac{\ln \Xi_*(t)}{t^2}\mathrm{d}t = 2\alpha, \tag{3.42}$$

since the integrand is even and again by considering (3.36), which indicates that we have integrability at the zero point. Here we have found that

$$\Theta_*^+(\xi) = 2\alpha\xi + O(|\xi|^2), \quad \xi \to 0. \tag{3.43}$$

From this we obtain the following estimate for $\Xi_*^+(\xi)$ as $\xi \to 0$:

$$\Xi_*^+(\xi) = 1 + \frac{\alpha\xi}{\pi i} + O(|\xi|^2), \quad \xi \to 0. \tag{3.44}$$

We now seek estimates of $\Theta_*^+(\xi)$ for $\xi \to \infty$ within the domain. To avoid problems caused by integrating along the real line, we consider $\xi \to \infty$ in such a way that $\mathrm{Im}(\xi) \to +\infty$. Integrating (3.41) by parts, splitting the integral in two and manipulating the resulting expression gives

$$\Theta_*^+(\xi) = \int_0^\infty \ln\left(\frac{1+t/\xi}{1-t/\xi}\right)\frac{\Xi_*'(t)}{\Xi_*(t)}\mathrm{d}t. \tag{3.45}$$

We introduce an arbitrary $R > 0$ and split this integral at R to give

$$\Theta_*^+(\xi) = \int_0^R \ln\left(\frac{1+t/\xi}{1-t/\xi}\right)\frac{\Xi_*'(t)}{\Xi_*(t)}\mathrm{d}t + \int_R^\infty \ln\left(\frac{1+t/\xi}{1-t/\xi}\right)\frac{\Xi_*'(t)}{\Xi_*(t)}\mathrm{d}t. \tag{3.46}$$

We then see that

$$\ln\left(\frac{1+t/\xi}{1-t/\xi}\right) = 2\frac{t}{\xi} + O\left(\frac{t^3}{|\xi|^3}\right), \quad \xi \to \infty, \quad 0 < t < R, \tag{3.47}$$

and from (3.34) we have

$$\frac{\Xi_*'(t)}{\Xi_*(t)} = -\frac{c}{t^2} + O\left(\frac{1}{t^3}\right), \quad t \to \infty. \tag{3.48}$$

This allows us to estimate

$$\Theta_*^+(\xi) = \int_R^\infty \left[-\frac{c}{t^2} + O\left(\frac{1}{t^3}\right)\right]\ln\left(\frac{\xi+t}{\xi-t}\right)\mathrm{d}t + O\left(\frac{R}{|\xi|}\right), \quad \xi \to \infty. \tag{3.49}$$

After integrating by parts and performing a change of variables, we find that

$$\int_R^\infty \frac{1}{t^2}\ln\left(\frac{\xi+t}{\xi-t}\right)\mathrm{d}t = -\frac{1}{\xi}\left(\ln\left|\frac{1}{\xi^2}\right| + i\arg\left(-\frac{1}{\xi^2}\right)\right) + O\left(\frac{1}{|\xi|}\right), \quad \xi \to \infty, \tag{3.50}$$

and so from (3.49), we deduce that

$$\Theta_*^+(\xi) = \frac{2c}{\xi}\ln(-i\xi) + O\left(\frac{1}{|\xi|}\right), \quad \mathrm{Im}(\xi) \to +\infty. \tag{3.51}$$

Recalling the relationship between our auxiliary function Θ_*^+ and Ξ_*^+ as we discussed after (3.41), we see that

$$\Xi_*^+(\xi) = 1 + \frac{c}{\pi i}\frac{\ln(-i\xi)}{\xi} + O\left(\frac{1}{|\xi|}\right), \quad \mathrm{Im}(\xi) \to +\infty. \tag{3.52}$$

□

We now apply Theorem 9 to our function $\Xi_*^+(\xi)$ and find that

$$\Xi_*^+(\xi) = 1 + \frac{\alpha\xi}{\pi i} + O(|\xi|^2), \quad \xi \to 0, \tag{3.53}$$

$$\Xi_*^+(\xi) = 1 + \frac{1}{\pi i}\frac{(\mu_1+\mu_2)}{\mu_1\mu_2\kappa}\frac{\ln(-i\xi)}{\xi} + O\left(\frac{1}{|\xi|}\right), \quad \mathrm{Im}(\xi) \to +\infty. \tag{3.54}$$

Here we have defined the asymptotic constant

$$\alpha = \int_0^\infty \frac{\ln \Xi_*(t)}{t^2}\mathrm{d}t. \tag{3.55}$$

The important expression (3.54) describing logarithmic asymptotics at infinity is needed later for equation (3.64).

3.1.6 Solution of the Wiener-Hopf equation

The factorised equation (3.25) is of the form

$$-\kappa(\lambda - i\xi)\Phi^+(\xi)\Xi_*^+(\xi) = \frac{1}{\lambda + i\xi}\xi^2\Phi^-(\xi)\frac{1}{\Xi_*^-(\xi)}. \tag{3.56}$$

Both sides of (3.56) represent analytic functions in the strip $-\gamma^+ < \mathrm{Im}(\xi) < \gamma^-$. Moreover we now have asymptotic estimates for $\Xi_*^\pm(\xi)$ at the zero point in equation (3.53) and for $\xi \to \pm\infty$ in (3.54). We deduce that since both sides of (3.56) exhibit the same behaviour at infinity in their respective domains according to (3.20), both sides must be equal to a constant, which we denote $\mathcal{A}$. We can therefore obtain explicit expressions for $\Phi^\pm$, which are as follows:

$$\Phi^+(\xi) = -\frac{\mathcal{A}}{\kappa(\lambda - i\xi)\Xi_*^+(\xi)}, \qquad \Phi^-(\xi) = \frac{\mathcal{A}(\lambda + i\xi)\Xi_*^-(\xi)}{\xi^2}, \tag{3.57}$$

We deduce that the Fourier transform of the weight functions $\mathcal{Y}_j$ are given by

$$\bar{\mathcal{Y}}_j(\xi, Y) = -\frac{\mathcal{A}\Phi^+(\xi)}{\mu_j \xi}\left\{\frac{\cosh(\xi(Y+(-1)^j H_j))}{\sinh(\xi(-1)^{j+1}H_j)}\right\}, \quad j = 1, 2. \tag{3.58}$$

This allows us to investigate the behaviour of $\bar{\mathcal{Y}}_j$ as $\xi \to \pm\infty$ and at the zero point. It also enables us to find the hitherto unknown real constants C_j and D_j.

3.1.7 Evaluation of constants C_j, D_j, $a_0^{(\mathcal{Y})}$, $\gamma^{\pm}$

In this subsection we evaluate the constants γ^+ (defined in (3.10)), γ^-, C_j, D_j (defined in (3.11)) and $a_0^{(\mathcal{Y})}$ (defined in (3.14)). We see from our expressions for $\bar{\mathcal{Y}}_j$ and Φ^+ (equations (3.57) and (3.58)), along with our asymptotic estimate for $\Xi_*^+(\xi)$ as $\xi \to 0$ that

$$\bar{\mathcal{Y}}_j(\xi) = \frac{(-1)^{j+1}\mathcal{A}}{\kappa\lambda\mu_j H_j}\left(\frac{1}{\xi^2} - \frac{i}{\xi}\left(-\frac{\alpha}{\pi} - \frac{1}{\lambda}\right)\right) + O(1), \quad \xi \to 0, \tag{3.59}$$

where α is the constant defined in (3.55). It follows from our definition of C_j and D_j in (3.16) that

$$C_j = \frac{(-1)^{j+1}\mathcal{A}}{\kappa\lambda\mu_j H_j}, \qquad D_j = \frac{(-1)^j \mathcal{A}}{\kappa\lambda\mu_j H_j}\left(\frac{\alpha}{\pi} + \frac{1}{\lambda}\right). \tag{3.60}$$

For normalisation we choose $\mathcal{A} = \kappa\lambda$, giving

$$C_j = \frac{(-1)^{j+1}}{\mu_j H_j}, \qquad D_j = \frac{(-1)^j}{\mu_j H_j}\left(\frac{\alpha}{\pi} + \frac{1}{\lambda}\right). \tag{3.61}$$

The chosen normalisation leaves $(3.61)_1$ in the same form as in [44], but it is clearly seen that the expression for D_j (which depends upon κ is different). Mishuris (2001) [40] demonstrates that near the crack tip (i.e. as $R \to 0$), $\mathcal{Y}_j(R, \theta)$ has behaviour described by (3.14). From this we see that

$$[\![\mathcal{Y}]\!] \sim -\kappa a_0^{(\mathcal{Y})}, \quad R \to 0. \tag{3.62}$$

The imperfect transmission conditions (3.6) therefore give that

$$\mu_1 \left.\frac{\partial \mathcal{Y}_1}{\partial Y}\right|_{Y=0+} \sim -a_0^{(\mathcal{Y})}, \quad X \to 0. \tag{3.63}$$

We earlier made an assumption in (3.20) regarding the behaviour of Φ^+ at infinity and now verify that this was correct. It follows from the expression for $\Phi^+(\xi)$ given in (3.57) and the asymptotic estimate for $\Xi_*^+(\xi)$ given in (3.54) that

$$\Phi^+(\xi) = \frac{\lambda}{i\xi} + \frac{(\mu_1+\mu_2)\lambda}{\mu_1\mu_2\pi\kappa\xi^2}\ln(-i\xi) + O\left(\frac{1}{|\xi|^2}\right), \quad \mathrm{Im}(\xi) \to +\infty, \tag{3.64}$$

which justifies our previous claim.

In order to find the constant $a_0^{(\mathcal{Y})}$, we will employ the following Abelian-type theorem, stated and proved below as Theorem 10. A number of Abelian-type theorems exist; a small collection can be found for instance in the paper of Piccolroaz [52]. Of particular relevance is Theorem A.5 in that paper, which describes the limit of a function near $x = 0$ provided its Fourier transform $\Phi^+(\xi)$ is a plus function displaying behaviour of the type

$$\Phi^+(\xi) = a_1\xi^{-1} + a_2\xi^{-2} + O(\xi^{-3}), \quad \xi \to \infty. \tag{3.65}$$

We seek to prove a similar Abelian-type theorem but with less favourable behaviour of Φ^+ of the form described in (3.64).

Theorem 10. *Let f(x) be the function*

$$f(x) = \frac{1}{2\pi}\int_{-\infty}^{\infty} \Phi^+(\xi)e^{-ix\xi}\mathrm{d}\xi. \tag{3.66}$$

If $\Phi^+(\xi)$ *is analytic in* $\mathbb{C}^+$ *and*

$$\Phi^+(\xi) = a_1\xi^{-1} + O(\xi^{-(1+\delta)}), \quad \xi \to \infty, \tag{3.67}$$

in the closed half-plane $\overline{\mathbb{C}}^+ = \mathbb{C}^+ \cup \mathbb{R}$ *where* $\delta > 0$ *is small, then* $f(x) = 0$ *for all* $x < 0$ *and*

$$\lim_{x \to 0^+} f(x) = -ia_1. \tag{3.68}$$

Proof. The fact that $f(x) = 0$ for all $x < 0$ is a direct consequence of the fact that $\Phi^+(\xi)$ is a '+' function. Assume now that $x > 0$. From the assumptions on the behaviour of the function $\Phi^+(\xi)$, it follows that $\Phi^+(\xi) = a_1\xi^{-1} + R(\xi)$, where $\xi R(\xi) \to 0$, as $\xi \to \infty$, $\xi \in \overline{\mathbb{C}}^+$ (including $\xi \to \pm\infty$, $\xi \in \mathbb{R}$).

We write

$$f(x) = \frac{1}{2\pi} \left\{ \int_a^\infty [\Phi^+(-\xi)e^{ix\xi} + \Phi^+(\xi)e^{-ix\xi}] \mathrm{d}\xi + \int_{-a}^{a} \Phi^+(\xi)e^{-ix\xi} \mathrm{d}\xi \right\}. \tag{3.69}$$

The first integral is

$$f_1(x, a) = \int_a^\infty [\Phi^+(-\xi)e^{ix\xi} + \Phi^+(\xi)e^{-ix\xi}] \mathrm{d}\xi = f_{11}(x, a) + f_{12}(x, a), \tag{3.70}$$

where we have defined the functions $f_{11}(x, a)$ and $f_{12}(x, a)$ by

$$f_{11}(x, a) = \int_a^\infty \left[-\frac{a_1}{\xi} e^{ix\xi} + \frac{a_1}{\xi} e^{-ix\xi} \right] \mathrm{d}\xi, \tag{3.71}$$

and

$$f_{12}(x, a) = \int_a^\infty \left[R(-\xi)e^{ix\xi} + R(\xi)e^{-ix\xi} \right] \mathrm{d}\xi. \tag{3.72}$$

Evaluating $f_{11}(x, a)$, we obtain

$$f_{11}(x, a) = -2ia_1 \int_{ax}^\infty \frac{\sin \xi}{\xi} \mathrm{d}\xi, \tag{3.73}$$

and so in particular we note that

$$f_{11}(x, x^{-1/2}) = -2ia_1 \int_{x^{1/2}}^\infty \frac{\sin \xi}{\xi} \mathrm{d}\xi \to -i\pi a_1 \text{ as } x \to 0+. \tag{3.74}$$

We evaluate $f_{12}(x,a)$ by parts. Let us first consider

$$\int_a^\infty R(\xi)e^{-ix\xi}\mathrm{d}\xi = e^{-ix\xi}F(\xi)\Big|_a^\infty - \int_a^\infty F(\xi)(-ix)e^{-ix\xi}\mathrm{d}\xi, \tag{3.75}$$

where

$$F(\xi) = -\int_\xi^\infty R(t)\mathrm{d}t. \tag{3.76}$$

Now, note that

$$F(\xi) = -\int_\xi^\infty R(t)\mathrm{d}t = \frac{A}{\xi^\delta} + O\left(\frac{1}{\xi^{\delta+\beta}}\right), \quad \xi \to +\infty, \tag{3.77}$$

for some small $\beta > 0$. We deduce that as $a \to \infty$, the first term in the right hand side of (3.75) tends to zero. Now consider the second term in the right hand side of (3.75). We again split the integral, writing that $F(\xi) = \frac{A}{\xi^\delta} + N(\xi)$, to obtain

$$\int_a^\infty ixF(\xi)e^{-ix\xi}\mathrm{d}\xi = ix\left[\int_a^\infty \frac{A}{\xi^\delta}e^{-ix\xi}\mathrm{d}\xi + \int_a^\infty N(\xi)e^{-ix\xi}\mathrm{d}\xi\right]. \tag{3.78}$$

We make the substitution $s = x\xi$ in the first integral, giving

$$\int_a^\infty ixF(\xi)e^{-ix\xi}\mathrm{d}\xi = iAx^\delta \int_{ax}^\infty \frac{e^{-is}}{s^\delta}\mathrm{d}s + ix\int_a^\infty N(\xi)e^{-ix\xi}\mathrm{d}\xi. \tag{3.79}$$

Now let $x \to 0+$ and $a = x^{-1/2}$; the first integral on the right hand side of (3.79) is bounded and so the first term tends to zero. Similarly the second integrand consists of higher order terms than the first, so also decays. It follows that

$$\int_a^\infty R(\xi)e^{-ix\xi}\mathrm{d}\xi \to 0 \text{ as } a \to \infty. \tag{3.80}$$

The same arguments give that $\int_a^\infty R(-\xi)e^{ix\xi}\mathrm{d}\xi$ also vanishes, and so

$$f_{12}(x, x^{-1/2}) \to 0 \text{ as } x \to 0^+. \tag{3.81}$$

Combining these results we see that

$$f_1(x, x^{1/2}) \to -i\pi a_1 \tag{3.82}$$

as $x \to 0+$.

Let us now consider the second integral in the right hand side of (3.69), that is

$$f_2(x, a) = \int_{-a}^{a} \Phi^+(\xi) e^{-ix\xi} \mathrm{d}\xi. \tag{3.83}$$

Similarly to how we manipulated f_1, we split the integral f_2 into the sum of f_{21} and f_{22}, where

$$f_{21}(x, a) = \int_{-a}^{a} \frac{a_1}{\xi} e^{-ix\xi} \mathrm{d}\xi, \tag{3.84}$$

and

$$f_{22}(x, a) = \int_{-a}^{a} R(\xi) e^{-ix\xi} \mathrm{d}\xi. \tag{3.85}$$

Let us now parameterise, writing $\xi = ae^{i\theta}$ by manipulating the analyticity of Φ^+ in the upper complex half-plane. Then

$$f_{21}(x, a) = -a_1 i \int_{0}^{\pi} e^{-ixae^{i\theta}} \mathrm{d}\theta; \tag{3.86}$$

and so as $ax \to 0$, $f_{21}(x, a) \to -i\pi a_1$. Again parameterising as $\xi = ae^{i\theta}$, we obtain to leading order

$$\int_{-a}^{a} R(\xi) e^{-ix\xi} \mathrm{d}\xi = \frac{i}{a^\delta} \int_{0}^{\pi} \frac{Ae^{i\theta}}{e^{i\theta(1+\delta)}} e^{-iaxe^{i\theta}} \mathrm{d}\theta. \tag{3.87}$$

The final integral in (3.87) is bounded as $a \to \infty$ while $x \to 0+$ in such a way that $ax \to 0$. Thus $f_{22}(x, x^{-1/2}) \to 0$ as $x \to 0+$. Combining these results for f_{21} and f_{22}, we see that

$$f_2(x, x^{-1/2}) \to i\pi a_1, \quad x \to 0+. \tag{3.88}$$

Finally, recall from (3.69) that

$$f(x) = \frac{1}{2\pi} \lim_{a \to +\infty} \{f_1(x,a) + f_2(x,a)\}. \tag{3.89}$$

Thus we can conclude that

$$f(x) \to \frac{1}{2\pi} (-i\pi a_1 - i\pi a_1) = -ia_1, \tag{3.90}$$

as $x \to 0^+$, which completes the proof.

□

Returning to the task of evaluating important constants, Theorem 10 (using $\mu_1 \frac{\partial \mathcal{Y}}{\partial Y}$ in place of 'f' in the statement of the theorem) yields that

$$\lim_{X \to 0+} \mu_1 \frac{\partial \mathcal{Y}}{\partial Y} = -\lambda, \tag{3.91}$$

where λ has been defined in (3.30) and so it follows that

$$a_0^{(\mathcal{Y})} = \lambda. \tag{3.92}$$

The constant $-\gamma^+$ is the imaginary part of the zero of the function $\Xi(\xi)$ in $\mathbb{C}^+$ that is closest to the real axis (see (3.26)). Manipulation of (3.26) indicates that zeros of $\Xi(\xi)$ satisfy

$$\frac{1}{\mu_1} \cot(\gamma^+ H_1) + \frac{1}{\mu_2} \cot(\gamma^+ H_2) - \kappa\gamma^+ = 0, \tag{3.93}$$

For the first zero below the axis, for large κ, γ^+ should be small, and so it can be shown that

$$\gamma^+(\kappa) = \lambda(\kappa)(1 + O(\kappa^{-1})), \quad \kappa \to \infty, \tag{3.94}$$

indicating that $\gamma^+(\kappa) = O(\kappa^{-1/2})$, $\kappa \to \infty$. We also see that

$$\gamma^+(0) \in \left(\frac{\pi}{2\max\{H_1, H_2\}}, \frac{\pi}{2\min\{H_1, H_2\}} \right). \tag{3.95}$$

The constant γ^- is given by

$$\gamma^- = \pi \min\left\{\frac{1}{H_1}, \frac{1}{H_2}\right\}. \tag{3.96}$$

In conjunction with (3.61) we have now found all constants describing the asymptotic behaviour of the weight function $\mathcal{Y}$.

3.2 Application to Analysis of Bloch-Floquet Waves

In this section, we present an application of the weight function derived in the previous section by addressing the problem of out-of plane shear Bloch-Floquet waves within a thin bi-material strip containing a periodic array of longitudinal cracks and imperfect interfaces. The problem addressed is an imperfect interface analogue to that studied in [44].

3.2.1 Geometry

The geometry of an elementary cell of the thin periodic structure considered is shown in Figure 3.2. The elementary cell is of length a and contains two materials of thicknesses εH_1 and εH_2, where $\varepsilon > 0$ is a small dimensionless parameter. These materials occupy respective domains $\Pi^{(j)}$, $j = 1, 2$, and the elementary cell is further split into smaller domains $\Omega_\varepsilon^{(m)}$, $m = 1, 2, 3, 4$, as shown in Figure 3.2. Along the join of the two materials and centered on the origin sits a crack of length $l < a$. Outside the crack, the interface is assumed to be imperfect, which models a thin layer of adhesive joining the materials together. The extent of this imperfection is represented by the parameter κ.

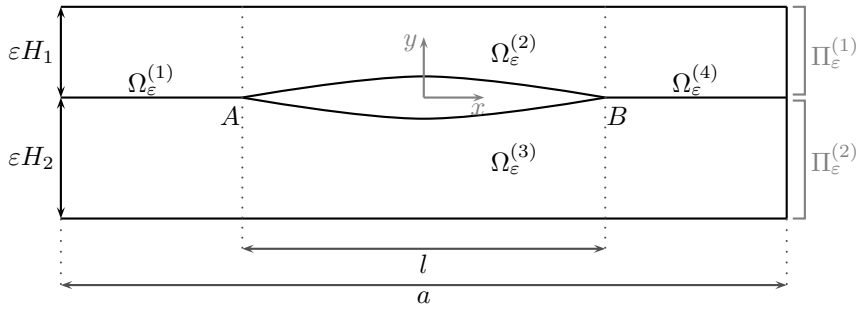

Figure 3.2: Geometry of the elementary cell.

The functions $u^{(j)}(x, y)$ are defined in $\Pi_\varepsilon^{(j)}$, $j = 1, 2$ as solutions of the Helmholtz equations

$$\nabla^2 u^{(j)}(x, y) + \frac{\omega^2}{c_j^2} u^{(j)}(x, y) = 0, \qquad (x, y) \in \Pi_\varepsilon^{(j)}, \quad j = 1, 2. \tag{3.97}$$

Here, $c_j = \sqrt{\mu_j/\rho_j}$ are the shear speeds in their respective domains $\Pi_\varepsilon^{(j)}$ $j = 1, 2$. The functions $u^{(j)}$ are regarded as out-of-plane displacements, μ_j denotes the shear modulus and ρ_j the mass density of the material occupying $\Pi_\varepsilon^{(j)}$. The quantity ω represents the radian frequency of the time-harmonic vibrations with amplitude u.

3.2.2 Boundary conditions

We impose boundary conditions along the horizontal parts of the boundary of Π_ε and on the crack face itself. We use similar notation to that in the previous section to denote the components of stress (see (3.2)).

We assume a zero stress component in the out-of-plane direction along the top and bottom of the strip, as well as along the face of the crack itself:

$$\sigma_{yz}^{(1)}(x, \varepsilon H_1) = 0, \qquad \sigma_{yz}^{(2)}(x, -\varepsilon H_2) = 0, \quad x \in (-a/2, a/2), \tag{3.98}$$

$$\sigma_{yz}^{(1)}(x, 0^+) = 0, \qquad \sigma_{yz}^{(2)}(x, 0^-) = 0, \quad x \in (-l/2, l/2). \tag{3.99}$$

Outside the crack, along the boundary between $\Pi_\varepsilon^{(1)}$ and $\Pi_\varepsilon^{(2)}$, there is an imperfect interface described by the conditions of continuity of tractions

$$\sigma_{yz}^{(1)}(x,0^+) = \sigma_{yz}^{(2)}(x,0^-), \quad x \in (-a/2,-l/2) \cup (l/2,a/2), \tag{3.100}$$

and a displacement jump across the interface that is proportional to the traction on the interface:

$$u^{(1)}(x,0^+) - u^{(2)}(x,0^-) = \varepsilon\kappa\sigma_{yz}^{(1)}(x,0^+), \quad x \in (-a/2,-l/2) \cup (l/2,a/2). \tag{3.101}$$

We seek the solutions $u^{(j)}$ which represent the Bloch-Floquet waves, so that at the ends of our elementary cell $x = \pm a/2$ we have for $j = 1,2$ the Bloch-Floquet conditions

$$u^{(j)}(-a/2,y) = e^{-iKa}u^{(j)}(a/2,y), \qquad y \in (-\varepsilon H_2, \varepsilon H_1), \tag{3.102}$$

$$\sigma_{xz}^{(j)}(-a/2,y) = e^{-iKa}\sigma_{xz}^{(j)}(a/2,y), \qquad y \in (-\varepsilon H_2, \varepsilon H_1). \tag{3.103}$$

For a fixed value of the Bloch parameter K, we seek the eigenvalues ω and the corresponding eigenfunctions $u^{(j)}$ with finite norm in $W_2^1(\Pi_\varepsilon^{(j)})$, $j = 1,2$.

In (3.101), the case in which $\kappa = 0$ corresponds to an ideal/perfect interface between the different materials; such a problem was considered in [44]. To summarise the approach used here, we approximate u in a certain form, derive a lower-dimensional model together with boundary layers in the vicinity of the vertices of the crack and then use our weight function to assist in the derivation of junction conditions for a skeleton model.

3.2.3 Asymptotic Ansatz

In the remainder of this chapter, we will often refer to $u(x,y)$, which we define for $(x,y) \in \Pi_\varepsilon^{(1)} \cup \Pi_\varepsilon^{(2)}$ by

$$u(x,y) = \begin{cases} u^{(1)}(x,y), & (x,y) \in \Pi_\varepsilon^{(1)}, \\ u^{(2)}(x,y), & (x,y) \in \Pi_\varepsilon^{(2)}. \end{cases} \tag{3.104}$$

The eigenfunctions $u(x,y)$ are approximated in the form

$$\begin{aligned} u(x,y,\varepsilon) &= \sum_{k=0}^{N} \varepsilon^k \left\{ \sum_{m=1}^{4} \chi_m \left(v_m^{(k)}(x) + \varepsilon^2 V_m^{(k)}(x,Y) \right) \right. \\ &+ \left. \left(W_A^{(k)}(X_A,Y) + W_B^{(k)}(X_B,Y) \right) \right\} + R_N(x,y,\varepsilon), \end{aligned} \tag{3.105}$$

with scaled co-ordinates X_A, X_B and Y introduced in the vicinity of the left and right vertices of the crack defined as

$$X_A = \frac{x - x_A}{\varepsilon}, \qquad X_B = \frac{x - x_B}{\varepsilon}, \qquad Y = \frac{y}{\varepsilon}. \tag{3.106}$$

Here, $v_m^{(k)}$ represent solutions of lower-dimensional problems within limit sets $\Omega_0^{(m)}$, $m = 1,2,3,4$ (see Figure 3.3 on page 53). $\chi_m = \chi_m(x,y,\varepsilon)$ are cut-off functions defined so that $\chi_m(x,y;\varepsilon) \equiv 1$ in $\Omega_\varepsilon^{(m)}$ and decay rapidly to zero outside $\Omega_\varepsilon^{(m)}$. They vanish near the so-called junction points A and B (the vertices of the crack). The terms $W_A^{(k)}$ and $W_B^{(k)}$ represent the boundary layers near A and B, and $V_m^{(k)}$ is the 'fast' change of eigenfunctions in the transverse direction in the domain $\Omega_\varepsilon^{(m)}$. R_N is the remainder term in the asymptotic approximation. The uppercase scaled co-ordinate X_B defined in (3.106) corresponds to X from the derivation of the weight function in Section 3.1.

More specifically, the smooth cut-off functions $\chi_m \in C^\infty(\mathbb{R})$, $m = 1,2,3,4$

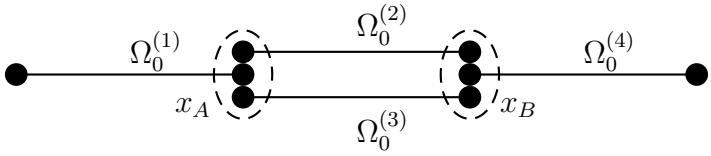

Figure 3.3: Geometry for the low dimensional model, consisting of four beams $\Omega_0^{(m)}$ in which the functions $v_m^{(k)}$ are sought. Dashed lines show the 'junction points' where the beams meet, which correspond to the crack tips.

are related to a function

$$\chi(\xi) = \begin{cases} 0, & \xi \leq 0, \\ 1, & \xi \geq 1, \end{cases} \tag{3.107}$$

by the formulae

$$\begin{aligned} &\chi_1(x, y; \varepsilon) = \chi(-X_A), \qquad \chi_2(x, y; \varepsilon) = \chi(X_A)\chi(-X_B)\mathcal{H}(y), \\ &\chi_3(x, y; \varepsilon) = \chi(X_A)\chi(-X_B)\mathcal{H}(-y), \qquad \chi_4(x, y; \varepsilon) = \chi(X_B), \end{aligned} \tag{3.108}$$

where $\mathcal{H}(y)$ is the Heaviside step function.

We note that this form of Ansatz relies upon the vital assumption that the boundary layers surrounding the crack vertices A and B are independent. That is, we assume that the exponential decay of both boundary layers is sufficiently rapid so that each boundary layer is negligible in the vicinity of the other crack tip in the given elementary cell and near the tips of other cracks in the periodic structure.

In this chapter we will consider the form of approximation given in (3.105) with $N = 1$ and will comment on the effect of taking higher order approximations.

3.2.4 One-dimensional model problems

Outside the vicinity of A and B, the boundary layers $W_A^{(j)}$ and $W_B^{(j)}$ decay (we later verify this to be the case) and so seek u in the form

$$u(x,y,\varepsilon) \sim \sum_{k=0}^{1} \varepsilon^k \left(v_m^{(k)}(x) + \varepsilon^2 V_m^{(k)}(x,Y) \right), \tag{3.109}$$

where $V_m^{(k)}$ have zero average over the cross-section of $\Omega_\varepsilon^{(m)}$ for all $m = 1,2,3,4$ and $x \in \Omega_\varepsilon^{(m)}$. That is,

$$\int_0^{H_1} V_m^{(k)}(x,Y)dY = 0, \qquad \int_{-H_2}^{0} V_m^{(k)}(x,Y)dY = 0, \tag{3.110}$$

for any $x \in \Omega_\varepsilon^{(m)}$. In the region above and below the crack (in $\Omega_\varepsilon^{(2)}$ and $\Omega_\varepsilon^{(3)}$), the low dimensional model problem is as in [44] and so for this part of the domain we proceed in a similar fashion. The problem is however differently formulated in $\Omega_\varepsilon^{(1)}$ and $\Omega_\varepsilon^{(4)}$ due to the imperfect transmission conditions in these domains.

Zero and first order approximations: $k = 0$ and $k = 1$.

We first consider the cases where $k = 0, 1$ and begin by concentrating on the part of the domain above and below the crack, that is $\Omega_\varepsilon^{(2)}$ and $\Omega_\varepsilon^{(3)}$. We use the notation $v_{1j}^{(k)}$ to denote the function $v_1^{(k)}$ in $\Pi_\varepsilon^{(j)}$. Substitution of the form of (3.109) into the Helmholtz equations (3.97) yields

$$\frac{\partial^2 V_m^{(k)}}{\partial Y^2}(x,Y) + (v_m^{(k)})''(x) + \frac{\omega^2}{d_m^2} v_m^{(k)}(x) = 0, \quad m = 2,3, \quad k = 0,1, \tag{3.111}$$

where $d_2 = c_1$ and $d_3 = c_2$. Furthermore, we have along the cut as well as on the top and bottom of our domain that

$$\left.\frac{\partial V_m^{(k)}}{\partial Y}\right|_{Y=0^\pm} = 0, \quad m = 2,3, \qquad \left.\frac{\partial V_2^{(k)}}{\partial Y}\right|_{Y=H_1} = \left.\frac{\partial V_3^{(k)}}{\partial Y}\right|_{Y=-H_2} = 0. \tag{3.112}$$

It is easily seen that these boundary value problems are solvable if and only if

$$(v_m^{(k)})''(x) + \frac{\omega^2}{d_m^2} v_m^{(k)}(x) = 0, \qquad |x| < l, \quad m = 2, 3; \quad k = 0, 1. \tag{3.113}$$

This gives us equations for the low dimensional model in the domains $\Omega_0^{(m)}$, $m = 2, 3$. Moreover, it follows from (3.112) and (3.113) that $V_m^{(k)}$ is a linear function in Y for $k = 0, 1$, and we conclude from the condition that the average of $V_m^{(k)}$ over the cross-section of the strip must be zero that

$$V_m^{(k)}(x, Y) = 0, \qquad m = 2, 3; \quad k = 0, 1. \tag{3.114}$$

Let us now focus our attention on the layered structure $\Omega_\varepsilon^{(1)}$; analogous arguments apply to $\Omega_\varepsilon^{(4)}$ The functions $V_{1j}^{(k)}$, $k = 0, 1$; $j = 1, 2$ satisfy the equations

$$\frac{\partial^2 V_{1j}^{(k)}}{\partial Y^2}(x, Y) + (v_{1j}^{(k)})''(x) + \frac{\omega^2}{c_j^2} v_{1j}^{(k)}(x) = 0. \tag{3.115}$$

Integration of (3.115) taking into account boundary conditions (3.98) yield that

$$\frac{\partial V_{11}^{(k)}}{\partial Y} = -(Y - H_1)\left((v_{11}^{(k)})''(x) + \frac{\omega^2}{c_1^2} v_{11}^{(k)}(x)\right) \tag{3.116}$$

$$\frac{\partial V_{12}^{(k)}}{\partial Y} = -(Y + H_2)\left((v_{12}^{(k)})''(x) + \frac{\omega^2}{c_2^2} v_{12}^{(k)}(x)\right) \tag{3.117}$$

It then follows from (3.100) that

$$\mu_1 H_1 \left((v_{11}^{(k)})''(x) + \frac{\omega^2}{c_1^2} v_{11}^{(k)}(x)\right) + \mu_2 H_2 \left((v_{12}^{(k)})''(x) + \frac{\omega^2}{c_2^2} v_{12}^{(k)}(x)\right) = 0. \tag{3.118}$$

We now utilise the transmission condition across the imperfect interface as

given in (3.101) to obtain

$$v_{11}^{(0)} + \varepsilon v_{11}^{(1)} + \varepsilon^2 v_{11}^{(2)} + \varepsilon^2 \, V_{11}^{(0)}\Big|_{Y=0^+} - v_{12}^{(0)} - \varepsilon v_{12}^{(1)} - \varepsilon^2 v_{12}^{(2)} - \varepsilon^2 \, V_{12}^{(0)}\Big|_{Y=0^-} = \mu_1 \kappa \frac{\partial}{\partial Y} \left\{ \varepsilon^2 \, V_{11}^{(0)}\Big|_{Y=0^+} \right\} + O(\varepsilon^3), \tag{3.119}$$

which upon comparing terms in ε^0, ε^1 and ε^2 gives the conditions

$$v_{11}^{(0)} - v_{12}^{(0)} = 0, \tag{3.120}$$

$$v_{11}^{(1)} - v_{12}^{(1)} = 0, \tag{3.121}$$

$$v_{11}^{(2)} + V_{11}^{(0)}\Big|_{Y=0^+} - v_{12}^{(2)} - V_{12}^{(0)}\Big|_{Y=0^-} = \mu_1 \kappa \left. \frac{\partial V_{11}^{(0)}}{\partial Y} \right|_{Y=0^+}. \tag{3.122}$$

For $k = 0, 1$ we have from equations (3.120) and (3.121) that $v_{11}^{(k)}(x) = v_{12}^{(k)}(x) = v^{(k)}(x)$, say. Equation (3.118) then gives that

$$(v^{(k)})''(x) + \frac{\omega^2}{d^2} v^{(k)}(x) = 0, \tag{3.123}$$

where

$$d = c_1 c_2 \sqrt{\frac{\mu_1 H_1 + \mu_2 H_2}{\mu_1 H_1 c_2^2 + \mu_2 H_2 c_1^2}}. \tag{3.124}$$

It follows that for $k = 0, 1$,

$$\frac{\partial V_{11}^{(k)}}{\partial Y}(x, Y) = \omega^2 \left(\frac{1}{c_1^2} - \frac{1}{d^2} \right) v^{(k)}(x) \, (Y - H_1), \tag{3.125}$$

$$\frac{\partial V_{12}^{(k)}}{\partial Y}(x, Y) = \omega^2 \left(\frac{1}{c_2^2} - \frac{1}{d^2} \right) v^{(k)}(x) \, (Y + H_2). \tag{3.126}$$

and so

$$V_{11}^{(k)}(x, Y) = \omega^2 \left(\frac{1}{c_1^2} - \frac{1}{d^2} \right) v^{(k)}(x) \left\{ \frac{(Y - H_1)^2}{2} + \mathcal{D}_1(x) \right\}, \tag{3.127}$$

$$V_{12}^{(k)}(x, Y) = \omega^2 \left(\frac{1}{c_2^2} - \frac{1}{d^2} \right) v^{(k)}(x) \left\{ \frac{(Y + H_2)^2}{2} + \mathcal{D}_2(x) \right\}, \quad k = 0, 1, \tag{3.128}$$

where $\mathcal{D}_1(x), \mathcal{D}_2(x)$ are functions which can be determined from the condition that the cross sectional averages of $V_m^{(k)}$ are zero as stated in equation (3.110). We find that $\mathcal{D}_1(x)$ and $\mathcal{D}_2(x)$ are the constants

$$\mathcal{D}_1(x) = -\frac{H_1^2}{6}, \qquad \mathcal{D}_2(x) = -\frac{H_2^2}{6}. \tag{3.129}$$

Second order approximation: $k = 2$.

We now consider the case $k = 2$. This analysis was not included in the paper corresponding to this chapter [62], but is included here to demonstrate that the asymptotic procedure can be extended further.

Hitherto we have only considered those cases in which $k = 0, 1$. When $k \geq 2$ our equations have an additional term in $V_m^{(k-2)}$:

$$\frac{\partial^2 V_m^{(k)}}{\partial Y^2}(x, Y) + (v_m^{(k)})''(x) + \frac{\omega^2}{c_j^2} v_m^{(k)}(x) + \frac{\omega^2}{c_j^2} V_m^{(k-2)} = 0. \tag{3.130}$$

Since we have already demonstrated that $V_m^{(0)}(x, Y) \equiv 0$ for $m = 2, 3$, this equation reduces to the same form as (3.111) when $k = 2$, implying that

$$V_m^{(k)}(x, Y) = 0, \quad m = 2, 3, \quad k = 0, 1, 2. \tag{3.131}$$

This also implies that (3.113) is true for $k = 2$ as well as for $k = 0, 1$.

In the layered structure $\Omega_\varepsilon^{(1)}$, we have that $V_1^{(0)}$ is the known function described in (3.127) and (3.128), giving

$$\begin{aligned} &\frac{\partial^2 V_{1j}^{(2)}}{\partial Y^2}(x, Y) + (v_{1j}^{(2)})''(x) + \frac{\omega^2}{c_j^2} v_{1j}^{(2)}(x) \\ &\qquad + \frac{\omega^4}{c_j^2}\left(\frac{1}{c_j^2} - \frac{1}{d^2}\right) v_{1j}^{(0)}(x) \left\{ \frac{(Y + (-1)^j H_j)^2}{2} - \frac{H_j^2}{6} \right\} = 0, \end{aligned} \tag{3.132}$$

together with boundary conditions

$$\left.\frac{\partial V_{11}^{(2)}}{\partial Y}\right|_{Y=H_1} = \left.\frac{\partial V_{12}^{(2)}}{\partial Y}\right|_{Y=-H_2} = 0, \qquad \mu_1 \left.\frac{\partial V_{11}^{(2)}}{\partial Y}\right|_{Y=0^+} = \mu_2 \left.\frac{\partial V_{12}^{(2)}}{\partial Y}\right|_{Y=0^-}. \tag{3.133}$$

Integrating once with respect to Y and taking into account the boundary conditions along the top and bottom of the strip give that

$$\frac{\partial V_{11}^{(2)}}{\partial Y} = -(Y - H_1)\left(\frac{\omega^2}{c_1^2} v_{11}^{(2)} + (v_{11}^{(2)})''\right) - \frac{\omega^2}{c_1^2} \int_0^Y V_{11}^{(0)}(x,T)\mathrm{d}T, \tag{3.134}$$

$$\frac{\partial V_{12}^{(2)}}{\partial Y} = -(Y + H_2)\left(\frac{\omega^2}{c_2^2} v_{12}^{(2)} + (v_{12}^{(2)})''\right) - \frac{\omega^2}{c_2^2} \int_0^Y V_{12}^{(0)}(x,T)\mathrm{d}T. \tag{3.135}$$

We note that the second boundary condition in (3.133) yields that equation (3.118) holds also for the case $k = 2$, that is for $k = 0, 1, 2$:

$$\mu_1 H_1 \left((v_{11}^{(k)})''(x) + \frac{\omega^2}{c_1^2} v_{11}^{(k)}(x)\right) + \mu_2 H_2 \left((v_{12}^{(k)})''(x) + \frac{\omega^2}{c_2^2} v_{12}^{(k)}(x)\right) = 0. \tag{3.136}$$

Moreover, it follows from (3.122) along with our equations for $V_{1j}^{(0)}$ ((3.127) and (3.128)) that

$$v_{11}^{(2)} - v_{12}^{(2)} = \mathcal{B} v^{(0)}(x), \tag{3.137}$$

where $\mathcal{B}$ is the constant

$$\mathcal{B} = \omega^2 \left\{ \frac{H_2^2}{3}\left(\frac{1}{c_2^2} - \frac{1}{d^2}\right) - \frac{H_1^2}{3}\left(\frac{1}{c_1^2} - \frac{1}{d^2}\right) - \mu_1 \kappa H_1 \left(\frac{1}{c_1^2} - \frac{1}{d^2}\right)\right\}, \tag{3.138}$$

derived by exploiting the condition that $V_m^{(k)}$ has zero average over the cross section of $\Omega_\varepsilon^{(m)}$ (see (3.110)). Substitution of (3.137) into (3.136) then gives the following ordinary differential equation for $v_{12}^{(2)}$:

$$(\mu_1 H_1 + \mu_2 H_2)(v_{11}^{(2)})''(x) + \frac{\omega^2}{c_1^2} v_{11}^{(2)}(x) = \mu_2 H_2 \mathcal{B}\left\{(v^{(0)})''(x) + \frac{\omega^2}{c_2^2} v^{(0)}(x)\right\}, \tag{3.139}$$

and taking into account (3.123) we have

$$(\mu_1 H_1 + \mu_2 H_2)(v_{11}^{(2)})''(x) + \frac{\omega^2}{c_1^2} v_{11}^{(2)}(x) = \left(\frac{\mu_2 H_2 \mathcal{B}}{c_2^2} - \frac{1}{d^2} \right) \omega^2 v^{(0)}(x). \quad (3.140)$$

This, in conjunction with (3.137) gives an expression for $v_{12}^{(2)}$.

To conclude this section, we have found that our problem with the imperfect interface has the same low dimensional model up to terms in ε as the case with the perfect interface studied in [44], but with a different distribution of the fast-changing part. The equations for $v_4^{(k)}$ and $V_4^{(k)}$ are of course similar to the case examined here where $m = 1$. We would like to stress that the imperfect interface impacts on the low dimensional model equations for terms in ε^k, $k \geq 2$. The equations gained in this section need to be complemented with the boundary conditions and junction conditions at the points x_A and x_B. In order to derive these junction conditions which depend on the imperfect parameter κ, we construct boundary layers in the vicinity of the vertices of the crack.

3.3 Junction conditions

The smooth cut-off functions χ_m that were defined in (3.108) allow us to extend the function (3.109) outside $\Omega_\varepsilon^{(m)}$, $m = 1, 2, 3, 4$, giving

$$u(x, y; \varepsilon) \sim \sum_{k=0}^{2} \varepsilon^k \sum_{m=1}^{4} \chi_m(x, y, \varepsilon) \left(v_m^{(k)}(x) + \varepsilon^2 V_m^{(k)}(x, Y) \right), \quad (3.141)$$

however this gives an error near the junction points x_A and x_B. We therefore introduce boundary layers $W_A(X_A, Y)$ and $W_B(X_B, Y)$, and so seek u in the

form

$$u(x,y,\varepsilon) \sim \sum_{k=0}^{2} \varepsilon^k \left\{ \sum_{m=1}^{4} \chi_m(x,y,\varepsilon)(v_m^{(k)}(x) + \varepsilon^2 V_m^{(k)}(x,Y)) + W_A^{(k)}(X_A,Y) + W_B^{(k)}(X_B,Y) \right\} \tag{3.142}$$

Here, substituting (3.142) into the original equation and comparing terms in the same degree of ε we have

$$\nabla^2_{X_\alpha Y} \left\{ W_\alpha^{(k)}(X_\alpha,Y) + \mathcal{F}_\alpha^{(k)}(X_\alpha,Y) \right\} = 0, \quad \alpha = A,B, \quad k = 0,1. \tag{3.143}$$

$$\nabla^2_{X_\alpha Y} \left\{ W_\alpha^{(2)}(X_\alpha,Y) + \mathcal{F}_\alpha^{(2)}(X_\alpha,Y) + \sum_{m=1}^{4} \chi_m(x,y;\varepsilon) V_m^{(0)}(x_\alpha,Y) \right\} \tag{3.144}$$

$$= -\sum_{m=1}^{4} \chi_m \frac{\omega^2}{c_j^2} v_m^{(0)}(x_\alpha) - \frac{\omega^2}{c_j^2} W_\alpha^{(0)}, \quad \alpha = A,B, \quad k = 2. \tag{3.145}$$

with the functions $\mathcal{F}$ given by

$$\mathcal{F}_A^{(0)} = \sum_{m=1}^{3} v_m^{(0)}(x_A)\chi_m(x,y;\varepsilon), \qquad \mathcal{F}_B^{(0)} = \sum_{m=2}^{4} v_m^{(0)}(x_B)\chi_m(x,y;\varepsilon), \tag{3.146}$$

$$\mathcal{F}_A^{(1)} = \sum_{m=1}^{3} \left\{ (v_m^{(0)})'(x_A)X_A + v_m^{(1)}(x_A) \right\} \chi_m(x,y;\varepsilon), \tag{3.147}$$

$$\mathcal{F}_B^{(1)} = \sum_{m=2}^{4} \left\{ (v_m^{(0)})'(x_B)X_B + v_m^{(1)}(x_B) \right\} \chi_m(x,y;\varepsilon), \tag{3.148}$$

$$\mathcal{F}_A^{(2)} = \sum_{m=1}^{3} \left\{ (v_m^{(0)})''(x_A)\frac{X_A^2}{2} + (v_m^{(1)})'(x_A)X_A + (v_m^{(2)})(x_A) \right\} \chi_m(x,y;\varepsilon), \tag{3.149}$$

$$\mathcal{F}_B^{(2)} = \sum_{m=2}^{4} \left\{ (v_m^{(0)})''(x_B)\frac{X_B^2}{2} + (v_m^{(1)})'(x_B)X_B + (v_m^{(2)})(x_B) \right\} \chi_m(x,y;\varepsilon). \tag{3.150}$$

We now focus our attention on the right-hand crack tip x_B; analogous arguments apply to x_A. We also restrict ourselves to the cases $k = 0, 1$ for the moment and will deal with the case $k = 2$ separately later. We will consider in the following analysis four functions g_i, $i = 1, 2, 3, 4$, which are solutions of the Laplace equation. These solutions also satisfy the boundary conditions corresponding to zero traction on the top and bottom edges of the strip as well as along the cut itself:

$$\mu_1 \frac{\partial g_i}{\partial Y}\bigg|_{Y=H_1} = \mu_2 \frac{\partial g_i}{\partial Y}\bigg|_{Y=-H_2} = 0, \quad X \in \mathbb{R}, \tag{3.151}$$

$$\mu_1 \frac{\partial g_i}{\partial Y}\bigg|_{Y=0^+} = \mu_2 \frac{\partial g_i}{\partial Y}\bigg|_{Y=0^-} = 0, \quad X < 0. \tag{3.152}$$

They also satisfy the transmission conditions across the imperfect interface

$$g_i|_{Y=0^+} - g_i|_{Y=0^-} = \mu_1 \kappa \frac{\partial g_i}{\partial Y}\bigg|_{Y=0^+}, \quad X > 0, \tag{3.153}$$

and

$$\frac{\partial g_i}{\partial Y}\bigg|_{Y=0^+} = \frac{\partial g_i}{\partial Y}\bigg|_{Y=0^-}, \quad X > 0. \tag{3.154}$$

These solutions are given by

$$g_1 = 1, \qquad g_2 = X_B, \qquad g_3 = \mathcal{Y}, \qquad g_4 = \frac{\partial \mathcal{Y}}{\partial X_B}, \tag{3.155}$$

where $\mathcal{Y}$ is the weight function derived earlier.

We expect that W_B behave as boundary layers, decaying exponentially as $X \to +\infty$ and behaving as $C_j^{(k)} X + D_j^{(k)}$ as $X \to -\infty$. We first express $C_j^{(k)}$, $D_j^{(k)}$, $k = 0, 1$ in terms of $v_m^{(k)}$ and their derivatives. We have from Green's formula that

$$0 = \sum_{j=1}^{2} \mu_j \int\limits_{\partial \Pi_B^{(j)}(L)} \left(g_i \frac{\partial}{\partial n}(W_B^{(k)} + \mathcal{F}_B^{(k)}) - (W_B^{(k)} + \mathcal{F}_B^{(k)}) \frac{\partial g_i}{\partial n} \right) \mathrm{d}S; \tag{3.156}$$

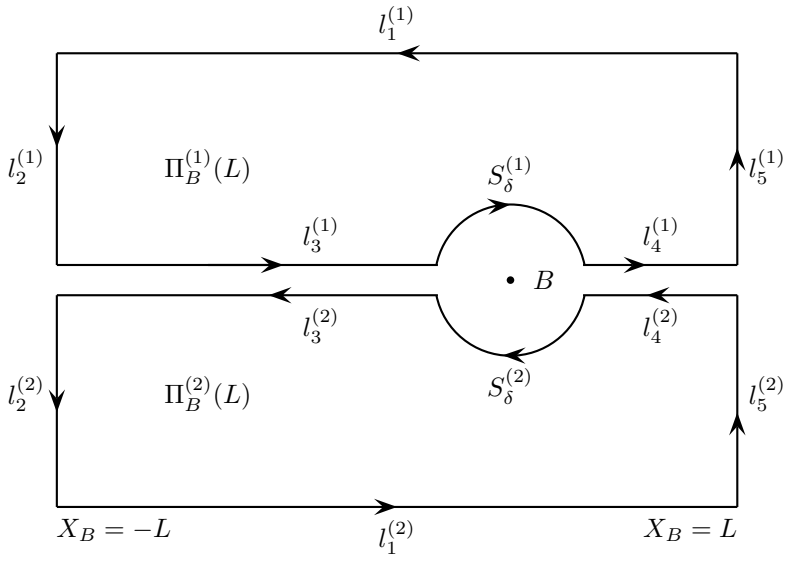

Figure 3.4: Contour of integration for (3.156)

the contour of integration $\partial\Pi_B^{(j)}(L)$ is shown in Figure 3.4. In the following subsections, we will consider a number of cases that correspond to different choices of the indices i and k.

3.3.1 The cases $k = 0, 1$, $i = 1, 2, 3$.

We see from boundary conditions that integrals over the horizontal parts of the boundary $l_1^{(j)}, l_3^{(j)}, l_4^{(j)}$, $j = 1, 2$ give zero contribution to the integral. Moreover, the contribution from S_δ also disappears as $\delta \to 0$ (see Figure 3.4) for g_1, g_2 and g_3, leaving contributions solely from $l_2^{(j)}$ and $l_5^{(j)}$ in these cases.

From the definitions of $\mathcal{F}_B^{(m)}$, we obtain the following limits as $X_B \to \pm\infty$

for $k = 0, 1$:

$$\mathcal{F}_B^{(0)} = v_4^{(0)}(x_B), \qquad X_B \to +\infty, \tag{3.157}$$

$$\mathcal{F}_B^{(0)} = v_2^{(0)}(x_B)\mathcal{H}(Y) + v_3^{(0)}(x_B)\mathcal{H}(-Y), \qquad X_B \to -\infty, \tag{3.158}$$

$$\mathcal{F}_B^{(1)} = (v_4^{(0)})'(x_B)X_B + v_4^{(1)}(x_B), \qquad X_B \to +\infty, \tag{3.159}$$

$$\begin{aligned}\mathcal{F}_B^{(1)} = &\left\{(v_2^{(0)})'(x_B)X_B + v_2^{(1)}(x_B)\right\}\mathcal{H}(Y) \\ &+ \left\{(v_3^{(0)})'(x_B)X_B + v_3^{(1)}(x_B)\right\}\mathcal{H}(-Y), \qquad X_B \to -\infty.\end{aligned} \tag{3.160}$$

Since $W_B^{(k)} \to 0$ as $X_B \to +\infty$, equation (3.156) reduces to

$$\begin{aligned}0 = \sum_{j=1}^{2} \mu_j \Bigg\{ &\int_{l_5^{(j)}} \left(g_i \frac{\partial}{\partial X_B} \mathcal{F}_B^{(k)} - \mathcal{F}_B^{(k)} \frac{\partial g_i}{\partial X_B} \right) \mathrm{d}S \\ &- \int_{l_2^{(j)}} \left(g_i \frac{\partial}{\partial X_B} \left(\mathcal{F}_B^{(k)} + W_B^{(k)} \right) - \left(\mathcal{F}_B^{(k)} + W_B^{(k)} \right) \frac{\partial g_i}{\partial X_B} \right) \mathrm{d}S \Bigg\}\end{aligned} \tag{3.161}$$

As an example of how to proceed, let us first consider the case where we use $g_1 = 1$ and $\mathcal{F}_B^{(0)}$. Then equation (3.161) becomes

$$0 = \sum_{j=1}^{2} \mu_j \left\{ \int_{l_5^{(j)}} 0 \mathrm{d}S - \int_{l_2^{(j)}} 1 \cdot C_j^{(0)} \mathrm{d}S \right\} = \mu_1 H_1 C_1^{(0)} + \mu_2 H_2 C_2^{(0)}. \tag{3.162}$$

Applying this procedure with g_1, g_2, g_3; $\mathcal{F}_B^{(0)}, \mathcal{F}_B^{(1)}$ and for brevity of notation defining the constants

$$\zeta_1 = \mu_1 H_1, \qquad \zeta_2 = \mu_2 H_2, \tag{3.163}$$

we obtain the following equations:

$$\zeta_1 C_1^{(0)} + \zeta_2 C_2^{(0)} = 0, \tag{3.164}$$

$$\zeta_1(v_2^{(0)}(x_B) + D_1^{(0)}) + \zeta_2(v_3^{(0)}(x_B) + D_2^{(0)}) = (\zeta_1 + \zeta_2)v_4^{(0)}(x_B), \tag{3.165}$$

$$\zeta_1((v_2^{(0)})'(x_B) + C_1^{(1)}) + \zeta_2((v_3^{(0)})'(x_B) + C_2^{(1)}) = (\zeta_1 + \zeta_2)(v_4^{(0)})'(x_B), \tag{3.166}$$

$$\zeta_1(v_2^{(1)}(x_B) + D_1^{(1)}) + \zeta_2(v_3^{(1)}(x_B) + D_2^{(1)}) = (\zeta_1 + \zeta_2)v_4^{(1)}(x_B), \tag{3.167}$$

$$\zeta_1(D_1 C_1^{(0)} - (v_2^{(0)}(x_B) + D_1^{(0)})C_1) + \zeta_2(D_2 C_2^{(0)} - (v_3^{(0)}(x_B) + D_2^{(0)})C_2) = 0, \tag{3.168}$$

$$\begin{aligned}\zeta_1(D_1(v_2^{(0)})'(x_B) + D_1 C_1^{(1)} - C_1 v_2^{(1)}(x_B) - C_1 D_1^{(1)}) \\ + \zeta_2(D_2(v_3^{(0)})'(x_B) + D_2 C_2^{(1)} - C_2 v_3^{(1)}(x_B) - C_2 D_2^{(1)}) = 0.\end{aligned} \tag{3.169}$$

3.3.2 The cases $k = 0, 1$; $i = 4$.

To obtain two further equations, we apply the same procedure to the solution $g_4 = \frac{\partial \mathcal{Y}}{\partial X_B}$. Again, the contribution from the horizontal parts of the contour of integration is zero, leaving nonzero contributions from the vertical parts of the contour, $l_2^{(j)}$ and $l_5^{(j)}$. Unlike with g_1, g_2 and g_3 however, the contribution from ${S_\delta}^{(j)}$ is non-zero. We investigate the behaviour of g_4 near the crack tip.

We have that

$$g_4^{(j)} = \frac{\partial \mathcal{Y}_j}{\partial X} = \frac{\partial \mathcal{Y}_j}{\partial R}\cos\theta - \frac{1}{R}\frac{\partial \mathcal{Y}_j}{\partial \theta}\sin\theta, \tag{3.170}$$

where (R, θ) is the usual polar co-ordinate system, with $R = \sqrt{X_B^2 + Y^2}$ and so from our asymptotic estimate for $\mathcal{Y}_j$ near the crack tip we deduce that near the crack tip,

$$g_4^{(j)} \sim \frac{(-1)^j}{\pi\mu_j}\left\{b_0^{(\mathcal{Y})} + a_0^{(\mathcal{Y})}\ln R + (-1)^{(j+1)}a_0^{(\mathcal{Y})}\sin 2\theta(\pi + (-1)^j\theta)\right\} \tag{3.171}$$

and so for small R,

$$\frac{\partial g_4^{(j)}}{\partial R} \sim \frac{(-1)^j a_0^{(\mathcal{Y})}}{\pi \mu_j R}. \tag{3.172}$$

Noting that the outward normal to $S_\delta^{(j)}$ is in the direction of $-R$, we have that as $\delta \to 0$

$$\begin{aligned}\mu_j \int_{S_\delta} \left(g_4 \left(-\frac{\partial}{\partial R} \right) (W_B^{(k)} + \mathcal{F}_B^{(k)}) - (W_B^{(k)} + \mathcal{F}_B^{(k)}) \left(-\frac{\partial g_4}{\partial R} \right) \right) \mathrm{d}S \\ = \mu_j \int_{S_\delta} \left((W_B^{(k)} + \mathcal{F}_B^{(k)}) \frac{\partial g_4}{\partial R} \right) R \mathrm{d}\theta \qquad (3.173) \\ = \mu_j \int_{S_\delta} \frac{(-1)^j a_0^{(\mathcal{Y})}}{\pi \mu_j R} \left(W_B^{(k)} + \mathcal{F}_B^{(k)} \right) R \mathrm{d}\theta. \qquad (3.174)\end{aligned}$$

Since W_B satisfies the same model problem as $\mathcal{Y}$, it too will possess asymptotic behaviour at the crack tip of the same form as g_4 in (3.171), but with different constants which we denote $a_{(k)}^{(W)}$ and $b_{(k)}^{(W)}$ for $k = 1, 2$. The contribution to the integral from the circular part of the contour is therefore given by

$$\begin{aligned}\frac{a_0^{(\mathcal{Y})}}{\pi} \left(\int_{-\pi}^{0} \left(W_B^{(k)}(0^+, \theta) + \mathcal{F}_B^{(k)}(0^+, \theta) \right) \mathrm{d}\theta - \int_{0}^{\pi} \left(W_B^{(k)}(0^+, \theta) + \mathcal{F}_B^{(k)}(0^+, \theta) \right) \mathrm{d}\theta \right) \\ = \frac{a_0^{(\mathcal{Y})}}{\pi} \int_{-\pi}^{0} \frac{\mu_1 \kappa}{\mu_1 + \mu_2} a_{(k)}^{(W)} \mathrm{d}\theta + \frac{a_0^{(\mathcal{Y})}}{\pi} \int_{0}^{\pi} \frac{\mu_2 \kappa}{\mu_1 + \mu_2} a_{(k)}^{(W)} \mathrm{d}\theta = \kappa a_0^{(\mathcal{Y})} a_{(k)}^{(W)}.\end{aligned} \tag{3.175}$$

With this information at hand, we are now able to apply (3.156) with g_4 and $\mathcal{F}_B^{(1)}, \mathcal{F}_B^{(2)}$, yielding our further two relationships

$$\mu_1 H_1 C_1 C_1^{(0)} + \mu_2 H_2 C_2 C_2^{(0)} = \kappa a_0^{(\mathcal{Y})} a_{(0)}^{(W)} \tag{3.176}$$

and

$$\mu_1 H_1 C_1 ((v_2^{(0)})'(x_B) + C_1^{(1)}) + \mu_2 H_2 C_2 ((v_3^{(0)})'(x_B) + C_2^{(1)}) = \kappa a_0^{(\mathcal{Y})} a_{(1)}^{(W)}. \tag{3.177}$$

Note that due to the chosen normalisation for the constants C_1 and C_2 (see 3.61 on page 43), we have that $\mu_j H_j C_j = (-1)^{j+1}$ for $j = 1, 2$.

3.3.3 The cases for which $k = 2$.

When studying the second order approximation, we again substitute our Ansatz (3.142) into our Helmholtz equations and compare terms in ε^0, yielding

$$\begin{aligned}\nabla^2_{X_BY}\Bigg\{W_B^{(2)}(X_B,Y) + \sum_{m=2}^{4}\chi_m(x,y;\varepsilon)\Bigg(v_m^{(2)}(x_B) + (v_m^{(1)})'(x_B)X_B \\ + (v_m^{(0)})''(x_B)\frac{X_B^2}{2} + V_m^{(0)}(x_B,Y)\Bigg)\Bigg\} \\ = -\sum_{m=2}^{4}\chi_m(x,y;\varepsilon)\frac{\omega^2}{d_m^2}v_m^{(0)}(x_B) - \frac{\omega^2}{d_m^2}W_B^{(0)}. \qquad (3.178)\end{aligned}$$

We can rewrite this as

$$\begin{aligned}\nabla^2_{X_BY}\Bigg\{W_B^{(2)}(X_B,Y) + \sum_{m=2}^{4}\chi_m(x,y;\varepsilon)\Bigg(v_m^{(2)}(x_B) + (v_m^{(1)})'(x_B)X_B \\ + (v_m^{(0)})''(x_B)\frac{X_B^2}{2} + V_m^{(0)}(x_B,Y)\Bigg)\Bigg\} \\ = -\sum_{m=2}^{4}\chi_m(x,y;\varepsilon)\left((v_m^{(0)})''(x_B) + \frac{\omega^2}{d_m^2}v_m^{(0)}(x_B)\right) - \frac{\omega^2}{d_m^2}W_B^{(0)}, \qquad (3.179)\end{aligned}$$

and since $(v_m^{(0)})''(x_B) + \frac{\omega^2}{d_m^2}v_m^{(0)}(x_B) = 0$, we have

$$\Delta_{X_BY}\left\{W_B^{(2)}(X_B,Y) + \mathcal{F}_B^{(2)}(X_B,Y)\right\} = -\frac{\omega^2}{d_m^2}W_B^{(0)}, \qquad (3.180)$$

where we have defined

$$\mathcal{F}_B^{(2)} = \sum_{m=2}^{4}\chi_m(x,y;\varepsilon)\left(v_m^{(2)}(x_B) + (v_m^{(1)})'(x_B)X_B + V_m^{(0)}(x_B,Y)\right). \qquad (3.181)$$

We see that $\mathcal{F}_B^{(2)}$ behaves at $\pm\infty$ as

$$\mathcal{F}_B^{(2)} = v_4^{(2)}(x_B) + (v_4^{(1)})'(x_B)X_B + V_4^{(0)}(x_B, Y), \quad X_B \to +\infty, \tag{3.182}$$

and behaves as follows as $X \to -\infty$:

$$\begin{aligned}\mathcal{F}_B^{(2)} = &\left\{v_2^{(2)}(x_B) + (v_2^{(1)})'(x_B)X_B + V_2^{(0)}(x_B, Y)\right\}\mathcal{H}(Y) \\ &+ \left\{v_3^{(2)}(x_B) + (v_3^{(1)})'(x_B)X_B + V_3^{(0)}(x_B, Y)\right\}\mathcal{H}(-Y).\end{aligned} \tag{3.183}$$

Green's formula then yields that

$$\begin{aligned}&\int_{\Pi_B} g_i \nabla^2_{X_B Y}(W_B^{(2)} + \mathcal{F}_B^{(2)})\mathrm{d}\Pi_B \\ &\qquad = \sum_{j=1}^{2} \mu_j \int_{\partial\Pi_B^{(j)}} \left(g_i \frac{\partial}{\partial n}(W_B^{(2)} + \mathcal{F}_B^{(2)}) - (W_B^{(2)} + \mathcal{F}_B^{(2)})\frac{\partial g_i}{\partial n}\right)\mathrm{d}S.\end{aligned} \tag{3.184}$$

We consider first the case where $i = 1$, that is $g_1 \equiv 1$. Then (3.184) reduces to

$$-\sum_{j=1}^{2} \int_{\Pi_B^{(j)}} \frac{\omega^2}{c_j^2} W_B^{(0)}\mathrm{d}\Pi_B^{(j)} = \sum_{j=1}^{2} \mu_j \int_{\partial\Pi_B^{(j)}} \frac{\partial}{\partial n}(W_B^{(2)} + \mathcal{F}_B^{(2)})\mathrm{d}S. \tag{3.185}$$

The contribution from the horizontal parts of the integral on the right hand side of (3.185) is zero, and so

$$\begin{aligned}-\sum_{j=1}^{2} \int_{\Pi_B^{(j)}} \frac{\omega^2}{c_j^2} W_B^{(0)}\mathrm{d}\Pi_B^{(j)} &= \sum_{j=1}^{2} \mu_j \left\{\int_{l_5^{(j)}} \frac{\partial}{\partial X_B}\mathcal{F}_B^{(2)}\mathrm{d}Y - \int_{l_2^{(j)}} \frac{\partial}{\partial X_B}(\mathcal{F}_B^{(2)} + W_B^{(2)})\mathrm{d}Y\right\} \\ &= (\zeta_1 + \zeta_2)(v_4^{(1)})'(x_B) - \zeta_1((v_2^{(1)})'(x_B) + C_1^{(2)}) - \zeta_2((v_3^{(1)})'(x_B) + C_2^{(2)}).\end{aligned} \tag{3.186}$$

Here we have used condition (3.110) which states that $V_m^{(0)}$ has zero average across the cross section (and therefore so does its X_B-derivative). Rearranging gives

$$\mu_1 H_1 C_1^{(2)} + \mu_2 H_2 C_2^{(2)} = (\mu_1 H_1 + \mu_2 H_2)(v_4^{(1)})'(x_B) - \mu_1 H_1 (v_2^{(1)})'(x_B) \\ -\mu_2 H_2 (v_3^{(1)})'(x_B) + \sum_{j=1}^{2} \int_{\Pi_B^{(j)}} \frac{\omega^2}{c_j^2} W_B^{(0)} \mathrm{d}\Pi_B^{(j)}. \tag{3.187}$$

3.3.4 Deriving the junction conditions

We define the column matrices

$$E^{(k)} = \begin{bmatrix} C_1^{(k)} & C_2^{(k)} & D_1^{(k)} & D_2^{(k)} \end{bmatrix}^T, \qquad k = 0, 1. \tag{3.188}$$

The eight equations obtained in the previous two subsections can then be rewritten as two matrix equations, the first of which is found to be

$$ME^{(0)} = \begin{bmatrix} 0 \\ (\mu_1 H_1 + \mu_2 H_2) v_4^{(0)}(x_B) - \mu_1 H_1 v_2^{(0)}(x_B) - \mu_2 H_2 v_3^{(0)}(x_B) \\ \mu_1 H_1 C_1 v_2^{(0)}(x_B) + \mu_2 H_2 C_2 v_3^{(0)}(x_B) \\ \kappa a_0^{(\mathcal{Y})} a_0^{(W)}, \end{bmatrix} \tag{3.189}$$

where M is the 4x4 matrix

$$\begin{bmatrix} \mu_1 H_1 & \mu_2 H_2 & 0 & 0 \\ 0 & 0 & \mu_1 H_1 & \mu_2 H_2 \\ \mu_1 H_1 D_1 & \mu_2 H_2 D_2 & -\mu_1 H_1 C_1 & -\mu_2 H_2 C_2 \\ \mu_1 H_1 C_1 & \mu_2 H_2 C_2 & 0 & 0 \end{bmatrix}, \tag{3.190}$$

where C_j and D_j are the asymptotic constants from the weight function defined in (3.61). The determinant of M is given by

$$\det(M) = -(\mu_1 H_1 + \mu_2 H_2)^2 < 0. \tag{3.191}$$

Therefore for $C_1^{(0)} = C_2^{(0)} = D_1^{(0)} = D_2^{(0)} = 0$ (that is, for W to vanish far away from the crack tip as we would expect for such a boundary layer), we have that the matrix in the right hand side of (3.189) must be equal to zero. From this follow the junction conditions

$$v_2^{(0)}(x_B) = v_3^{(0)}(x_B) = v_4^{(0)}(x_B), \tag{3.192}$$

$$a_{(0)}^{(W)} = 0. \tag{3.193}$$

The latter condition (3.193) yields that $W_B^{(0)} \equiv 0$. The second matrix equation is

$$ME^{(1)} = \tag{3.194}$$

$$\begin{bmatrix} (\mu_1 H_1 + \mu_2 H_2)(v_4^{(0)})'(x_B) - \mu_1 H_1 (v_2^{(0)})'(x_B) - \mu_2 H_2 (v_3^{(0)})'(x_B) \\ (\mu_1 H_1 + \mu_2 H_2) v_4^{(1)}(x_B) - \mu_1 H_1 v_2^{(1)}(x_B) - \mu_2 H_2 v_3^{(1)}(x_B) \\ \mu_1 H_1 C_1 v_2^{(1)}(x_B) + \mu_2 H_2 C_2 v_3^{(1)}(x_B) - \mu_1 H_1 D_1 (v_2^{(0)})'(x_B) - \mu_2 H_2 D_2 (v_3^{(0)})'(x_B) \\ \kappa a_0^{(\mathcal{Y})} a_1^{(W)} - \mu_1 H_1 C_1 (v_2^{(0)})'(x_B) - \mu_2 H_2 C_2 (v_3^{(0)})'(x_B) \end{bmatrix}$$

where M is the matrix given in (3.190). For $C_1^{(1)} = C_2^{(1)} = D_1^{(1)} = D_2^{(1)} = 0$, the right hand matrix is again set to zero. Noting that $a_0^{(\mathcal{Y})} = \lambda$ (see (3.92)) and that $\mu_1 H_1 C_1 + \mu_2 H_2 C_2 = 0$, setting the fourth row of the RHS matrix to zero then yields that

$$a_{(1)}^{(W)} = \frac{1}{\kappa\lambda} \Delta\{(v^{(0)})'\}. \tag{3.195}$$

where

$$\Delta\{(v^{(0)})'\}(x_B) = (v_2^{(0)})'(x_B) - (v_3^{(0)})'(x_B). \tag{3.196}$$

The other conditions imply

$$v_2^{(1)}(x_B) = v_4^{(1)}(x_B) - \tfrac{\mu_2 H_2}{\mu_1 H_1 + \mu_2 H_2}\left(\tfrac{\alpha}{\pi} + \tfrac{1}{\lambda}\right)\Delta\{(v^{(0)})'\}(x_B), \quad (3.197)$$

$$v_3^{(1)}(x_B) = v_4^{(1)}(x_B) + \tfrac{\mu_1 H_1}{\mu_1 H_1 + \mu_2 H_2}\left(\tfrac{\alpha}{\pi} + \tfrac{1}{\lambda}\right)\Delta\{(v^{(0)})'\}(x_B), \quad (3.198)$$

along with the relationship

$$(\mu_1 H_1 + \mu_2 H_2)(v_4^{(0)})'(x_B) - \mu_1 H_1 (v_2^{(0)})'(x_B) - \mu_2 H_2 (v_3^{(0)})'(x_B) = 0. \quad (3.199)$$

We stress that α and λ are functions of κ and so expressions (3.197) and (3.198) describe how the junction conditions depend upon the extent of imperfection of the interface. In particular, $(\alpha/\pi + 1/\lambda)$ is a constant that plays a crucial physical role since it defines the proportionality between the displacement jump in the first order approximation and the angle of opening in the zero order approximation. Equation (3.199) complements conditions (3.192) and (3.193) to give full information for the zero order approximation. We later present numerical results for the normalized constant $\alpha_I = ((\alpha/\pi) + 1/\lambda)/(H_1 + H_2)$.

The conditions regarding the first order approximation (3.195), (3.197) and (3.198) can be complemented by a further equation in $(v_m^{(1)})'(x_B)$, which follows from the next level of approximation, i.e. taking $N = 2$ in (3.105):

$$\mu_1 H_1 (v_2^{(1)})'(x_B) + \mu_2 H_2 (v_3^{(1)})'(x_B) - (\mu_1 H_1 + \mu_2 H_2)(v_4^{(1)})'(x_B) = \sum_{j=1}^{2} \int_{\Pi_B^{(j)}} \frac{\omega^2}{c_j^2} W_B^{(0)} \mathrm{d}\Pi_B^{(j)}, \quad (3.200)$$

and by our earlier comment that $W_B^{(0)} \equiv 0$, the right side of this expression is zero. At this point we would like to comment that taking higher order approximations and evaluating higher order junction conditions is possible but much more advanced. For example, integrals analogous to that on the right

hand side of the above expression would depend upon $W_B^{(1)}$ and boundary layers from higher order approximations, and so would not in general be zero. However, since we focus on thin strips, ε is small and so terms in ε^2 would give significantly less contribution than the lower order approximations. We later comment on the accuracy of the zero order approximation by comparing computations against FEM results in a case where ε is not too small. While the accuracy of the low dimensional model will increase for smaller ε, finite element computations become difficult and inefficient for very small values which correspond to very thin strips.

3.3.5 Summary of low dimensional model and boundary layer analysis

Figure 3.5 on page 72 summarises the results obtained in this section by illustrating the right-hand junction point/crack tip x_B for both the low dimensional model (illustrated by three beams meeting near the junction point) and the boundary layer near the crack tip. Red lines correspond to the crack faces while blue lines illustrate the imperfect interface.

In the zero order low dimensional model, displacement is continuous at the junction point (see (3.192)) and the boundary layer has zero opening at the crack tip (3.193). However, the low dimensional model allows an opening angle of the beams of size $\Delta\{(v^{(0)})'\}$ as defined in (3.196).

For the first order low dimensional model, there is a displacement jump at the junction point proportional to the angle of opening in the zero order model as demonstrated by (3.197) and (3.198) on page 70; the constant of proportionality is α_I. For the first order approximation, there is a displacement opening at the crack tip whose size is also proportional to $\Delta\{(v^{(0)})'\}$.

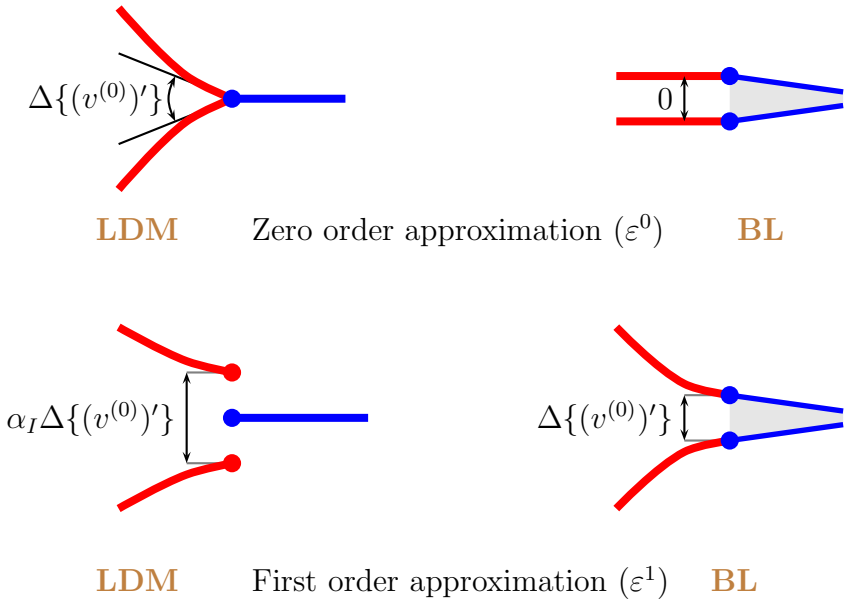

Figure 3.5: Zero and first order behaviours of the low dimensional model (LDM) and boundary layer (BL) near the right-hand junction point/crack tip x_B.

3.4 Numerical simulations and discussions

To enable us to compare results with the perfect interface case discussed in [44] effectively, we seek normalized constants. We first seek a normalized representation of α as defined in equation (3.55) on page 42. We introduce the notation

$$H = H_1 + H_2,\ H_* = \frac{H_1 - H_2}{H_1 + H_2},\ \mu_* = \frac{\mu_1 - \mu_2}{\mu_1 + \mu_2},\ \kappa_* = \frac{\kappa(\mu_1 + \mu_2)}{H},\ \lambda_* = \lambda H, \tag{3.201}$$

where H_*, μ_* and κ_* are non-dimensional parameters which respectively describe the geomterical, mechanical and imperfect properties of the problem. λ is the constant dependent on μ_j, H_j and κ defined in (3.30). λ_* can be

expressed in terms of the other dimensionless parameters as

$$\lambda_*^2 = \frac{8(1+\mu_* H_*)}{\kappa_*(1-\mu_*^2)(1-H_*^2)}. \tag{3.202}$$

We also introduce the function

$$\Xi_{**}(t) = \frac{t}{\lambda_*^2 + t^2}\left(t + \frac{2}{\kappa_*(1+\mu_*)}\coth\frac{t(1+H_*)}{2} + \frac{2}{\kappa_*(1-\mu_*)}\coth\frac{t(1-H_*)}{2}\right),$$

which satisfies the relationship $\Xi_{**}(t) = \Xi_*\left(\frac{t}{H}\right)$, and so we can write

$$\alpha = \int_0^\infty \frac{\ln \Xi_*(\xi)}{\xi^2}\mathrm{d}\xi = \int_0^\infty \frac{H^2 \ln \Xi_{**}(t)}{t^2}\frac{\mathrm{d}t}{H} = H\int_0^\infty \frac{\ln \Xi_{**}(t)}{t^2}\mathrm{d}t = H\alpha_*, \tag{3.203}$$

where we have defined the non-dimensional quantity α_*. We find through asymptotic analysis that

$$\frac{\ln \Xi_{**}(t)}{t^2} = \frac{1}{12}\frac{H_*^3\mu_* - H_*^2 - \mu_* H_* + 1}{1+\mu_* H_*} + O(t^2), \quad t \to 0. \tag{3.204}$$

Mishuris, Movchan and Bercial [44] showed that in the analogous problem to that discussed in this chapter with a perfect interface instead of an imperfect interface,

$$D_j = \alpha_P(H_1 + H_2)C_j, \tag{3.205}$$

where

$$\begin{aligned}\alpha_P =& \frac{1}{\pi}\ln\left\{\left(\frac{1+H_*}{2}\right)^{\frac{1+H_*}{2}}\left(\frac{1-H_*}{2}\right)^{\frac{1-H_*}{2}}\right\} \\ &- \frac{\mu_*}{\pi}\int_0^\infty \frac{H_* - \tanh(tH_*)\coth(t)}{(\sinh(t) + \mu_*\sinh(tH_*))t}\mathrm{d}t.\end{aligned} \tag{3.206}$$

We have demonstrated (see the form of the constants C_j, D_j in (3.61)) that for the imperfect interface problem,

$$D_j = \alpha_I(H_1 + H_2)C_j, \tag{3.207}$$

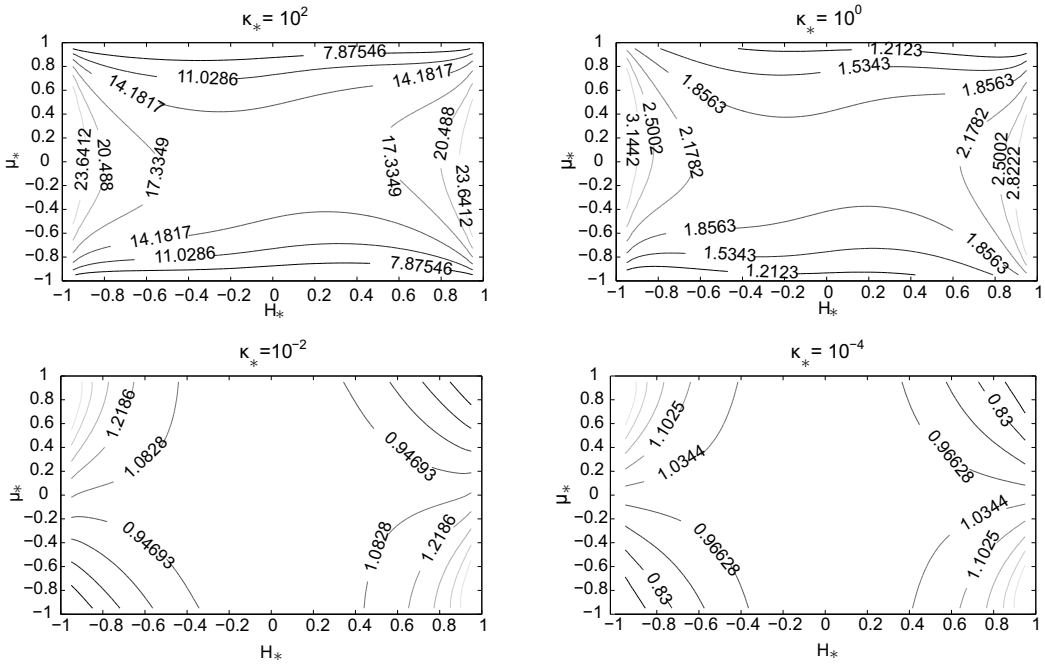

Figure 3.6: Contour plots of the ratio α_I/α_P for four different values of κ_*, a dimensionless parameter describing the extent of imperfection of the interface between the two materials. The axes of each plot are μ_* and H_*, dimensionless parameters respectively describing the mechanical and geometric properties of the problem. The ratio α_I/α_P gets closer to 1 as κ_* decreases in value towards 0.

where

$$\alpha_I = -\left(\frac{1}{\pi}\int_0^\infty \frac{\ln \Xi_{**}(t)}{t^2}\mathrm{d}t + \frac{1}{\lambda_*}\right), \tag{3.208}$$

and since small κ_* correspond to an interface which is 'almost perfect', we would expect $\alpha_I \to \alpha_P$ as $\kappa_* \to 0$. Figure 3.6 shows a plot of the ratio α_I/α_P on axes of μ_* against H_* for four different values of κ_*. From this it is easily seen that as $\kappa_* \to 0$, α_I/α_P gets close to 1 as expected. The behaviour of the weight functions near the crack tip are however absolutely different since

the problem is singularly perturbed, that is:

$$[\![\mathcal{Y}]\!] \sim \sqrt{\eta\kappa}, \quad \kappa \to 0, \tag{3.209}$$

$$\mu_1 \left.\frac{\partial \mathcal{Y}}{\partial Y}\right|_{Y=0+} \sim -\sqrt{\frac{\eta}{\kappa}}, \quad X \to 0, \quad \kappa \to 0, \tag{3.210}$$

where η is defined in (3.33). In the plots showing the ratio for small values of κ_*, the highest deviations from 1 occur near the corner of the plot. These correspond to the cases where there is a high contrast between the shear moduli and thicknesses of the two materials. We see that in the cases where the materials have similar shear moduli and thicknesses (nearer the center of the plot), the ratio α_I/α_P quickly approaches 1 as $\kappa_* \to 0$.

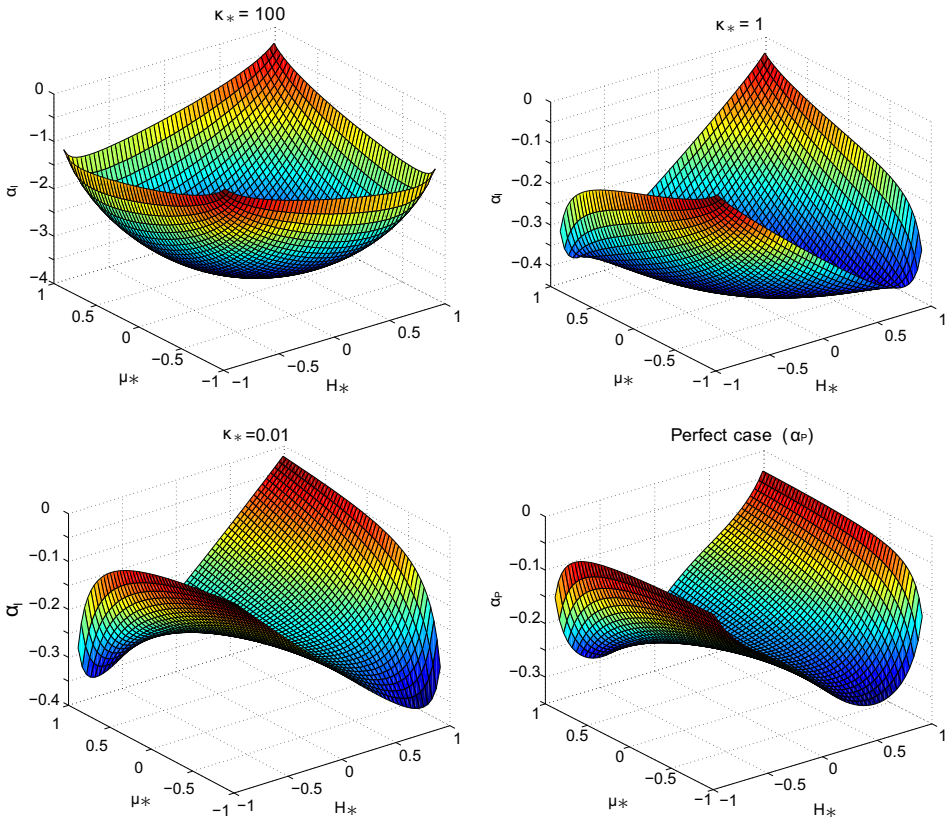

Figure 3.7: Surface plots of α_I for $\kappa_* = 100$, 1 and 0.01; also of α_P, all plotted on axes of μ_* and H_*.

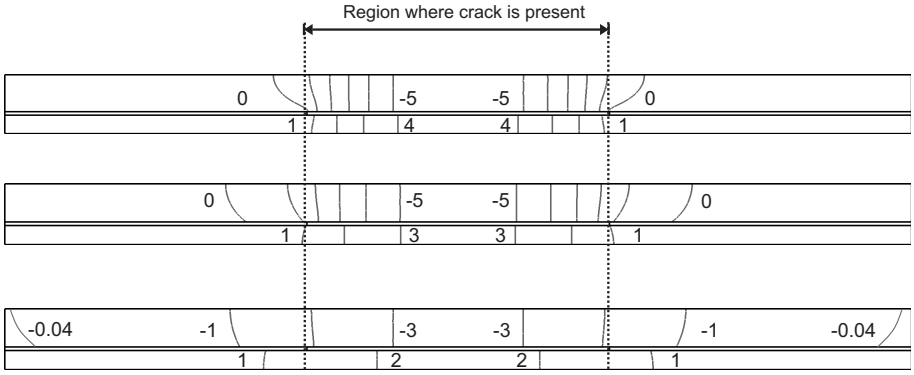

Figure 3.8: Finite element computation (COMSOL) contour plot of the eigensolution corresponding to the standing Bloch-Floquet waves for three different values of κ. **Top:** Bonding material with shear modulus $1000\mu_{\text{resin}}$. **Middle:** Bonding material is epoxy resin. **Bottom:** Bonding material with shear modulus $\mu_{\text{resin}}/10$. Countours join points of integer values, and the dotted vertical lines indicate the location of the crack tips.

Figure 3.7 on page 75 shows surface plots of α_I on axes of μ_* and H_* for $\kappa_* = 100$, 1, and 0.01. This constant describes the impact that the imperfect interface has upon the junction conditions as described in equations (3.197) and (3.198). Also shown in the figure is a plot of α_P. The similarity between the plot of α_I for $\kappa_* = 0.01$ and the plot of α_P is evident here. For the cases with larger κ_* values, we see that α_P is differently dependent upon the mechanical and geometric parameters of the problem.

Figure 3.8 shows finite-element plots (using the COMSOL Multiphysics software package) of standing wave eigensolutions. For these simulations we use the following geometrical parameters for the elementary cell:

$$l = 0.8[\text{m}], \quad a = 2.4[\text{m}], \quad H_1 = 0.1[\text{m}], \quad H_2 = 0.05[\text{m}],$$

and the following material constants which correspond to iron (in $\Pi_\varepsilon^{(2)}$) and

aluminium (in $\Pi_\varepsilon^{(1)}$):

$$\mu_2 = 82 \cdot 10^9 [\mathrm{N/m^2}], \quad \mu_1 = 26 \cdot 10^9 [\mathrm{N/m^2}],$$
$$\rho_2 = 7860 [\mathrm{kg/m^3}], \quad \rho_1 = 2700 [\mathrm{kg/m^3}].$$

Presented in this figure are three plots corresponding to Al-Fe strips with different materials bonding them together, with the vertical dotted lines indicating the location of the crack tips. The imperfect interface is modelled in the COMSOL simulations by a thin layer occupied by an adhesive material; this approach was justified in [40, 43], among others. Provided that h_{resin}/H_2 is sufficiently small and μ_{resin} is small in comparison to μ_1 and μ_2, this gives $\kappa = h_{\mathrm{resin}}/\mu_{\mathrm{resin}}$.

The second of the three plots in Figure 3.8 uses epoxy resin as the bonding material with parameters

$$\mu_{\mathrm{resin}} = 2.5 \cdot 10^9 [\mathrm{N/m^2}], \quad \rho_{\mathrm{resin}} = 1850 [\mathrm{kg/m^3}], \quad h_{\mathrm{resin}} = 0.01 [\mathrm{m}].$$

For comparison, the first plot shows a simulation with a gluing layer of shear modulus 1000 greater than that of epoxy resin. The third plot uses a material with shear modulus 10 times less than epoxy resin. Equivalently, these three cases in the top, middle and bottom parts of the figure correspond to $\kappa_* = 2.88 \cdot 10^{-3}$, $\kappa_* = 2.88$, and $\kappa_* = 28.8$, respectively. The plots show that the standing wave is more localised and intense in the locality of the crack when the bonding material is stiffer. Conversely, when the bonding material is less stiff, the standing wave extends further beyond the locality of the crack and is less intense. Closely packed contours indicate areas where stress is high; as we would expect, the highest stress intensity is found in the case with the stiffest bonding material.

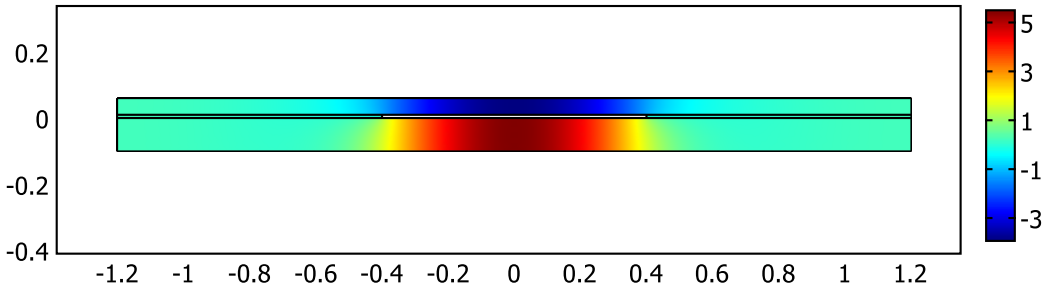

Figure 3.9: Finite element computation (COMSOL) of the eigensolution corresponding to the standing Bloch-Floquet wave. Note that the standing wave is localised within the region above and below the crack.

It is readily seen in the bottom plot of Figure 3.8 (which corresponds to a highly imperfect interface) that the boundary layer support extends almost to the edge of the elementary cell. This extension far away from the crack tips suggests that the boundary layers decay slowly from the crack tips and so may not be assumed independent. In this case, therefore, our analysis may become invalid due to the assumption in our asymptotic procedure that the exponentially decaying boundary layer does not influence the Bloch-Floquet conditions. This assumption is satisfied if γ^+ is far from zero, so if κ is not too large. More accurately, we assume $\gamma^+ \gg \frac{\varepsilon}{a-l}$ (see (3.94) for large κ). If the imperfect interface is too weak and this condition is violated then the junction conditions evaluated here will no longer be accurate and other analysis should be sought.

Figures 3.9 and 3.10 show two different eigensolutions computed in COMSOL. Figure 3.9 shows a standing wave eigensolution. It is clearly seen from this plot that the standing wave is localised within the region directly above and below the crack, as we would expect. Figure 3.10 shows an eigensolution corresponding to a propagating wave. This wave travels through the strip and is largely uninfluenced by the presence of the crack.

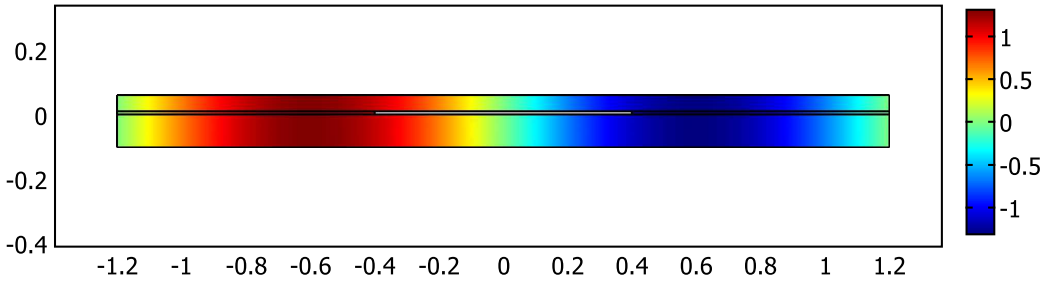

Figure 3.10: Finite element computation (COMSOL) of another eigensolution. This eigensolution corresponds to a wave that propagates through the strip.

For the moment, we do not present dispersion diagrams since we will devote the next chapter to the analysis and improvement of the low dimensional model. Nevertheless it is worth mentioning that dispersion diagrams computed from the low dimensional model display excellent agreement with the COMSOL simulations for the eigenfrequencies of propagating waves with a typical discrepancy between finite element and asymptotic results of around 0.3% in the case where the strip has the same dimensions as used throughout this section, which corresponds to $\varepsilon = 0.0625$. A discrepancy is apparent in the case of standing waves, however. The size of this discrepancy varies depending upon the mechanical and geometric parameters considered but may typically lie somewhere within the region of 5-10%. A similar discrepancy in standing wave eigenfrequencies was observed by Mishuris *et al.* for the perfect interface case in [44].

For engineering applications, this discrepancy may be an important shortcoming, since the standing waves may cause the crack to propagate. To justify this statement, consider equation (3.195) on page 69 which demonstrates that the first non-zero term in the asymptotic expansion of the boundary layer near the right hand crack tip, $a^{(W)}_{(1)}$, is proportional to $\Delta\{(v^{(0)})'\}(x_B)$, the angle of opening of the crack in the zero order skeleton model. Thus if

the crack opening angle is small or zero in the zero order low dimensional model (as is the case for waves that propagate through the strip), then the crack tip opening displacement in the boundary layer will be small or zero. For standing waves, however, (3.195) yields that the crack tip opening displacement will be larger, since the angle of opening in the low dimensional model is much greater in the case of standing waves. It is therefore important to identify their frequencies with as much precision as possible. This motivates our work in the next chapter, in which we offer a computationally efficient method that significantly improves the accuracy of standing wave eigenfrequencies.

Chapter 4

Eigenfrequency correction for the low dimensional model

4.1 Introduction

In this chapter we focus in greater detail on the low dimensional model considered in the previous chapter. An analogous LDM was derived in [44] for the perfect interface version of the problem discussed in Chapter 3. In order to verify the accuracy of the low dimensional models for both the perfect and imperfect cases, we can compare computations against finite element method (FEM) simulations like those presented at the end of the previous chapter in Figures 3.9 and 3.10.

While finite element simulations are useful for geometries which are not too thin, they become inefficient in cases where the thickness of the strip $H_1 + H_2$ is much smaller than the length of the elementary cell a. This problem with FEM simulations is further heightened by the fact that the imperfect interface is implemented by means of placing a very thin layer with

a small shear modulus between $\Pi_\varepsilon^{(1)}$ and $\Pi_\varepsilon^{(2)}$. Thus for problems involving a thin strip, the layer representing the interface is very thin indeed, making computations inefficient.

For this reason an easily computable low dimensional model and asymptotic approach is very useful; moreover, the weight function approach yields analytic expressions for the behaviour of the solution near the crack tip, which a FEM approach alone could not. The asymptotic model derived in the previous chapter which we will adapt in the present chapter is designed for use in very thin strips (i.e. small ε) with geometries such that boundary layers near the crack tips are independent; we will however demonstrate that it is possible to obtain useful information even in cases where the strip is not particularly thin or crack tips in the periodic structure are close to each other, with some limitations which we will discuss.

As we discussed at the end of the previous chapter, upon comparing the eigenfrequencies computed from the LDM with FEM simulations, a discrepancy arises in the frequency of the standing waves. The size of this discrepancy depends greatly upon material and geometrical parameters but is typically somewhere in the region of 3-15%. In this present chapter, we devise an improved model which significantly lowers the size of this discrepancy, typically by at least an order of magnitude.

4.2 Problem formulation

The full problem formulation is as given in Chapter 3. As discussed in that chapter, the problem is singularly perturbed and so the case $\kappa = 0$ which corresponds to the perfect interface case requires different analysis [44] to

the imperfect case. The distance between adjacent cracks is $a - l$, and we assume that a, l and H_j are all of the same order. The functions $u^{(j)}(x, y)$, $j = 1, 2$, are respectively defined above and below the interface as solutions of the Helmholtz equations

$$\Delta u^{(j)}(x, y) + \frac{\omega^2}{c_j^2} u^{(j)}(x, y) = 0, \quad (x, y) \in \Pi_\varepsilon^{(j)}, \tag{4.1}$$

where

$$\Pi_\varepsilon^{(j)} = \left\{ (x, y) \in \mathbb{R} : x \in \left(-\frac{a}{2}, \frac{a}{2} \right), \ (-1)^{j+1} y \in (0, \varepsilon H_j) \right\}. \tag{4.2}$$

We will consider low range frequencies; high frequency treatments are available in [28] and high frequency long wavelength analysis of hard and soft interfaces can be found in [29]. As in the previous chapter, the sought solutions $u^{(j)}$ represent Bloch-Floquet waves, so at the ends of our elementary cell $x = \pm a/2$ we have for $j = 1, 2$ the Bloch-Floquet conditions

$$u^{(j)}(-a/2, y) = e^{-iKa} u^{(j)}(a/2, y), \qquad y \in (-\varepsilon H_2, \varepsilon H_1), \tag{4.3}$$

$$\sigma_{xz}^{(j)}(-a/2, y) = e^{-iKa} \sigma_{xz}^{(j)}(a/2, y), \qquad y \in (-\varepsilon H_2, \varepsilon H_1). \tag{4.4}$$

Again, eigenfunctions $u(x, y)$ are approximated in the form

$$\begin{aligned} u(x, y, \varepsilon) &= \sum_{k=0}^{N} \varepsilon^k \left\{ \sum_{m=1}^{4} \chi_m \left(v_m^{(k)}(x) + \varepsilon^2 V_m^{(k)}(x, Y) \right) \right. \\ &+ \left. \left(W_A^{(k)}(X_A, Y) + W_B^{(k)}(X_B, Y) \right) \right\} + R_N(x, y, \varepsilon), \end{aligned} \tag{4.5}$$

with scaled co-ordinates X_A, X_B and Y introduced in the vicinity of the left and right vertices of the crack defined as

$$X_A = \frac{x - x_A}{\varepsilon}, \qquad X_B = \frac{x - x_B}{\varepsilon}, \qquad Y = \frac{y}{\varepsilon}. \tag{4.6}$$

When solving the low dimensional model to find the functions $v_m^{(k)}$, computations display a discrepancy for standing wave eigenfrequencies between

the low order model and finite element simulations of the problem; these computations are presented in Section 4.5. In order to address the discrepancies that arise in this asymptotic model, in this chapter we further consider the square of the frequency, ω^2, as an asymptotic quantity, writing

$$\omega^2 = \sum_{k=0}^{N} \varepsilon^k \omega_k^2. \tag{4.7}$$

It is not immediately apparent *a priori* that this amendment will lead to a large correction in the approximations of eigenfrequencies, but we will later see that this allows us to solve the first order low dimensional model which causes a significant improvement in the accuracy of the model in those cases where the zero order model displays large discrepancies. Interestingly, in cases where the zero order model gives high accuracy, the corrections are very small. As an example, in one case we consider in Section 4.5, the first order correction method alters the frequency of the first *standing wave* (for which the zero order model gives a significant discrepancy) by 11% of its zero order value, while the *propagating waves* (for which the zero order model displays high accuracy) are only corrected by 10^{-6}.

4.3 Solution of low dimensional model equations

Since the boundary layers W_A and W_B (see (4.5)) decay exponentially, we have that far from the crack tip, $\chi_m = 1$,

$$u \approx \sum_{k=0}^{N} \varepsilon^k \sum_{m=1}^{4} \left(v_m^{(k)} + \varepsilon^2 V_m^{(k)} \right). \tag{4.8}$$

Substitution of this expression into the Helmholtz equation (4.1) and comparing coefficients of terms in ε^k, $k = 0, 1$ respectively yields the two equations

$$(v_m^{(0)})'' + \frac{\partial^2 V_m^{(0)}}{\partial Y^2} + \frac{\omega_0^2}{c_j^2} v_m^{(0)} = 0, \quad m = 1, 2, 3, 4; \quad j = 1, 2, \tag{4.9}$$

$$(v_m^{(1)})'' + \frac{\partial^2 V_m^{(1)}}{\partial Y^2} + \frac{\omega_1^2}{c_j^2} v_m^{(0)} + \frac{\omega_0^2}{c_j^2} v_m^{(1)} = 0, \quad m = 1, 2, 3, 4; \quad j = 1, 2. \tag{4.10}$$

Expression (4.9) corresponding to terms in $k = 0$ is the same as before when ω was not treated as an asymptotic series, but (4.10) is new. Above and below the crack, that is for $m = 2, 3$, we therefore have that

$$\frac{\partial^2 V_m^{(1)}}{\partial Y^2} = -\left[(v_m^{(1)})'' + \frac{\omega_1^2}{d_m^2} v_m^{(0)} + \frac{\omega_0^2}{d_m^2} v_m^{(1)}\right], \quad m = 2, 3, \tag{4.11}$$

where $d_2 = c_1$ and $d_3 = c_2$, which after integration and application of the boundary condition $\left.\frac{\partial V_m^{(1)}}{\partial Y}\right|_{Y=0\pm} \equiv 0$ yields the equation

$$(v_m^{(1)})''(x) + \frac{\omega_0^2}{d_m^2} v_m^{(1)}(x) + \frac{\omega_1^2}{d_m^2} v_m^{(0)}(x) = 0, \quad m = 2, 3. \tag{4.12}$$

For $m = 1, 4$ (where no crack is present), rearranging and integrating (4.10) and applying the condition for continuity of tractions across the imperfect interface yields the equation

$$(v_m^{(1)})''(x) + \frac{\omega_0^2}{d^2} v_m^{(1)}(x) + \frac{\omega_1^2}{d^2} v_m^{(0)}(x) = 0, \tag{4.13}$$

where as in the preceding chapter

$$d = c_1 c_2 \sqrt{\frac{\mu_1 H_1 + \mu_2 H_2}{\mu_1 H_1 c_2^2 + \mu_2 H_2 c_1^2}}. \tag{4.14}$$

For the zero order approximation,

$$(v_m^{(0)})''(x) + \frac{\omega_0^2}{d_m^2} v_m^{(0)}(x) = 0, \quad m = 1, 2, 3, 4. \tag{4.15}$$

4.3.1 Junction conditions and crack tip asymptotics

The asymptotic representation of ω does not affect junction conditions on the first two levels of the approximation. Junction conditions for the zero order approximation have been derived in Chapter 3 and read

$$v_1^{(0)}(x_A) = v_2^{(0)}(x_A) = v_3^{(0)}(x_A); \quad v_2^{(0)}(x_B) = v_3^{(0)}(x_B) = v_4^{(0)}(x_B), \tag{4.16}$$

along with the conditions for flux

$$\mu_1 H_1 (v_2^{(0)})'(x_A) + \mu_2 H_2 (v_3^{(0)})'(x_A) = (\mu_1 H_1 + \mu_2 H_2)(v_1^{(0)})'(x_A). \tag{4.17}$$

$$\mu_1 H_1 (v_2^{(0)})'(x_B) + \mu_2 H_2 (v_3^{(0)})'(x_B) = (\mu_1 H_1 + \mu_2 H_2)(v_4^{(0)})'(x_B). \tag{4.18}$$

The junction conditions for the first order approximation at the right hand crack tip are given for $m = 2, 3$, by

$$v_m^{(1)}(x_B) = v_4^{(1)}(x_B) + (-1)^{m+1} \frac{\mu_2 H_2}{\mu_1 H_1 + \mu_2 H_2} \alpha_N \Delta\{(v^{(0)})'\}(x_B), \tag{4.19}$$

where by α_N we mean α_P if $\kappa = 0$ (the perfect interface case) and α_I if $\kappa > 0$ (the imperfect interface case), and

$$\Delta\{(v^{(0)})'\}(x) = (v_2^{(0)})'(x) - (v_3^{(0)})'(x). \tag{4.20}$$

The junction conditions (4.19) are valid for both perfect and imperfect cases, but the form of the corresponding constants α_P and α_I are absolutely different and come from different analyses; this arises from the fact that the problem is singularly perturbed and so different analysis is needed in the cases $\kappa > 0$ to the case $\kappa = 0$. The definition of the constant α_P is given in [44] while the constant α_I was derived in the previous chapter of this thesis; both are stated below. For the perfect interface case, the constant is defined

as

$$\alpha_P = \frac{H_1 + H_2}{\pi} \left\{ \mu_* \int_0^\infty f(t)\mathrm{d}t - \ln \left\{ \left(\frac{1+H_*}{2} \right)^{\frac{1+H_*}{2}} \left(\frac{1-H_*}{2} \right)^{\frac{1-H_*}{2}} \right\} \right\}, \tag{4.21}$$

where

$$f(t) = \frac{H_* - \tanh(tH_*)\coth(t)}{(\sinh(t) + \mu_* \sinh(tH_*))t}, \quad \mu_* = \frac{\mu_1 - \mu_2}{\mu_1 + \mu_2}, \quad H_* = \frac{H_1 - H_2}{H_1 + H_2}. \tag{4.22}$$

In the imperfect interface case, the constant is given by

$$\alpha_I = (H_1 + H_2) \left\{ \frac{1}{\pi} \int_0^\infty \frac{\ln g(t)}{t^2} \mathrm{d}t + \frac{1}{\lambda_*} \right\}, \tag{4.23}$$

where

$$g(t) = \frac{t}{\lambda_*^2 + t^2} \left(t + \frac{2}{\kappa_*(1+\mu_*)} \coth \frac{t(1+H_*)}{2} + \frac{2}{\kappa_*(1-\mu_*)} \coth \frac{t(1-H_*)}{2} \right), \tag{4.24}$$

$$\lambda_* = (H_1 + H_2) \sqrt{\frac{\mu_1 H_1 + \mu_2 H_2}{\mu_1 \mu_2 H_1 H_2 \kappa}}, \quad \kappa_* = \frac{\kappa(\mu_1 + \mu_2)}{(H_1 + H_2)}. \tag{4.25}$$

We stress that α_I is a constant that depends heavily upon κ and so describes how the junction conditions are impacted by the imperfect interface. The first order fluxes satisfy the relationship

$$(\mu_1 H_1 + \mu_2 H_2)(v_4^{(1)})'(x_B) - \mu_1 H_1 (v_2^{(1)})'(x_B) - \mu_2 H_2 (v_3^{(1)})'(x_B) = 0. \tag{4.26}$$

The analogous conditions for $m = 2, 3$, at the other vertex can be obtained by replacing B by A and $m+1$ by m in equation (4.19). The other crack tip's condition for fluxes is as in equation (4.26), but again replacing B by A.

The zero order and first order constants describing the singular behaviour of the full solution near the crack tips derived for the perfect and imperfect

interface cases are unaffected by the consideration of ω as an asymptotic series. However, if one continues to deeper levels of the asymptotics, the junction conditions of fifth order and higher would be affected by taking ω as an asymptotic series.

4.3.2 Corrected low dimensional model

Zero order low dimensional model

Solutions of the zero order equation (4.15) for $m = 1, 2, 3, 4$ are of the form

$$v_m^{(0)}(x) = A_m^{(0)} \sin\left(\frac{\omega_0}{d_m}x\right) + B_m^{(0)} \cos\left(\frac{\omega_0}{d_m}x\right), \tag{4.27}$$

The first order equation (4.15) has solutions in the form

$$v_m^{(1)}(x) = A_m^{(1)} \sin\left(\frac{\omega_0}{d_m}x\right) + B_m^{(1)} \cos\left(\frac{\omega_0}{d_m}x\right) + \omega_1^2 F_m(x), \tag{4.28}$$

where

$$F_m(x) = \frac{x}{2d_m\omega_0}\left\{A_m^{(0)} \cos\left(\frac{\omega_0}{d_m}x\right) - B_m^{(0)} \sin\left(\frac{\omega_0}{d_m}x\right)\right\}. \tag{4.29}$$

We note that assuming the zero order system has been solved, all constants in this expression for $F_m(x)$ are considered known.

Let us first consider the zero order case. We see from (4.27) that eight constants need to be evaluated, $A_m^{(0)}$ and $B_m^{(0)}$ for $m = 1, 2, 3, 4$ which we write in the column vector $A^{(0)}$ defining the notation

$$A^{(k)} = \left[\begin{array}{cccccccc} A_1^{(k)} & B_1^{(k)} & A_2^{(k)} & B_2^{(k)} & A_3^{(k)} & B_3^{(k)} & A_4^{(k)} & B_4^{(k)} \end{array}\right]^T. \tag{4.30}$$

We have six junction conditions to apply: two from (4.16) and one from each of (4.17) and (4.18), which can be complemented by the two Bloch-Floquet conditions to yield the 8×8 matrix equation

$$M_{8\times 8} A^{(0)} = 0. \tag{4.31}$$

We introduce notation to abbreviate the entries of $M_{8\times 8}$ as follows:

$$S_m = \sin\left(\frac{d}{d_m}\varpi_0 x_B\right); \quad C_m = \sin\left(\frac{d}{d_m}\varpi_0 x_B\right); \quad m = 1,2,3,4; \tag{4.32}$$

$$\psi_j = \frac{\mu_j H_j}{\mu_1 H_1 + \mu_2 H_2}\frac{d}{d_{j+1}};\ j = 1,2;\ S_a = \sin\left(\varpi_0\frac{a}{2}\right); C_a = \cos\left(\varpi_0\frac{a}{2}\right), \tag{4.33}$$

where $\varpi_j = \omega_j/d$ is introduced for normalisation. Now, $M_{8\times 8} =$

$$\begin{bmatrix}
0 & 0 & S_2 & C_2 & 0 & 0 & -S_4 & -C_4 \\
0 & 0 & 0 & 0 & S_3 & C_3 & -S_4 & -C_4 \\
0 & 0 & \psi_1 C_2 & -\psi_1 S_2 & \psi_2 C_3 & -\psi_2 S_3 & -C_4 & S_4 \\
-S_1 & -C_1 & S_2 & C_2 & 0 & 0 & 0 & 0 \\
S_1 & -C_1 & 0 & 0 & -S_3 & C_3 & 0 & 0 \\
-C_1 & -S_1 & \psi_1 C_2 & \psi_1 S_2 & \psi_2 C_3 & \psi_2 S_3 & 0 & 0 \\
-S_a & C_a & 0 & 0 & 0 & 0 & -e^{-iKa}S_a & -e^{-iKa}C_a \\
C_a & S_a & 0 & 0 & 0 & 0 & -e^{-iKa}C_a & e^{-iKa}S_a
\end{bmatrix} \tag{4.34}$$

The determinant of $M_{8\times 8}$ can be written in the form

$$\det(M_{8\times 8}) = \mathcal{A}(\omega_0)e^{-2iKa} + \mathcal{B}(\omega_0)e^{-iKa} + \mathcal{A}(\omega_0). \tag{4.35}$$

It can be shown that for the case in which all wave speeds d_m are equal to d, say, both $\mathcal{A}(\omega_0)$ and $\mathcal{B}(\omega_0)$ are zero when $\omega_0 = n\pi d/(2x_B)$, $n \in \mathbb{N}$. It follows that in this case, the standing waves have no dependence upon the Bloch-Floquet parameter K. This observation motivates us to consider the special case discussed in Subsection 4.4.1.

First order low dimensional model

Applying the junction and Bloch-Floquet conditions for the first order equation (4.15) yields the matrix equation

$$M_{8\times 8}A^{(1)} = \varpi_1^2 N_{8\times 8}A^{(0)} + B_A\Delta\{(v^{(0)})'\}(x_A) + B_B\Delta\{(v^{(0)})'\}(x_B). \quad (4.36)$$

Here, $M_{8\times 8}$ is the matrix defined in (4.34), $A^{(0)}$ and $A^{(1)}$ are the coefficients defined in (4.30). Since $M_{8\times 8}$, is singular, this equation gives a solvability condition which will allow us to find the correction term, ω_1. The matrix $N_{8\times 8}$ is defined as

$$\begin{bmatrix}
0 & 0 & \frac{-dx_BC_2}{2d_2\varpi_0} & \frac{dx_BS_2}{2d_2\varpi_0} & 0 & 0 & \frac{x_BC_4}{2\varpi_0} & \frac{-x_BS_4}{2\varpi_0} \\
0 & 0 & 0 & 0 & \frac{-dx_BC_3}{2d_3\varpi_0} & \frac{dx_BS_3}{2d_3\varpi_0} & \frac{x_BC_4}{2\varpi_0} & \frac{-x_BS_4}{2\varpi_0} \\
0 & 0 & N_{3,3} & N_{3,4} & N_{3,5} & N_{3,6} & N_{3,7} & N_{3,8} \\
\frac{-x_BC_1}{2\varpi_0} & \frac{-x_BS_1}{2\varpi_0} & \frac{dx_BC_2}{2d_2\varpi_0} & \frac{dx_BS_2}{2d_2\varpi_0} & 0 & 0 & 0 & 0 \\
\frac{-x_BC_1}{2\varpi_0} & \frac{-x_BS_1}{2\varpi_0} & 0 & 0 & \frac{dx_BC_3}{2d_3\varpi_0} & \frac{dx_BS_3}{2d_3\varpi_0} & 0 & 0 \\
N_{6,1} & N_{6,2} & N_{6,3} & N_{6,4} & N_{6,5} & N_{6,6} & 0 & 0 \\
\frac{aC_a}{4\varpi_0} & \frac{aS_a}{4\varpi_0} & 0 & 0 & 0 & 0 & \frac{aZC_a}{4\varpi_0} & \frac{-aZS_a}{4\varpi_0} \\
N_{8,1} & N_{8,2} & 0 & 0 & 0 & 0 & N_{8,7} & N_{8,8}
\end{bmatrix} \quad (4.37)$$

where $Z = e^{-iKa}$ and for $q \in \{3,4,5,6,7,8\}$,

$$\begin{aligned}
N_{3,q} &= \frac{d}{d_{\lfloor\frac{q+1}{2}\rfloor}}x_B\left(\left(\frac{1+(-1)^q}{2}\right)C_{\lfloor\frac{q+1}{2}\rfloor} + \left(\frac{1-(-1)^q}{2}\right)S_{\lfloor\frac{q+1}{2}\rfloor}\right) \\
&- \frac{1}{\varpi_0}\left(\left(\frac{1-(-1)^q}{2}\right)C_{\lfloor\frac{q+1}{2}\rfloor} - \left(\frac{1+(-1)^q}{2}\right)S_{\lfloor\frac{q+1}{2}\rfloor}\right). \quad (4.38)
\end{aligned}$$

Here, the notation $\lfloor\cdot\rfloor$ denotes the usual floor function. For $q \in \{1,2,3,4,5,6\}$,

$$\begin{aligned}
N_{6,q} &= \frac{(-1)^{q+1}d}{d_{\lfloor\frac{q+1}{2}\rfloor}}x_B\left(\left(\frac{1+(-1)^q}{2}\right)C_{\lfloor\frac{q+1}{2}\rfloor} + \left(\frac{1-(-1)^q}{2}\right)S_{\lfloor\frac{q+1}{2}\rfloor}\right) \\
&+ \frac{(-1)^q}{\varpi_0}\left(\left(\frac{1-(-1)^q}{2}\right)C_{\lfloor\frac{q+1}{2}\rfloor} - \left(\frac{1+(-1)^q}{2}\right)S_{\lfloor\frac{q+1}{2}\rfloor}\right), \quad (4.39)
\end{aligned}$$

and the expressions of the eighth row are given by

$$N_{8,1} = \frac{a}{4}S_a - \frac{1}{2\varpi_0}C_a, \quad N_{8,2} = \frac{1}{2\varpi_0}S_a - \frac{a}{4}C_a, \tag{4.40}$$

$$N_{8,7} = e^{-iKa}\left(\frac{1}{2\varpi_0}C_a - \frac{a}{4}S_a\right), \quad N_{8,8} = -e^{-iKa}\left(\frac{1}{2\varpi_0}S_a + \frac{a}{4}C_a\right). \tag{4.41}$$

The vectors B_A and B_B are given by

$$B_A = \alpha_N \left[\begin{array}{cccccccc} 0 & 0 & 0 & -\frac{\mu_2 H_2}{\mu_1 H_1 + \mu_2 H_2} & \frac{\mu_1 H_1}{\mu_1 H_1 + \mu_2 H_2} & 0 & 0 & 0 \end{array}\right]^T, \tag{4.42}$$

$$B_B = \alpha_N \left[\begin{array}{cccccccc} -\frac{\mu_2 H_2}{\mu_1 H_1 + \mu_2 H_2} & \frac{\mu_1 H_1}{\mu_1 H_1 + \mu_2 H_2} & 0 & 0 & 0 & 0 & 0 & 0 \end{array}\right]^T. \tag{4.43}$$

To conclude this section, we have obtained a matrix equation (4.36) involving the correction term ϖ_1^2. In the following section, we will solve this equation, firstly for a simple special case which allows a closed-form solution to be obtained, before considering the general case.

4.4 Derivation of first order correction term, ω_1

4.4.1 Homogeneous symmetric case

In this section, we condsider the symmetric case in which $H_1 = H_2$ and $\mu_1 = \mu_2$. This simple case is instructive since the symmetry enables us to analytically determine the eigenfrequency of the first standing wave in an easily traceable process; we will later make indications on how the method for the general case relates to and differs from this procedure. Moreover, this eigenfrequency does not have any K-dependence as is the case for inhomogeneous setups, which enables us to easily separate the first standing wave solution

from the others. In the case of the standing wave, the beams above and below the crack vibrate while the others do not (that is, $v_1^{(k)}(x) = v_4^{(k)}(x) = 0$ for $k = 0, 1$).

The problem formulation for the symmetric case is as follows. For the zero order approximation, solutions satisfy (4.15) with $d_m = d$ for all $m = 1, 2, 3, 4$. To isolate the standing waves (whose frequencies we wish to impose a correction upon) we impose the condition

$$v_1^{(0)}(x) \equiv v_4^{(0)}(x) \equiv 0. \tag{4.44}$$

The junction conditions for the zero order approximation then simplify to

$$v_2^{(0)}(x_A) = v_2^{(0)}(x_B) = 0, \quad v_3^{(0)}(x_A) = v_3^{(0)}(x_B) = 0, \tag{4.45}$$

along with

$$(v_2^{(0)})'(x_A) + (v_3^{(0)})'(x_A) = 0, \quad (v_2^{(0)})'(x_B) + (v_3^{(0)})'(x_B) = 0. \tag{4.46}$$

For $m = 2, 3$, we have that the general solution of the zero order LDM is of the form (4.27) with $d_m = d$. Applying conditions (4.45)-(4.46) yields

$$v_2^{(0)}(x) = B\cos\left(\frac{\omega_0}{d}x\right), \quad v_3^{(0)}(x) = -B\cos\left(\frac{\omega_0}{d}x\right). \tag{4.47}$$

The first order approximation equation is of the form (4.12) with $d_m = d$. Since $v_m^{(0)}$ are now known functions, the corresponding system consists of the two ordinary differential equations

$$(v_2^{(1)})''(x) + \frac{\omega_0^2}{d^2}v_2^{(1)}(x) + \frac{\omega_1^2}{d^2}B\cos\left(\frac{\omega_0}{d}x\right) = 0, \tag{4.48}$$

$$(v_3^{(1)})''(x) + \frac{\omega_0^2}{d^2}v_3^{(1)}(x) - \frac{\omega_1^2}{d^2}B\cos\left(\frac{\omega_0}{d}x\right) = 0. \tag{4.49}$$

These ODEs have respective elementary solutions

$$v_2^{(1)}(x) = A_2^{(1)}\sin\left(\frac{\omega_0}{d}x\right) + B_2^{(1)}\cos\left(\frac{\omega_0}{d}x\right) - \omega_1^2\frac{Bx\sin\left(\frac{\omega_0}{d}x\right)}{2\omega_0 d}, \tag{4.50}$$

$$v_3^{(1)}(x) = A_3^{(1)} \sin\left(\frac{\omega_0}{d}x\right) + B_3^{(1)} \cos\left(\frac{\omega_0}{d}x\right) + \omega_1^2 \frac{Bx \sin\left(\frac{\omega_0}{d}x\right)}{2\omega_0 d}, \qquad (4.51)$$

complemented by the junction conditions (which follow from the previous chapter)

$$v_m^{(1)}(x_\beta) = \frac{(-1)^{m+p}}{2}\alpha_N \Delta\left\{(v^{(0)})'\right\}(x_\beta), \quad m = 2, 3;\ \beta = A, B, \qquad (4.52)$$

where $p = 0$ if $\beta = A$ and $p = 1$ if $\beta = B$.

For the first standing wave, $\omega_0 = \pi d/l$, and so applying (4.52) with $\beta = B$, $m = 2$, we see that

$$A_2^{(1)} = B\left(\omega_1^2 \frac{l^2}{4\pi d^2} + \frac{\pi \alpha_N}{l}\right). \qquad (4.53)$$

Applying the condition (4.52) with $\beta = A$, $m = 2$, yields the condition

$$A_2^{(1)} = -B\left(\omega_1^2 \frac{l^2}{4\pi d^2} + \frac{\pi \alpha_N}{l}\right). \qquad (4.54)$$

Summing equations (4.53) and (4.54), we see that $A_2^{(1)} = 0$, and deduce that

$$\omega_1^2 = -\frac{4\pi^2 d^2 \alpha_N}{l^3}. \qquad (4.55)$$

Thus, for the symmetrical case where both materials are the same, we have found an expression for the correction term ω_1^2. Note that in this case, $\omega_1^2 < 0$; we remind the reader that the asymptotic expansion used was

$$\omega^2 = \omega_0^2 + \varepsilon\omega_1^2 + O(\varepsilon^2) \qquad (4.56)$$

and so the negative sign of ω_1^2 indicates that the correction decreases the standing wave eigenfrequency.

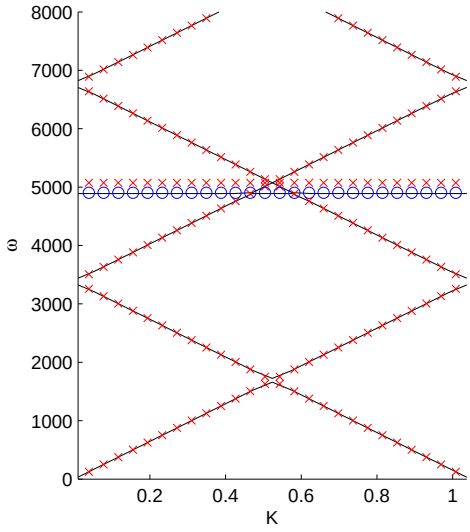

Figure 4.1: Dispersion diagram for the perfect interface case with medium crack length $l = 2$m in an elementary cell with $a = 6$m. The material above and below the crack is iron. The solid black lines show finite element results, while red crosses ($\times$) show the zero order approximation and blue circles ($\circ$) show the corrected regime, with the first standing wave corrected by the analytic derivation of ω_1 as presented in equation (4.55).

Figure 4.1 shows the dispersion diagram for this homogeneous, symmetric case. The red crosses on the diagram indicate the zero order approximation (ω_0) of the eigenfrequencies, while the blue circles show the corrected first order approximation. The black lines result from a finite element computation. The derived correction method improves the standing wave frequency discrepancy from 3.7% to just 0.26%.

4.4.2 General case

We now consider the general case in which the materials above and below the crack and interface may have different thicknesses and shear moduli. For the first order approximation, after the application of junction and Bloch-Floquet conditions we obtain a matrix equation of the form

$$MA^{(1)} = \omega_1^2 NA^{(0)} + B_A \Delta\{(v^{(0)})'\}(x_A) + B_B \Delta\{(v^{(0)})'\}(x_B). \tag{4.57}$$

Here, M and N are both 8×8 matrices as defined earlier in (4.34) and (4.37) respectively whose elements depend on the Bloch-Floquet parameter K and the eigenfrequency ω_0 which is such that $\det(M) = 0$. Because $\det(M) = 0$, M has zero among its eigenvalues. We can write

$$M = VDV^{-1} \tag{4.58}$$

where V is a matrix whose columns are eigenvectors of M and D is a diagonal matrix with the respective eigenvalues of M along the diagonal. Premultiplying (4.57) by V^{-1}, we can write

$$V^{-1}MVV^{-1}A^{(1)} = V^{-1}(\omega_1^2 NA^{(0)} + B_A \Delta\{(v^{(0)})'\}(x_A) + B_B \Delta\{(v^{(0)})'\}(x_B)), \tag{4.59}$$

which upon substitution of (4.58) becomes

$$DV^{-1}A^{(1)} = \omega_1^2 V^{-1}NA^{(0)} + V^{-1}B_A \Delta\{(v^{(0)})'\}(x_A) + V^{-1}B_B \Delta\{(v^{(0)})'\}(x_B). \tag{4.60}$$

Since M is singular, it posesses zero as an eigenvalue, and so one row of the left hand side matrix in (4.60) is equal to zero. Let us denote that row l. Then

$$\omega_1^2 \left(V^{-1}NA^{(0)}\right)_l + \left(V^{-1}B_A\right)_l \Delta\{(v^{(0)})'\}(x_A) + \left(V^{-1}B_B\right)_l \Delta\{(v^{(0)})'\}(x_B) = 0. \tag{4.61}$$

All matrices and parameters in this equation are now known, with the exception of ω_1^2 which can now be written in terms of known quantities:

$$\omega_1^2 = -\frac{\left(V^{-1}(B_A\Delta\{(v^{(0)})'\}(x_A) + B_B\Delta\{(v^{(0)})'\}(x_B))\right)_l}{(V^{-1}NA^{(0)})_l}. \tag{4.62}$$

A potential problem with this computational method is that the matrix V may have a determinant which is close to zero when eigenvalues of M are close together. To eliminate any possible errors arising from this, we introduce a second computational scheme for computing ω_1.

The Schur decomposition states that if A is a $n \times n$ square matrix with complex entries, then A can be expressed in the form $A = QUQ^{-1}$ where Q is unitary and U is upper triangular, with the eigenvalues of A. In our case, we apply Schur decomposition to the transpose of M:

$$M^T = QUQ^{-1}. \tag{4.63}$$

Schur decomposition is not unique; we may place the smallest eigenvalue in the first position along the leading diagonal, and since M is singular, this eigenvalue is zero. The first column of the upper triangular matrix U is therefore a row of zeros. Since $M = (Q^{-1})^T U^T Q^T$, we can premultiply the first order matrix equation by Q^T and substutite to obtain

$$U^T Q^T A^{(1)} = \omega_1^2 Q^T N A^{(0)} + Q^T B_A \Delta\{(v^{(0)})'\}(x_A) + Q^T B_B \Delta\{(v^{(0)})'\}(x_B). \tag{4.64}$$

The first row of the left hand side is zero, whence

$$\omega_1^2 = -\frac{\left(Q^T(B_A\Delta\{(v^{(0)})'\}(x_A) + B_B\Delta\{(v^{(0)})'\}(x_B))\right)_1}{(Q^T NA^{(0)})_1}. \tag{4.65}$$

4.5 Numerical results

4.5.1 Materials and geometries used in numerical simulations

For our numerical calculations we will consider a strip whose elementary cell is of length $a = 6\text{m}$ with an overall thickness of $H_1 + H_2 = 0.15\text{m}$. This geometry corresponds to a value of $\varepsilon = 0.025$. We will compare results from the low dimensional model against those from finite element simulations (computed using COMSOL). We stress that finite element simulations are efficient for comparison only in cases when the strip is not too thin, i.e. when ε is not too small. The low dimensional model, however, remains valid as $\varepsilon \to 0$.

For our computations we vary four parameters. These parameters (detailed in the following list) are the type of interface (perfect, imperfect, highly imperfect), length of crack (shorter, medium, longer), materials (iron/aluminium [similar wave speeds], magnesium/aluminium [less similar wave speeds]) and thicknesses of each material (symmetric geometry, asymmetric geometry).

1. **Type of interface**

   - Perfect.
   - Imperfect — in the finite element computations, a thin layer of epoxy resin is used. This corresponds to a value of $\kappa_* = 2.88$ in the asymptotic model (recall that $\kappa_* = \kappa(\mu_1 + \mu_2)/(H_1 + H_2)$ as defined on page 72).
   - Highly imperfect — in this case, the bonding material has a shear modulus a tenth that of epoxy resin. This corresponds to a value of $\kappa_* = 28.8$.

2. **Length of crack**

   - Shorter — Crack length of $l = a/10 = 0.6$m.
   - Medium — Crack length of $l = a/3 = 2$m. This can be viewed as a 'sensible' crack length.
   - Longer — Crack length of $l = 9a/10 = 5.4$m.

3. **Materials**

   - Iron/Aluminium — see Figure 4.2 on page 99 for shear moduli, densities and wave speeds.
   - Magnesium/Aluminium — both materials have similar wave speeds.

4. **Thicknesses of each material**

   - Symmetrical geometry — $\varepsilon H_1 = \varepsilon H_2 = 0.075$m.
   - Asymmetrical geometry — $\varepsilon H_1 = 0.01$m, $\varepsilon H_2 = 0.14$m.

Material	Shear modulus $[\mathrm{Nm}^{-2}]$	Mass density $[\mathrm{kgm}^{-3}]$	Wave speed $[\mathrm{ms}^{-1}]$
Iron	82×10^9	7860	3230
Magnesium	17×10^9	1738	3128
Aluminium	26×10^9	2700	3103
Epoxy resin	2.5×10^9	1850	1162

Figure 4.2: Material parameters used in computations.

We will present in the following subsections a number of dispersion diagrams, plotting frequency ω against the Bloch-Floquet parameter K. We refer to plots of $\omega = \omega_0$ as the zero order approximation, and to plots of ω calculated according to (4.7) (that is, $\omega^2 = \omega_0^2 + \varepsilon\omega_1^2 + O(\varepsilon^2)$) as the first order approximation, or the corrected frequency.

4.5.2 Correction in the perfect interface case

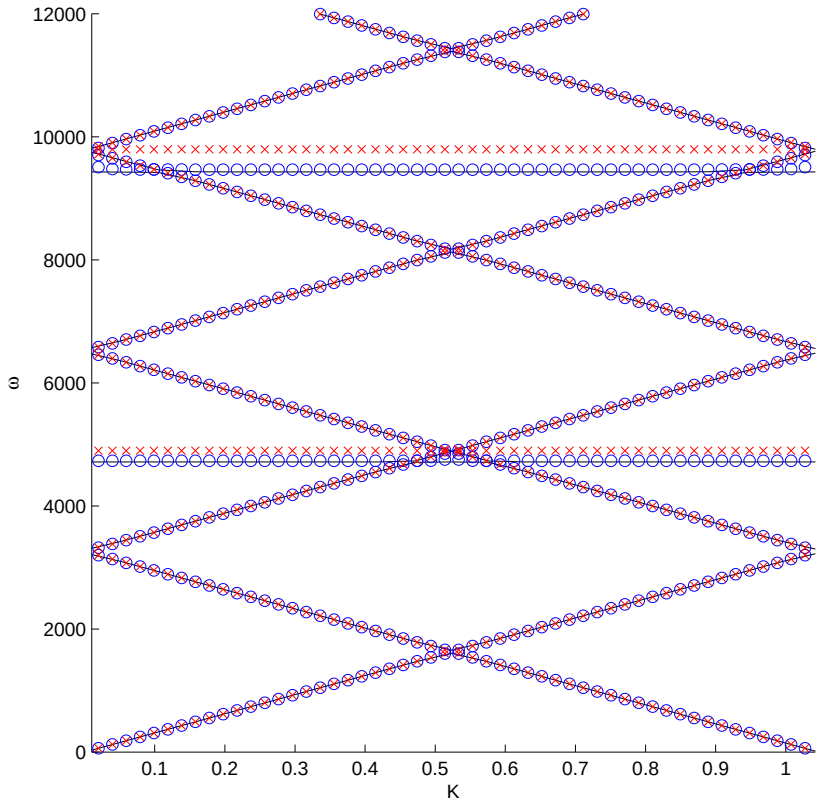

Figure 4.3: Dispersion diagram for a perfect interface strip composed of equal thicknesses of aluminium and magnesium with a medium length crack ($l = 2$m). The solid black lines show the finite element results, while red crosses ($\times$) show the zero order approximation and blue circles ($\circ$) show the corrected first order approximation.

Materials with similar wave speeds

Figure 4.3 demonstrates the effectiveness of the method of eigenfrequency correction for the standing waves. This dispersion diagram results from computations corresponding to the case of a strip with a 'sensible' crack

length, composed of equal thicknesses of magnesium and aluminium (materials possessing similar wave speeds, see the table in Figure 4.2 for the precise values). The diagram demonstrates that the zero order approximation agrees to a very high degree of accuracy with the finite element results in the cases of the waves which propagate through the strip (the slanted lines). Typically the zero order approximation for these waves' eigenfrequencies differs from the finite element simulation only by a factor of around 10^{-6}. However, it is clear that there is a discrepancy between the zero order model and the finite element results in the case of the standing waves (horizontal lines on the dispersion diagram). The corrected first order model retains the excellent accuracy for propagating waves, slightly increasing the accuracy while remaining of the order of 10^{-6}, and significantly improves the discrepancy of the standing wave frequencies. While the correction is not completely uniform since the standing waves' frequencies depend upon the Bloch-Floquet parameter K except in the case where materials have *identical* wave speeds, a typical discrepancy for the first standing wave has decreased from 3.9% to 0.38%. This can be considered as a surprisingly useful correction, since there is no reason *a priori* to suspect that considering ω as an asymptotic quantity should cause such an improvement in the accuracy of the low dimensional model's approximation of the standing wave frequency. The lack of uniformity becomes more clear for the second standing wave than the first, particularly near the edges of the dispersion diagram. We will later see that such effects become more pronounced for materials with more contrasting wave speeds.

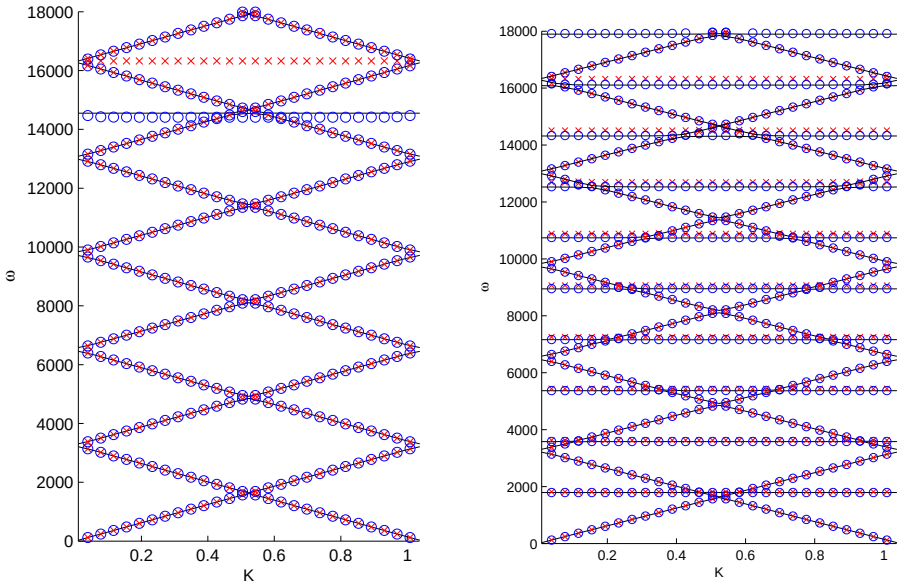

Figure 4.4: Dispersion diagrams for a perfect interface strip composed of equal thicknesses of aluminium and magnesium **Left:** Shorter crack ($l = 0.6$m) **Right:** Longer crack ($l = 5.4$m). The solid black lines show the finite element results, while red crosses ($\times$) show the zero order approximation and blue circles ($\circ$) show the corrected regime.

The dispersion diagrams for the cases with shorter and longer crack lengths, again with materials of similar wave speeds, perfect interfaces and the same thicknesses of both material are contained within Figure 4.4. As one would expect, the length of the crack does not significantly alter the eigenfrequencies of those waves that propagate through the strip (again the correction is on the level of 10^{-6}), since they are not strongly influenced by the presence of the crack. In similar agreement with physical intuition, the first standing wave for the longer crack is of much lower frequency than in the geometry housing the particularly shorter crack. The correction offered by the first order approach is relatively small in the longer crack case, but

since the zero order model in this case already gave good accuracy with only a 1.3% discrepancy for the first standing wave, this is not surprising. The corrected eigenfrequency of this wave agrees with finite element results to within 10^{-5}. This can be seen as a surprisingly effective correction since in the longer crack geometry, the crack tips are close to the ends of the elementary cell. This gives the boundary layers surrounding the crack tips a small area in which to decay so that they do not influence the Bloch-Floquet conditions.

In the case of the shorter crack, the zero order approximation of the first standing wave eigenfrequency is easily seen to be significantly different to the true value found in the finite element simulation, with a 12.2% discrepancy. After applying the correction method, the discrepancy decreases to 0.95%. Together, the computations for the longer and shorter cracks demonstrate that the decay of the boundary layers is sufficiently rapid for them to remain independent even while crack tips are quite close to each other. We will see later (see Figure 4.6 on page 107) that in the imperfect interface case, this is not true when the extent of imperfection is very high and similarly we would expect the model to break down if they crack was much shorter or longer than the lengths used.

We noted in the introduction the assumption that only lower range frequencies are considered by the model, specifically we assume $\omega \ll c_j/\varepsilon$. In this case of the aluminium/magnesium strip with the geometry considered here, we therefore assume that ω is much less than around $1.2 \times 10^5 \mathrm{s}^{-1}$. The dispersion diagrams demonstrate that there are many standing waves with frequencies significantly lower than this value.

4.5.3 Discussion of model limitations

The figures presented in the previous subsection gave results for strips whose materials possessed similar wave speeds and demonstrated that the amended model provides a useful correction. In the remainder of this chapter we will present results in which the correction is less uniform but often still an improvement on the zero order model.

In performing the comparisons between finite element models and the low dimensional model, we have chosen geometric parameters for the strip to be such that it is not too thin to make finite element computations too onerous. The asymptotic model, however, increases in accuracy as $\varepsilon \to 0$. Performing computations using a value for ε that is not *very* small may therefore be pushing the model outside of its designed range of validity. While this causes lack of uniformity in the correction of standing wave eigenfrequencies, especially for higher frequencies, the computations demonstrate that useful information can be obtained with ε outside the originally intended regime.

Moreover, problems can be caused by communicating boundary layers which may occur if their decay is insufficiently rapid. For our analysis we have assumed that boundary layers are independent; this is not always a suitable assumption. For instance, if κ is very large, then the decay of the boundary layer surrounding one crack tip may not be fast enough to maintain independence with the boundary layer surrounding the other crack tip. Moreover, if the cracks are very long then boundary layers surrounding crack tips in one elementary cell may interact with boundary layers surrounding tips of different cracks in adjacent elementary cells.

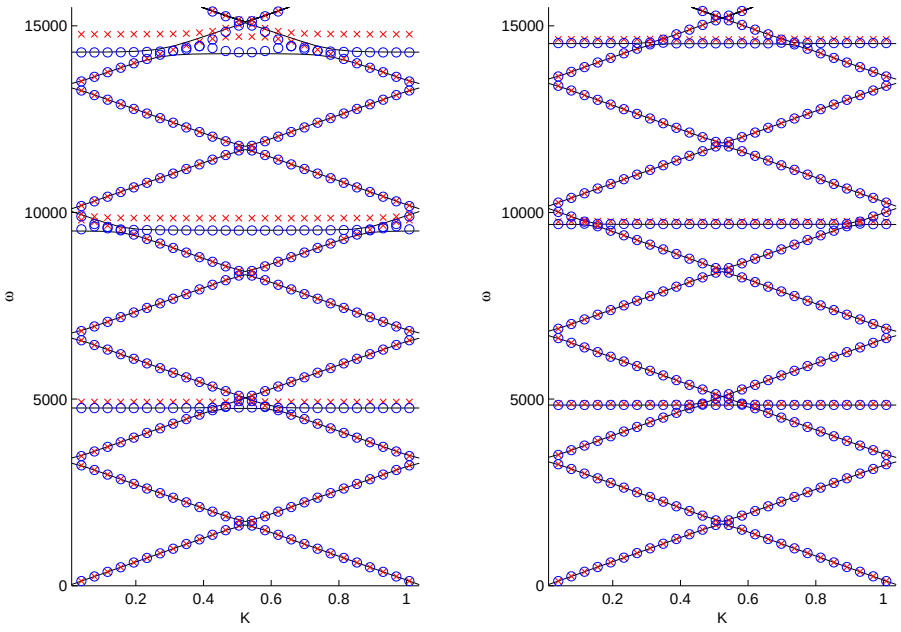

Figure 4.5: Dispersion diagrams for a perfect interface strip composed of aluminium and iron containing a medium-length crack ($l = 2$m). **Left:** Equal thicknesses of iron and aluminium. **Right:** Different thicknesses ($\varepsilon H_1 = 0.01$m thickness of aluminium, $\varepsilon H_2 = 0.14$m thickness of iron). The solid black lines show the finite element results, while red crosses ($\times$) show the zero order approximation and blue circles ($\circ$) show the corrected regime.

Materials with more contrasting wave speeds

We first emphasise that the computations presented in the following figures correspond to $\varepsilon = 0.025$; this is not vanishingly small but allows comparison against finite element simulations. In particular, during the construction of the asymptotic model we made the assumption that $\omega \ll c_j/\varepsilon$ and so when ε is not too small, the model may be pushed near to (or beyond) its range of applicability, especially for higher frequencies. We will see from the following

computations that this often leads to good agreement between finite element simulations and asymptotic model results for at least the first standing wave eigenfrequency, but approximations of the higher frequency eigenfrequencies display less accuracy and uniformity. Despite these limitations, the model continues to give useful predictions in most cases.

The standing wave dispersion diagrams for a strip of aluminium and magnesium are presented in Figure 4.5 on page 105, for both the symmetrical and asymmetrical cases. The correction is largest, as is the zero order discrepancy, in the symmetrical case. However, it is readily seen that the correction is less uniform in the symmetric case, particularly for higher frequencies; due to this lack of uniformity is is harder to quantify the exact size of a typical discrepancy. This can be attributed to the fact that the low dimensional model considers the part of the bi-material elementary cell that does not contain the crack as a single rod; this approximation becomes less appropriate if the two materials of similar thickness have more contrasting wave speeds. In the right-hand subfigure of Figure 4.5 corresponding to the case where the iron is 14 times thicker than the aluminium, the correction maintains its uniformity to higher frequencies, suggesting that this structure (in which most of the thickness is composed of one material) is better modelled as a single rod.

4.5.4 Correction in the imperfect interface case

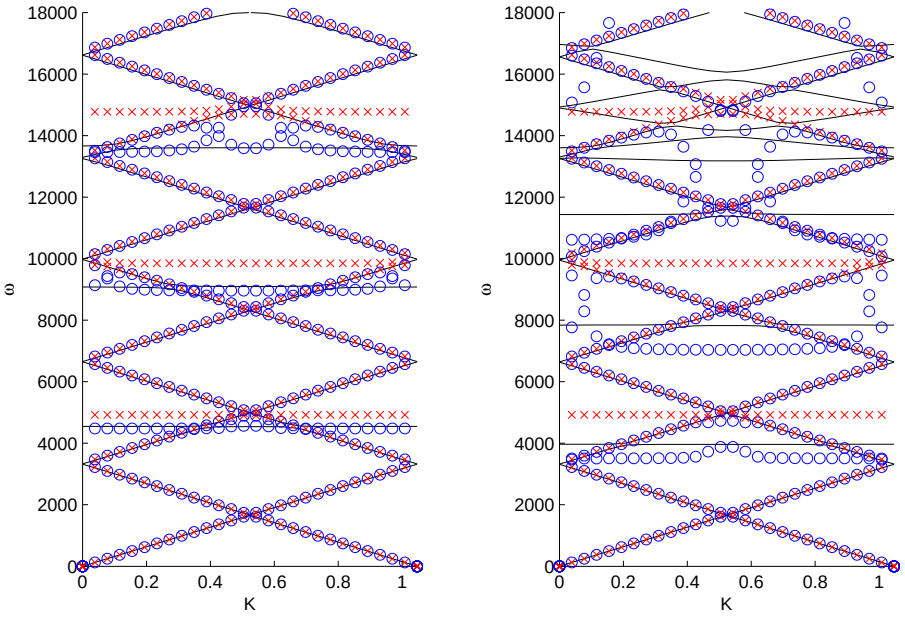

Figure 4.6: Dispersion diagrams for imperfect interface strips composed of equal thicknesses of aluminium and iron **Left:** Bonding material corresponding to epoxy resin ($\kappa_* = 2.88$). **Right:** A highly imperfect interface ($\kappa_* = 28.8$) representing an extremely soft bonding material. This rightmost subfigure demonstrates an example in which the low dimensional model is not effective. The solid black lines show the finite element results, while red crosses ($\times$) show the zero order approximation and blue circles ($\circ$) show the corrected regime.

The results in the case of the imperfect interface analogue follow broadly the same qualitative pattern as in the perfect interface case. The left hand subfigure of Figure 4.6 gives the dispersion diagram for an iron-aluminium strip, joined with a thin layer of epoxy resin adhesive. Due to the different wave speeds, the sizes of the standing wave corrections are dependent on

the Bloch-Floquet parameter K, but in most cases the correction gives a significant improvement in accuracy. An interesting phenomenon can be observed when eigenvalues are close to each other in this subfigure; a zoomed section of the dispersion diagram to illustrate this is given in Figure 4.7. In Figure 4.7, some of the circles have been replaced by squares; these are the points which approximated propagating waves in the zero order model which are corrected to approximate the standing waves for some values of K. In doing so, a crossing-over phenomenon occurs, where the order of eigenfrequencies switches after correction. The phenomenon becomes more pronounced at higher frequencies and indicate that the parameters have been pushed outside the limitations of the model's validity.

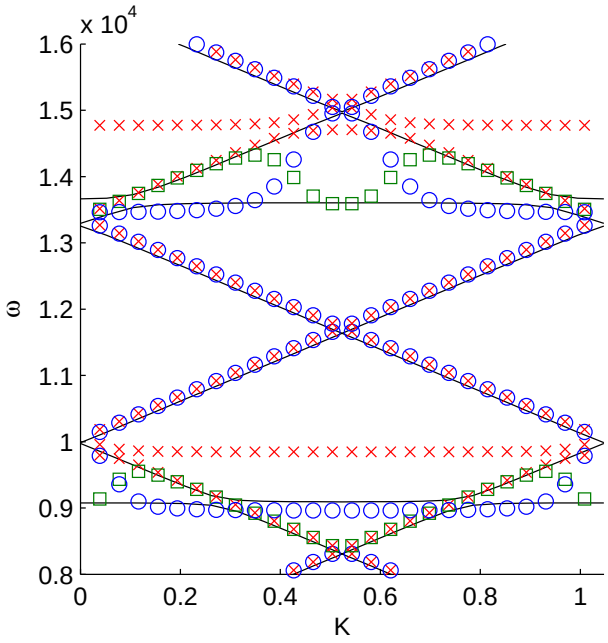

Figure 4.7: Zoomed section of the imperfect interface case, showing how the eigenfrequency correction method causes a crossing-over phenomenon.

The right hand figure of Figure 4.6 corresponds to a case where the materials are bonded in a highly imperfect fashion, using an adhesive with a shear modulus just a tenth that of the epoxy resin whose parameters are given in Figure 4.2 (i.e. a material with shear modulus $2.5 \times 10^8 \mathrm{Nm}^{-2}$ and mass density $1850 \mathrm{kgm}^{-3}$). This subfigure serves the purpose of presenting a case in which the low dimensional model ceases to provide entirely useful approximations. Here the finite element simulation displays qualitatively different features which the low dimensional model does not predict at all. The fact that the low dimensional model breaks down is not surprising; we found a required condition on κ in Section 3.4 on page 78 for the analysis on which the low dimensional model is based to be valid. The key point of this condition is that if κ is too large, the boundary layers W_A and W_B (see equation (4.5) on page 83) decay sufficiently slowly for the assumption that they are independent to cease to hold. Moreover, if the boundary layers decay slowly from the crack tip, the Bloch-Floquet conditions will be influenced by the boundary layers. This case is interesting in itself and requires separate analysis; the phenomenon has been discussed in [5].

4.5.5 Conclusions

The comparisons between the low dimensional model and the finite element simulations demonstrate that the proposed method of eigenfrequency correction is highly effective in most cases, typically improving accuracy for the standing wave eigenfrequency by an order of magnitude for setups where ε is not too small and even where crack tips are close to each other. Thus the corrected model continues to give useful information in setups where the parameters are being pushed near to the limits of the model's range

of validity. Moreover, the correction itself is computationally very efficient. The correction becomes less uniform for materials with significantly different wave speeds, improving the accuracy by different amounts in different parts of the dispersion diagram, and misses qualitative features for setups with highly imperfect interfaces. Practically, however, such highly imperfect interfaces are unlikely to be encountered. Fracture parameters are not affected by the analysis and for that reason are omitted in this chapter and refer the reader to [44] and the previous chapter of this thesis, where discussions and details relating to these parameters can be found. We only underline here that SIF (in the perfect interface case) or imperfect interface analogues can be constructed as functionals on the low dimensional model without further work.

Chapter 5

Weight function and perturbation analysis for a crack and imperfect interface in a bi-material plane

5.1 Introduction

In this chapter we consider a problem of out-of-plane shear in the whole plane (as opposed to the strip geometries in which we have hitherto formulated problems), with different materials occupying the regions above and below the crack line. The geometry considered contains a semi-infinite crack situated along an imperfect interface; we will formulate and solve a weight funtion problem in this geometry. By using Betti's identity in the imperfect interface case, we will use the weight function to derive important constants in a related physical problem. We then conduct perturbation analysis to de-

termine how the presence of small defects in the material affects the stresses near the main crack tip.

5.2 Formulation

5.2.1 Physical formulation

We consider an infinite two-phase plane with an imperfect interface positioned along the x-axis. A semi-infinite crack is placed occupying the line $\{(x, y) : x < 0, y = 0\}$. We refer to the half-planes respectively above and below the crack and interface as $\Pi^{(1)}$ and $\Pi^{(2)}$. The material occupying $\Pi^{(j)}$ has shear modulus μ_j and mass density ρ_j for $j = 1, 2$. The out-of-plane shear displacement function u satisfies the Laplace equation

$$\nabla^2 u(x, y) = 0. \tag{5.1}$$

The plane also contains a micro-defect whose centre is at the point $\boldsymbol{Y}$; we will consider in particular elliptic inclusions although other types of defect may be incorporated into the model provided a suitable dipole matrix can be obtained (see for example the paper of Piccolroaz [45] in which micro-cracks and rigid line inclusions are considered). The defect g_ε has shear modulus μ_{in}, is placed at a distance d from the crack tip, makes an angle ϕ with the imperfect interface and is oriented at an angle α to the horizontal as shown in Figure 5.1. The value of μ_{in} may be greater than or less than the value of μ_{out} (which may be μ_1 or μ_2 depending where the defect is placed), and so both stiff and soft defects can be considered.

We assume continuity of tractions across the crack and interface, and

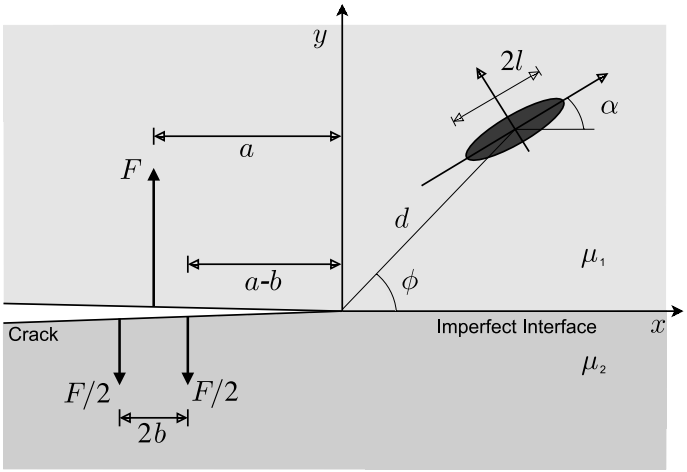

Figure 5.1: Geometry for the physical setup. The crack tip is placed at the origin of an infinite plane composed of materials with shear modulus μ_j occupying half-planes $\Pi^{(j)}$ above and below the the crack and imperfect interface for $j = 1, 2$. The central point $\mathbf{Y}$ of a micro-defect is situated at a distance d from the tip of the main crack.

introduce imperfect interface conditions ahead of the crack:

$$\mu_1 \left.\frac{\partial u}{\partial y}\right|_{y=0+} = \mu_2 \left.\frac{\partial u}{\partial y}\right|_{y=0-}, \quad x > 0, \tag{5.2}$$

$$[\![u]\!] - \kappa\mu_1 \left.\frac{\partial u}{\partial y}\right|_{y=0+} = 0, \quad x > 0, \tag{5.3}$$

where (as in the previous chapters) the notation $[\![u]\!]$ defines the jump in displacement across $y = 0$, i.e. $[\![u]\!](x) = u_1(x, 0^+) - u_2(x, 0^-)$. The parameter $\kappa > 0$ describes the extent of imperfection of the interface, with larger κ corresponding to more imperfect interfaces. We further impose prescribed tractions $p_\pm$ on the crack faces:

$$\mu_1 \left.\frac{\partial u}{\partial y}\right|_{y=0+} = p_+(x), \qquad \mu_2 \left.\frac{\partial u}{\partial y}\right|_{y=0-} = p_-(x); \quad x < 0. \tag{5.4}$$

These tractions are assumed to be self-balanced; that is

$$\int_{-\infty}^{0} p_+(x)\mathrm{d}x - \int_{-\infty}^{0} p_-(x)\mathrm{d}x = 0, \tag{5.5}$$

and it is further assumed that $p_\pm(x)$ vanishes in a neighbourhood of the crack tip. Although the techniques we will establish can be applied to any permissible loading, we will particularly focus our attention on the case where these loadings are point loadings, with a loading on the upper crack face positioned at $x = -a$ (where $a > 0$) balanced by two equal point loadings on the lower crack face positioned at $x = -a - b$ and $x = -a + b$, where $0 < b < a$. This loading makes computations more difficult to perform than for the smooth loadings considered by Antipov *et al.* [1], but is more illustrative for showing the asymmetry of the load.

Near the crack tip as $r \to 0$, the physical displacement behaves as

$$u_j(r,\theta) = \frac{(-1)^{j+1}a_0}{\pi\mu_j}\left\{\frac{\mu_1\mu_2\kappa\pi}{\mu_1+\mu_2} + \left(1 - \ln\left(\frac{r}{b_0}\right)\right) r\cos\theta \right. \\ \left. + (-1)^{j+1}(\pi + (-1)^j\theta) r\sin\theta\right\} + O(r^2\ln^2 r), \quad (5.6)$$

as demonstrated by Mishuris in [40]. It follows that the displacement jump is approximated by

$$[\![u]\!](x) = \kappa a_0 + O(x\ln|x|), \quad x \to 0^{\pm}, \tag{5.7}$$

as the crack tip is approached along the x-axis.

In the neighbourhood of the crack tip, the out-of-plane component of stress behaves as

$$\sigma_j \sim \frac{(-1)^j}{\pi}\left\{a_0 \ln r \sin\theta + c_0\sin\theta + (-1)^j a_0(\pi + (-1)^j\theta)\cos\theta\right\}, \quad r \to 0, \tag{5.8}$$

in the usual polar co-ordinate system and so along the interface,

$$\sigma \sim a_0, \quad x \to 0^+. \tag{5.9}$$

These estimates demonstrate that Fourier transforms of the displacement jump and out-of-plane stress components can be taken, which implies that as $\xi \to \infty$:

$$[\![\bar{u}]\!](\xi) = -\kappa a_0 i\xi^{-1} + O(\xi^{-(1+\delta)}), \quad \xi \to \infty, \quad \delta > 0. \tag{5.10}$$

Moreover, along the axis, the out-of-plane stress component decays as

$$\bar{\sigma} = a_0 i\xi^{-1} + O(\xi^{-(1+\delta)}), \quad \xi \to \infty, \quad \delta > 0. \tag{5.11}$$

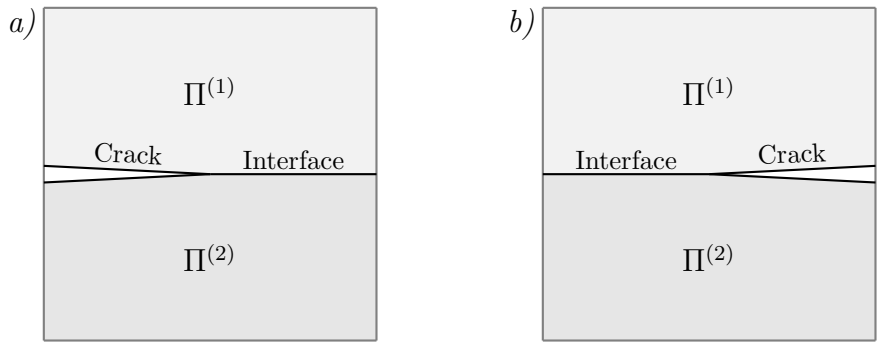

Unperturbed physical problem for imperfect interface

Weight function configuration for imperfect interface

Figure 5.2: Geometries for the unperturbed physical (Figure 2*a*) and weight function (Figure 2*b*) setups.

5.2.2 Weight function formulation

The sought weight function U also satisfies the Laplace equation, but with the crack occupying $\{(x, y) : x > 0, y = 0\}$. We define the functions Σ_j in their respective half-planes by

$$\Sigma_j(x, y) := \mu_j \frac{\partial U_j}{\partial y}, \quad j = 1, 2. \tag{5.12}$$

Boundary conditions analogous to the physical set-up apply. That is,

$$\Sigma_1(x, 0^+) = \Sigma_2(x, 0^-), \quad x < 0, \tag{5.13}$$

$$[\![U]\!](x) - \kappa \Sigma_1(x, 0^+) = 0, \quad x < 0, \tag{5.14}$$

$$\Sigma_1(x, 0^+) = 0, \quad x > 0, \tag{5.15}$$

$$\Sigma_2(x, 0^-) = 0, \quad x > 0. \tag{5.16}$$

We expect that along the interface, the displacement jump behaves as

$$[\![U]\!](x) = O(1), \quad x \to 0^-; \qquad [\![U]\!](x) = O(|x|^{-1/2}), \quad x \to -\infty, \tag{5.17}$$

while along the crack,

$$[\![U]\!](x) = c_1 + c_2 x \log x + c_3 x + o(x), \quad x \to 0^+, \tag{5.18}$$

and

$$[\![U]\!](x) = c_4 + c_5\sqrt{x} + o(\sqrt{x}), \quad x \to +\infty, \tag{5.19}$$

where c_i are constants. We further expect that

$$\Sigma_j = O(1), \quad x \to 0^-; \qquad \Sigma_j = O(x^{-1/2}), \quad x \to -\infty. \tag{5.20}$$

5.2.3 Derivation of Wiener-Hopf type equation for the weight function

The asymptotic behaviour of U_j allows us to apply Fourier transforms. Moreover, the behaviour near $r = 0$ demonstrates that the Fourier transform exists as a Cauchy value integral. Applying the Fourier transform with respect to x

$$\bar{U}_j(\xi, y) = \int_{-\infty}^{\infty} U_j(x, y) e^{i\xi x} \mathrm{d}x \tag{5.21}$$

and taking into account the behaviour of U at infinity, we obtain that the transformed solutions of (5.1) are of the form

$$\bar{U}_j(\xi, y) = A_j(\xi) e^{-|\xi y|}, \tag{5.22}$$

with the corresponding expressions for tractions at $y = 0^{\pm}$ given by

$$\bar{\Sigma}_j(\xi, 0^{\pm}) = (-1)^j \mu_j |\xi| A_j(\xi). \tag{5.23}$$

We define the functions $\Phi^{\pm}(\xi)$ by

$$\Phi^-(\xi) = \bar{\Sigma}|_{y=0^+}, \tag{5.24}$$

$$\Phi^+(\xi) = [\![\bar{U}]\!] - \kappa\bar{\Sigma}|_{y=0^+}. \tag{5.25}$$

These functions $\Phi^{\pm}(\xi)$ are analytic in the complex half-planes denoted by their superscripts. We expect that as $\xi \to \infty$ in their respective domains, asymptotic estimates for $\Phi^{\pm}(\xi)$ are

$$\Phi^{\pm}(\xi) = O\left(\frac{1}{\xi}\right), \quad \xi \to \infty, \tag{5.26}$$

and near zero,

$$\Phi^+(\xi) = O(\xi^{-3/2}), \qquad \Phi^-(\xi) = O(\xi^{-1/2}), \quad \xi \to 0; \tag{5.27}$$

we verify this later (see equations (5.52)-(5.55)). The condition of continuity of tractions across the crack and interface (5.2) gives that

$$\mu_1 A_1(\xi) = -\mu_2 A_2(\xi), \tag{5.28}$$

and the Fourier transform of the jump function $[\![U]\!]$ can be seen from (5.21) to be

$$[\![\bar{U}]\!](\xi) = A_1(\xi) - A_2(\xi). \tag{5.29}$$

Combining these conditions (5.28)-(5.29), we conclude that the functions $\Phi^{\pm}(\xi)$ satisfy the functional equation of the Wiener-Hopf type

$$\Phi^+(\xi) = -\kappa\Xi(\xi)\Phi^-(\xi), \tag{5.30}$$

where

$$\Xi(\xi) = 1 + \frac{\mu_0}{|\xi|}, \tag{5.31}$$

with the constant μ_0 given by

$$\mu_0 = \frac{\mu_1 + \mu_2}{\mu_1\mu_2\kappa}. \tag{5.32}$$

This Wiener-Hopf kernel $\Xi(\xi)$ is the same as that found in the paper of Antipov *et al.* [1] which considered a similar geometry but with a perfect

interface in place of the presently considered imperfect interface between materials. The authors factorise this function as $\Xi(\xi) = X^+(\xi)/X^-(\xi)$, where $X^\pm(\xi)$ are the limiting values of

$$X^\pm(\xi) = \exp\left\{\frac{1}{2\pi i}\int_{-\infty}^{\infty} \ln\left(1+\frac{\mu_0}{|\beta|}\right)\frac{\mathrm{d}\beta}{\beta-\xi}\right\}, \quad \xi \in \mathbb{C}^\pm. \tag{5.33}$$

Asymptotic behaviours of the functions $X^\pm$ are presented; we note in particular that

$$X^+(\xi) = O(\xi^{-1/2}), \quad \xi \to 0,\ \xi \in \mathbb{C}^+. \tag{5.34}$$

This bad behaviour of $X^+(\xi)$ as $\xi \to 0$ would make computations difficult; while asymptotic estimates are given, no computations are performed. Moreover, the authors do not construct a weight function for this problem. These points inspire the following section in which we obtain a different more computationally convenient factorisation of $\Xi(\xi)$.

5.3 Factorisation

In this section we factorise the function $\Xi(\xi)$ which is defined in (5.31). As we just remarked, despite this function having been previously factorised in [1], we provide here an alternative factorisation which is more convenient for computations. We define an auxiliary function Ξ_* by

$$\Xi_*(\xi) = \frac{\xi_+^{1/2}\xi_-^{1/2}}{\xi}\tanh\left(\frac{\xi}{\mu_0}\right)\left(1+\frac{\mu_0}{|\xi|}\right), \tag{5.35}$$

with the functions $\xi_\pm^{1/2}$ given by

$$\xi_\pm^{1/2} = \sqrt{\mp i\xi}. \tag{5.36}$$

Here $\sqrt{\cdot}$ is the standard square root function with its branch cut positioned along the negative real axis. Thus $\xi_\pm^{1/2}$ are analytic functions in half-planes

corresponding to their respective subscripts; note that their product is equal to the absolute value of ξ, that is $\xi_+\xi_- = |\xi|$. Now, $\Xi_*(\xi)$ is an even function and behaves at zero and infinity as follows:

$$\Xi_*(\xi) = 1 + \frac{|\xi|}{\mu_0} - \frac{5}{6}\left(\frac{|\xi|}{\mu_0}\right)^2 + O\left(\left(\frac{|\xi|}{\mu_0}\right)^3\right), \quad \xi \to 0, \tag{5.37}$$

$$\Xi_*(\xi) = 1 + \frac{\mu_0}{|\xi|} + O(e^{-2|\xi|/\mu_0}), \quad |\xi| \to \infty. \tag{5.38}$$

The kernel function $\Xi(\xi)$ can be factorised as

$$\Xi(\xi) = \frac{\xi}{\xi_+^{1/2}\xi_-^{1/2}}\Xi_*(\xi)\Xi_0(\xi), \tag{5.39}$$

where

$$\Xi_0(\xi) = \coth\left(\frac{\xi}{\mu_0}\right). \tag{5.40}$$

This function can itself be factorised as

$$\Xi_0(\xi) = \frac{\pi\mu_0}{\xi}\Xi_0^+(\xi)\Xi_0^-(\xi), \tag{5.41}$$

where

$$\Xi_0^\pm(\xi) = \frac{\Gamma\left(1 \mp \frac{i\xi}{\pi\mu_0}\right)}{\Gamma\left(\frac{1}{2} \mp \frac{i\xi}{\pi\mu_0}\right)}. \tag{5.42}$$

The functions $\Xi_0^\pm(\xi)$ satisfy $\Xi_0^+(\xi) = \Xi_0^-(-\xi)$, with $\Xi_0^+(\xi)$ being regular and non-zero in the half-plane $\mathrm{Im}(\xi) > -\pi\mu_0/2$. Moreover, Stirling's formula gives that the behaviour as $\xi \to \infty$ in an upper half-plane is

$$\Xi_0^+(\xi) = \beta^{1/2} + \frac{1}{8}\beta^{-1/2} + \frac{1}{128}\beta^{-3/2} + O(\beta^{-5/2}), \quad \xi \to \infty, \tag{5.43}$$

where $\beta = i\xi/(\pi\mu_0)$. Analogous asymptotics for $\Xi_0^-(\xi)$ are easily obtained by noting that $\Xi_0^+(\xi) = \Xi_0^-(-\xi)$ and exploiting standard asymptotic expansions of the Gamma function. Near $\xi = 0$, the asymptotics for $\Xi_0^+(\xi)$ are given by

$$\Xi_0^+(\xi) = \frac{1}{\sqrt{\pi}} - \frac{2\ln(2)i\xi}{\pi^{3/2}\mu_0} - \frac{(\pi^2 + 12\ln^2(2))\xi^2}{6\mu_0^2\pi^{5/2}} + O\left(\xi^3\right), \quad \xi \to 0. \tag{5.44}$$

The function $\Xi_*(\xi)$ can be written in the form

$$\Xi_*(\xi) = \Xi_*^+(\xi)\Xi_*^-(\xi), \quad \xi \in \mathbb{C}^{\pm} \tag{5.45}$$

where

$$\Xi_*^{\pm}(\xi) = \exp\left\{\frac{\pm 1}{2\pi i}\int_{-\infty}^{\infty}\frac{\ln \Xi_*(t)}{t-\xi}\mathrm{d}t\right\}. \tag{5.46}$$

In particular, we stress that the functions $\Xi_*^{\pm}(\xi)$ are easy to compute. Near zero, we find that

$$\Xi_*^+(\xi) = 1 + \frac{\alpha\xi}{\pi i} + O(\xi^2), \quad \xi \to 0, \tag{5.47}$$

where

$$\alpha = \int_0^{\infty}\frac{\ln \Xi_*(t)}{t^2}\mathrm{d}t. \tag{5.48}$$

This result follows from Theorem 9 which we stated and proved earlier on page 39.

Moreover, applying Theorem 9 further yields that behaviour near infinity in a suitable domain is described by

$$\Xi_*^+(\xi) = 1 + \frac{\mu_0}{\pi i}\frac{\ln(-i\xi)}{\xi} + O\left(\frac{1}{\xi}\right), \quad \mathrm{Im}(\xi) \to +\infty. \tag{5.49}$$

These expressions again emphasise the well behaved nature of the functions $\Xi_*^{\pm}(\xi)$. The 'bad' behaviour of the kernel near $\xi = 0$ is all contained in the function $\Xi_0(\xi)$ which has subsequently been factorised into the product of readily computable analytic functions.

5.4 Solution to the Wiener-Hopf equation (5.30)

Substituting our factorised expressions for $\Xi_0^{\pm}(\xi)$ and $\Xi_*^{\pm}(\xi)$ into (5.30), we arrive at the Wiener-Hopf type equation

$$\frac{\xi\Phi^+(\xi)\xi_+^{1/2}}{\Xi_0^+(\xi)\Xi_*^+(\xi)} = -\kappa\pi\mu_0\Phi^-(\xi)\Xi_*^-(\xi)\Xi_0^-(\xi)\frac{\xi}{\xi_-^{1/2}}. \tag{5.50}$$

Both sides of (5.50) represent analytic functions in their respective half-planes and do not have any poles along the real axis. The asymptotic estimates as $\xi \to \infty$ given in (5.26), (5.43) and (5.49), demonstrate that both sides of equation (5.50) behave as $O(1)$ as $\xi \to \infty$ in their respective domains. We therefore deduce that both sides must be equal to a constant, which we denote $\mathcal{A}$.

We deduce that the functions $\Phi^{\pm}(\xi)$ are given by

$$\Phi^-(\xi) = \frac{-\mathcal{A}\xi_-^{1/2}}{\kappa\pi\mu_0\Xi_*^-(\xi)\Xi_0^-(\xi)\xi}, \qquad \Phi^+(\xi) = \frac{\mathcal{A}}{\xi\xi_+^{1/2}}\Xi_0^+(\xi)\Xi_*^+(\xi). \tag{5.51}$$

These expressions validate our earlier expectations (see equations (5.26) and (5.27) on page 118) regarding the asymptotic estimates for $\Phi^{\pm}$. In particular, accurate estimates near zero are given by

$$\Phi^-(\xi) = -\frac{\mathcal{A}}{\kappa\mu_0\sqrt{\pi}}\frac{\xi_-^{1/2}}{\xi}\left\{1 + \left(\frac{\alpha\mu_0 + 2\ln 2}{\pi i\mu_0}\right)\xi + O(\xi^2)\right\}, \quad \xi \to 0, \tag{5.52}$$

$$\Phi^+(\xi) = \frac{\mathcal{A}}{\sqrt{\pi}\xi\xi_+^{1/2}}\left\{1 + \left(\frac{\alpha\mu_0 + 2\ln 2}{\pi i\mu_0}\right)\xi + O(\xi^2)\right\}, \quad \xi \to 0, \tag{5.53}$$

and as $\xi \to \infty$ in the appropriate domains,

$$\Phi^-(\xi) = \frac{-\mathcal{A}}{\xi\kappa\sqrt{\mu_0\pi}}\left(1 - \frac{\mu_0}{\pi i}\frac{\ln(-i\xi)}{\xi} + O\left(\frac{1}{\xi}\right)\right), \quad \xi \to \infty, \tag{5.54}$$

$$\Phi^+(\xi) = \frac{\mathcal{A}}{\xi}\left(\frac{1}{\sqrt{\pi\mu_0}} + \frac{\sqrt{\pi\mu_0}}{i\pi^2}\frac{\ln(-i\xi)}{\xi} + O\left(\frac{1}{\xi}\right)\right), \quad \xi \to \infty. \tag{5.55}$$

It also follows from (5.51) that the Fourier transform of U is given by

$$\bar{U}_j(\xi, y) = \frac{(-1)^{j+1}\mathcal{A}e^{-|\xi y|}}{\mu_j \kappa \pi \mu_0 \Xi_*^-(\xi)\Xi_0^-(\xi)\xi_+^{1/2}\xi}, \quad j = 1, 2. \tag{5.56}$$

Expressions for the transforms of the displacement jump and the mean displacement across the interface are therefore respectively given by

$$[\![\bar{U}]\!](\xi) = \frac{\mathcal{A}}{\pi \Xi_*^-(\xi)\Xi_0^-(\xi)\xi_+^{1/2}\xi}, \tag{5.57}$$

$$\langle \bar{U} \rangle(\xi) := \frac{1}{2}\left(\bar{U}_1(\xi, 0^+) + \bar{U}_2(\xi, 0^-)\right) = \frac{-\mathcal{A}\mu_*}{2\pi \Xi_*^-(\xi)\Xi_0^-(\xi)\xi_+^{1/2}\xi}, \tag{5.58}$$

where μ_* is the dimensionless mechanical contrast parameter

$$\mu_* = \frac{(\mu_1 - \mu_2)}{(\mu_1 + \mu_2)}. \tag{5.59}$$

These expressions will be useful in Section 5.5 where we consider the Betti identity in an imperfect interface setting. In particular we note that $[\![\bar{U}]\!]$ has asymptotic expansions near zero and infinity as follows

$$[\![\bar{U}]\!](\xi) = \frac{\mathcal{A}\sqrt{\pi\mu_0}}{\pi\xi\xi_+^{1/2}\xi_-^{1/2}}\left(1 + \frac{\mu_0 \ln(i\xi)}{\pi\xi} + O\left(\frac{1}{\xi}\right)\right), \quad \xi \to \infty, \tag{5.60}$$

$$[\![\bar{U}]\!](\xi) = \frac{\mathcal{A}}{\pi^{3/2}\xi\xi_+^{1/2}}\left(1 + \frac{(2\ln(2) - \alpha)i\xi}{\pi\mu_0} + O(\xi^2)\right), \quad \xi \to 0. \tag{5.61}$$

The function $\langle \bar{U} \rangle$ behaves similarly, as

$$\langle \bar{U} \rangle(\xi) = \frac{-\mathcal{A}\mu_*\sqrt{\pi\mu_0}}{2\pi\xi\xi_+^{1/2}\xi_-^{1/2}}\left(1 + \frac{\mu_0 \ln(i\xi)}{\pi\xi} + O\left(\frac{1}{\xi}\right)\right), \quad \xi \to \infty, \tag{5.62}$$

$$\langle \bar{U} \rangle(\xi) = \frac{-\mathcal{A}\mu_*}{2\pi^{3/2}\xi\xi_+^{1/2}}\left(1 + \frac{(2\ln(2) - \alpha)i\xi}{\pi\mu_0} + O(\xi^2)\right), \quad \xi \to 0. \tag{5.63}$$

Another key difference between the imperfect and perfect interface (as considered in [52]) cases is also readily seen here. Due to the condition of continuity of displacement across perfect interfaces, the function $[\![\bar{U}]\!](\xi)$ is a

plus function in the perfect case, since $[\![U]\!](x)$ is zero for x lying along the negative real axis. However, across an imperfect interface, the displacement is no longer continuous and so $[\![\bar{U}]\!]$ is neither a plus function nor a minus function.

5.5 Betti identity in the imperfect interface setting

In this section we refer to the physical fields for displacement and stress as u and σ respectively, and the weight function fields for displacement and stress as U and Σ respectively. We will use the reciprocal theorem (Betti formula) as in [71] to relate the physical solution to the weight function.

Applying the Betti formula to the physical fields and to the upper and lower half-plane we obtain

$$\int_{-\infty}^{\infty} \left\{U(x'-x,0^+)\sigma(x,0^+) - \Sigma(x'-x,0^+)u(x,0^+)\right\} \mathrm{d}x = 0, \tag{5.64}$$

and

$$\int_{-\infty}^{\infty} \left\{U(x'-x,0^-)\sigma(x,0^-) - \Sigma(x'-x,0^-)u(x,0^-)\right\} \mathrm{d}x = 0. \tag{5.65}$$

These identities were proved under the assumption that the integrand decays faster at infinity than $1/R$ along any ray. It is clear from the asymptotic estimates for the physical solution and the weight function given in subsections 5.2.1 and 5.2.2 that this condition is satisfied. Subtracting (5.65) from (5.64)

we obtain

$$\int_{-\infty}^{\infty} \{U(x'-x,0^+)\sigma(x,0^+) - U(x'-x,0^-)\sigma(x,0^-) \\ - [\Sigma(x'-x,0^+)u(x,0^+) - \Sigma(x'-x,0^-)u(x,0^-)]\}\mathrm{d}x = 0. \tag{5.66}$$

We split the terms for physical stress into two parts, writing

$$\sigma(x,0^\pm) = p_\pm^{(-)}(x) + \sigma^{(+)}(x), \tag{5.67}$$

where $p_\pm^{(-)}$ and $\sigma^{(+)}$ are defined as follows

$$p_\pm^{(-)}(x) = \mathcal{H}(-x)\sigma(x,0^\pm), \qquad \sigma^{(+)}(x) = \mathcal{H}(x)\sigma(x,0); \tag{5.68}$$

here $\mathcal{H}(x)$ denotes the Heaviside step function. The functions $p_\pm^{(-)}(x)$ represent the prescribed loading on the crack faces. After this splitting, equation (5.66) becomes

$$\int_{-\infty}^{\infty} \{[\![U]\!](x'-x)\sigma^{(+)}(x) - \Sigma(x'-x,0)[\![u]\!](x)\}\mathrm{d}x \\ = -\int_{-\infty}^{\infty} \{U(x'-x,0^+)p_+^{(-)}(x) - U(x'-x,0^-)p_-^{(-)}(x)\}\mathrm{d}x. \tag{5.69}$$

We introduce notation for symmetric and skew-symmetric parts of the loading:

$$\langle p\rangle^{(-)}(x) = \frac{1}{2}(p_+^{(-)}(x) + p_-^{(-)}(x)), \quad [\![p]\!]^{(-)}(x) = p_+^{(-)}(x) - p_-^{(-)}(x). \tag{5.70}$$

This allows us to rewrite the right hand side of (5.69), giving

$$\int_{-\infty}^{\infty} \{[\![U]\!](x'-x)\sigma^{(+)}(x) - \Sigma(x'-x,0)[\![u]\!](x)\}\mathrm{d}x \\ = -\int_{-\infty}^{\infty} \{[\![U]\!](x'-x)\langle p\rangle(x) + \langle U\rangle(x'-x)[\![p]\!](x)\}\mathrm{d}x. \tag{5.71}$$

We now split $[\![U]\!]$ into the sum of $[\![U]\!]^{(\pm)}$ in the spirit of (5.67), and similarly split $[\![u]\!]$ into the sum of $[\![u]\!]^{(\pm)}$. We will use the usual notation of $f * g$ to denote the convolution of f and g. Rewriting (5.71) using these expressions gives

$$[\![U]\!]^{(+)} * \sigma^{(+)} + [\![U]\!]^{(-)} * \sigma^{(+)} - \Sigma * [\![u]\!]^{(+)} - \Sigma * [\![u]\!]^{(-)} = \\ - [\![U]\!] * \langle p \rangle^{(-)} - \langle U \rangle * [\![p]\!]^{(-)}. \tag{5.72}$$

Taking Fourier transforms in x yields

$$\overline{[\![U]\!]^{(+)}}(\xi)\overline{\sigma^{(+)}}(\xi) + \overline{[\![U]\!]^{(-)}}(\xi)\overline{\sigma^{(+)}}(\xi) - \overline{\Sigma}(\xi)\overline{[\![u]\!]^{(+)}}(\xi) - \overline{\Sigma}(\xi)\overline{[\![u]\!]^{(-)}}(\xi) = \\ - [\![\bar{U}]\!](\xi)\langle \bar{p} \rangle(\xi) - \langle \bar{U} \rangle(\xi)[\![\bar{p}]\!](\xi). \tag{5.73}$$

We now make use of the transmission conditions which state that

$$\overline{[\![U]\!]^{(-)}}(\xi) = \kappa\overline{\Sigma}(\xi), \qquad \overline{[\![u]\!]^{(+)}}(\xi) = \kappa\overline{\sigma^{(+)}}(\xi). \tag{5.74}$$

This causes the second and third terms in the left hand side of (5.73) to cancel, leaving

$$\overline{[\![U]\!]^{(+)}}(\xi)\overline{\sigma^{(+)}}(\xi) - \overline{\Sigma}(\xi)\overline{[\![u]\!]^{(-)}}(\xi) = -[\![\bar{U}]\!](\xi)\langle \bar{p} \rangle(\xi) - \langle \bar{U} \rangle(\xi)[\![\bar{p}]\!](\xi), \quad \xi \in \mathbb{R}. \tag{5.75}$$

We note that

$$\overline{[\![U]\!]^{(+)}}(\xi) \equiv \Phi^{+}(\xi), \qquad \bar{\Sigma}(\xi) \equiv \Phi^{-}(\xi), \tag{5.76}$$

and can therefore combine the asymptotic estimates in (5.10), (5.11), (5.54) and (5.55) to yield that

$$\overline{[\![U]\!]^{(+)}}(\xi)\overline{\sigma^{(+)}}(\xi) = \frac{a_0 i}{\sqrt{\pi\mu_0}\xi^2} + O(\xi^{-(2+\delta)}), \qquad \xi \to \infty \text{ in } \mathbb{C}^{+}, \tag{5.77}$$

$$\bar{\Sigma}(\xi)\overline{[\![u]\!]^{(-)}}(\xi) = \frac{a_0 i}{\sqrt{\pi\mu_0}\xi^2} + O(\xi^{-(2+\delta)}), \qquad \xi \to \infty \text{ in } \mathbb{C}^{-}, \tag{5.78}$$

where $\delta > 0$. We now multiply both sides of (5.75) by ξ, giving

$$\xi\left(\overline{[\![U]\!]^{(+)}}(\xi)\overline{\sigma^{(+)}}(\xi) - \overline{\Sigma}(\xi)\overline{[\![u]\!]^{(-)}}(\xi)\right) = -\xi\left([\![\bar{U}]\!](\xi)\langle\bar{p}\rangle(\xi) + \langle\bar{U}\rangle(\xi)[\![\bar{p}]\!](\xi)\right). \tag{5.79}$$

Then, and similarly to the expression obtained for the perfect interface Betti formula approach of Willis and Movchan [71], the left hand side now has asymptotics at infinity (in appropriate domains) of the form

$$\xi\left(\overline{[\![U]\!]^{(+)}}(\xi)\overline{\sigma^{(+)}}(\xi) - \overline{\Sigma}(\xi)\overline{[\![u]\!]^{(-)}}(\xi)\right) \sim \frac{a_0 i}{\sqrt{\pi\mu_0}}\left[\frac{1}{\xi + i0} - \frac{1}{\xi - i0}\right], \quad \xi \to \infty, \tag{5.80}$$

where the term in square brackets is the regularization of the Dirac delta function, namely $-2\pi i\delta(\xi)$. Integrating both sides of (5.79), we can derive an expression for the constant a_0 in terms of known, readily computable functions:

$$a_0 = \frac{1}{2}\sqrt{\frac{\mu_0}{\pi}}\int_{-\infty}^{\infty}\xi\left([\![\bar{U}]\!](\xi)\langle\bar{p}\rangle(\xi) + \langle\bar{U}\rangle(\xi)[\![\bar{p}]\!](\xi)\right)\mathrm{d}\xi. \tag{5.81}$$

We note that since $[\![\bar{U}]\!](\xi)$ and $\langle\bar{U}\rangle(\xi)$ behave as $O(\xi^{-2})$ as $\xi \to \infty$, and the functions $[\![\bar{p}]\!](\xi)$ and $\langle\bar{p}\rangle(\xi)$ behave as bounded oscillations as $\xi \to \infty$ for point loadings, the integrand is well behaved at infinity. Moreover, near $\xi = 0$ the integrand is also sufficiently well behaved, acting as $O(\xi_+^{-1/2})$.

Equation (5.81) is a particularly important result; it gives an expression for the leading order of the out-of-plane component of stress near the crack tip (see (5.9)) in terms of known functions and acts as an imperfect interface analogue to the stress intensity factor from the perfect interface setting.

5.5.1 The functions $[\![\bar{p}]\!]$ and $\langle\bar{p}\rangle$ for specific point loadings

As we stated in the introduction to this chapter, although the methods described are applicable to any permissible loading, we will later perform computations using the specific point loading configuration shown in Figure 5.1 on page 113.

For this configuration, the loadings are defined as a point load on the upper crack face at $x = -a$ balanced by two equal loads at $x = -a + b$ and $x = -a - b$, that is

$$p_+^{(-)}(x) = F\delta(x+a), \qquad p_-^{(-)}(x) = \frac{F}{2}\left(\delta(x+a+b) + \delta(x+a-b)\right). \quad (5.82)$$

The corresponding explicit expressions for $\langle p\rangle(x)$ and $[\![p]\!](x)$ are

$$\langle p\rangle(x) = \frac{F}{2}\left\{\delta(x+a) + \frac{1}{2}\left(\delta(x+a+b) + \delta(x+a-b)\right)\right\}, \quad (5.83)$$

$$[\![p]\!](x) = F\left\{\delta(x+a) - \frac{1}{2}\left(\delta(x+a+b) + \delta(x+a-b)\right)\right\}, \quad (5.84)$$

which have Fourier transforms given by

$$\langle\bar{p}\rangle(\xi) = \frac{F}{4}(e^{ib\xi}+1)^2 e^{-i(a+b)\xi}, \quad (5.85)$$

$$[\![\bar{p}]\!](\xi) = -\frac{F}{2}(e^{ib\xi}-1)^2 e^{-i(a+b)\xi}. \quad (5.86)$$

These expressions are useful in generating the numerical results which are later presented in Section 5.10.

5.6 The unperturbed solution, u_0

We will later require a method to evaluate the *unperturbed physical solution* u_0 and its first order partial derivatives with respect to x and y. This problem

has been solved by Antipov *et al.* [1] by approximating the loading by a linear combination of exponentials; this approximation is however not ideal for point loadings.

Tractions on the upper and lower crack faces can be written as

$$\bar{\sigma}_1(\xi, 0^+) = \bar{p}_1(\xi) + \varphi_1^+(\xi), \tag{5.87}$$

$$\bar{\sigma}_2(\xi, 0^-) = \bar{p}_2(\xi) + \varphi_2^+(\xi). \tag{5.88}$$

It follows immediately from continuity of tractions across the imperfect interface that

$$\varphi_1^+(\xi) = \varphi_2^+(\xi) =: \varphi^+(\xi). \tag{5.89}$$

We further define minus functions, φ_1^- and φ_2^- as

$$\varphi_1^-(\xi) = [\![\bar{u}]\!](\xi) - \kappa\bar{\sigma}_1(\xi, 0^+), \tag{5.90}$$

$$\varphi_2^-(\xi) = [\![\bar{u}]\!](\xi) - \kappa\bar{\sigma}_2(\xi, 0^-). \tag{5.91}$$

We expect that the unknown functions $\varphi^+(\xi)$ and $\varphi_j^-(\xi)$ behave at infinity as

$$\varphi_j^{\pm}(\xi) = O\left(\frac{1}{\xi}\right), \quad \xi \to \infty, \quad \pm\mathrm{Im}(\xi) > 0. \tag{5.92}$$

From these expressions follow the relationships

$$[\![\bar{\sigma}]\!](\xi) \equiv [\![\bar{p}]\!](\xi), \tag{5.93}$$

$$\langle\bar{\sigma}\rangle(\xi) \equiv \langle\bar{p}\rangle(\xi) + \varphi^+(\xi), \tag{5.94}$$

and also

$$-\kappa[\![\bar{\sigma}]\!](\xi) \equiv \varphi_1^-(\xi) - \varphi_2^-(\xi), \tag{5.95}$$

$$2[\![\bar{u}]\!](\xi) - 2\kappa\langle\bar{\sigma}\rangle(\xi) \equiv \varphi_1^-(\xi) + \varphi_2^-(\xi). \tag{5.96}$$

Moreover, since transformed solutions are of the form

$$\bar{u}_j(\xi, y) = A_j(\xi)e^{-|\xi y|}, \tag{5.97}$$

we further have the relationships

$$[\![\bar{u}]\!](\xi) = A_1(\xi) - A_2(\xi), \tag{5.98}$$

$$[\![\bar{\sigma}]\!](\xi) = -|\xi|(\mu_1 A_1(\xi) + \mu_2 A_2(\xi)), \tag{5.99}$$

and

$$\langle\bar{\sigma}\rangle(\xi) = \frac{|\xi|}{2}(\mu_2 A_2(\xi) - \mu_1 A_1(\xi)). \tag{5.100}$$

These seven equations in eight unknowns reduce to the following Wiener-Hopf type equation relating $\varphi^+(\xi)$ and $\varphi_1^-(\xi)$:

$$-\kappa\left\{1 + \frac{\mu_0}{|\xi|}\right\}\varphi^+(\xi) - \kappa\left\{1 + \frac{\mu_0}{|\xi|}\right\}\langle\overline{p}\rangle(\xi) = \varphi_1^-(\xi) + \frac{\kappa}{2}\left\{1 - \frac{\mu_*\mu_0}{|\xi|}\right\}[\![\overline{p}]\!](\xi). \tag{5.101}$$

Noting that the term in braces on the left hand side of (5.101) is the function we earlier defined as $\Xi(\xi)$ and have already suitably factorised, we can write

$$-\kappa\Xi(\xi)\varphi^+(\xi) - \kappa\Xi(\xi)\langle\overline{p}\rangle(\xi) = \varphi_1^-(\xi) + \kappa\Lambda(\xi)[\![\overline{p}]\!](\xi), \tag{5.102}$$

where

$$\Lambda(\xi) = \frac{1}{2}\left\{1 - \frac{\mu_*\mu_0}{|\xi|}\right\}. \tag{5.103}$$

Recall that $\Xi(\xi)$ can be factorised in the form

$$\Xi(\xi) = \pi\mu_0 B^+(\xi)B^-(\xi), \tag{5.104}$$

where we have defined the functions $B^{\pm}(\xi)$ for the sake of notational brevity by

$$B^+(\xi) = \frac{\Xi_0^+(\xi)\Xi_*^+(\xi)}{\xi_+^{1/2}}, \qquad B^-(\xi) = \frac{\Xi_0^-(\xi)\Xi_*^-(\xi)}{\xi_-^{1/2}}, \tag{5.105}$$

which are analytic in the half-planes indicated by their superscripts. These functions have behaviour near zero and infinity given by

$$B^{\pm}(\xi) = O(\xi^{-1/2}), \qquad \xi \to 0, \tag{5.106}$$

$$B^{\pm}(\xi) = O(1), \qquad \xi \to \infty. \tag{5.107}$$

Thus

$$-\kappa\pi\mu_0 B^+(\xi)\varphi^+(\xi) = \frac{\varphi_1^-(\xi)}{B^-(\xi)} + \kappa\frac{\Lambda(\xi)}{B^-(\xi)}[\![\overline{p}]\!](\xi) + \kappa\pi\mu_0 B^+(\xi)\langle\overline{p}\rangle(\xi). \tag{5.108}$$

We can decompose the final term on the right hand side as usual into

$$\kappa\frac{\Lambda(\xi)}{B^-(\xi)}[\![\overline{p}]\!](\xi) + \kappa\pi\mu_0 B^+(\xi)\langle\overline{p}\rangle(\xi) = L^+(\xi) - L^-(\xi), \tag{5.109}$$

where $L^{\pm}(\xi)$ are given by

$$L^{\pm}(\xi) = \frac{1}{2\pi i}\int_{-\infty}^{\infty}\left\{\kappa\frac{\Lambda(\beta)}{B^-(\beta)}[\![\overline{p}]\!](\beta) + \kappa\pi\mu_0 B^+(\beta)\langle\overline{p}\rangle(\beta)\right\}\frac{\mathrm{d}\beta}{\beta-\xi}, \quad \xi \in \mathbb{C}^{\pm}. \tag{5.110}$$

We expect that $L^{\pm}(\xi)$ behave as $O(\xi^{-1})$ as $\xi \to \infty$.

The Wiener-Hopf equation becomes

$$-\kappa\pi\mu_0 B^+(\xi)\varphi^+(\xi) - L^+(\xi) = \frac{\varphi_1^-(\xi)}{B^-(\xi)} - L^-(\xi). \tag{5.111}$$

Both terms of on each side of (5.111) decay as $O(1/\xi)$, $\xi \to \infty$. Moreover, each side is analytic in the half-plane denoted by the superscripts. Liouville's theorem yields that both sides are equal to zero, and so

$$\varphi^+(\xi) = \frac{-L^+(\xi)}{\kappa\pi\mu_0 B^+(\xi)}, \qquad \varphi_1^-(\xi) = L^-(\xi)B^-(\xi). \tag{5.112}$$

These expressions verify that our expectations of the behaviour of $\varphi^+(\xi)$ and $\varphi_1^-(\xi)$ as $\xi \to \infty$ were correct. Moreover, (5.95) enables us to express $\varphi_2^-(\xi)$ as

$$\varphi_2^-(\xi) = L^-(\xi)B^-(\xi) + \kappa[\![\bar{p}]\!](\xi). \tag{5.113}$$

Condition (5.96) then yields an expression for the transform of the displacement jump

$$[\![\bar{u}]\!](\xi) = \frac{\varphi_1^-(\xi)}{2} + \frac{\varphi_2^-(\xi)}{2} + \kappa\langle\bar{\sigma}\rangle(\xi) = \varphi_1^-(\xi) + \kappa\varphi^+(\xi) + \kappa\langle\bar{p}\rangle(\xi) + \frac{\kappa}{2}[\![\bar{p}]\!](\xi), \tag{5.114}$$

from which we can obtain expressions for $A_1(\xi)$ and $A_2(\xi)$ as follows

$$A_1(\xi) = -\frac{1}{\mu_1|\xi|}\left\{\varphi^+(\xi) + \langle\bar{p}\rangle(\xi) + \frac{1}{2}[\![\bar{p}]\!](\xi)\right\}, \tag{5.115}$$

$$A_2(\xi) = \frac{1}{\mu_2|\xi|}\left\{\varphi^+(\xi) + \langle\bar{p}\rangle(\xi) - \frac{1}{2}[\![\bar{p}]\!](\xi)\right\}. \tag{5.116}$$

These expressions now enable us (see (5.97)) to compute the Fourier transform of the unperturbed solution (i.e. the setup with no small defect present) $\bar{u}_j(\xi, y)$ for any ξ, y.

5.7 Perturbation analysis

We shall construct an asymptotic solution of the problem using the method of Movchan and Movchan [46], that is the asymptotics of the solution will be taken in the form

$$u_{1,2}(\boldsymbol{x}, \varepsilon) = u_{1,2}^{(0)}(\boldsymbol{x}) + \varepsilon W^{(1)}(\boldsymbol{\xi}) + \varepsilon^2 u_{1,2}^{(1)}(\boldsymbol{x}) + o(\varepsilon^2), \quad \varepsilon \to 0. \tag{5.117}$$

In (5.117), the leading term $u_{1,2}^{(0)}(\boldsymbol{x})$ corresponds to the unperturbed solution, which is described in the previous section. The term $\varepsilon W^{(1)}(\boldsymbol{\xi})$ corresponds to the boundary layer concentrated near the defect and needed to satisfy the transmission conditions for the elastic inclusion g_ε

$$u_{\text{in}} = u_{\text{out}}, \quad \mu_{\text{in}}\frac{\partial u_{\text{in}}}{\partial n} = \mu_{\text{out}}\frac{\partial u_{\text{out}}}{\partial n} \quad \text{on } \partial g_\varepsilon. \tag{5.118}$$

The term $\varepsilon^2 u_{1,2}^{(1)}(\boldsymbol{x})$ is introduced to fulfil the original boundary conditions (5.4) on the crack faces and the interface conditions (5.2), (5.3) disturbed by

the boundary layer; this term, in turn, will produce perturbations of the crack tip fields and correspondingly of the constant a_0.

We shall consider an elastic inclusion, situated in the upper (or lower) half-plane. The leading term $u^{(0)}_{1,2}$ clearly does not satisfy the transmission conditions (5.118) on the boundary ∂g_ε. Thus, we shall correct the solution by constructing the boundary layer $W^{(1)}(\boldsymbol{\xi})$, where the new scaled variable $\boldsymbol{\xi}$ is defined by

$$\boldsymbol{\xi} = \frac{\boldsymbol{x} - \boldsymbol{Y}}{\varepsilon}, \tag{5.119}$$

with $\boldsymbol{Y} = (X, Y)$ being the "centre" of the inclusion g_ε (see Figure 5.1).

For $W^{(1)}(\boldsymbol{\xi}) = \{W^{(1)}_{\rm in},\ \boldsymbol{\xi} \in g;\ W^{(1)}_{\rm out},\ \boldsymbol{\xi} \in \mathbb{R}^2 \setminus \overline{g}\}$ we consider the following problem

$$\nabla^2 W^{(1)}_{\rm in}(\boldsymbol{\xi}) = 0, \quad \boldsymbol{\xi} \in g, \quad \nabla^2 W^{(1)}_{\rm out}(\boldsymbol{\xi}) = 0, \quad \boldsymbol{\xi} \in \mathbb{R}^2 \setminus \overline{g}, \tag{5.120}$$

where

$$g = \varepsilon^{-1} g_\varepsilon \equiv \{\boldsymbol{\xi} \in \mathbb{R}^2 : \varepsilon\boldsymbol{\xi} + \boldsymbol{Y} \in g_\varepsilon\}.$$

The function $W^{(1)}$ remains continuous across the interface ∂g, that is,

$$W^{(1)}_{\rm in} = W^{(1)}_{\rm out} \quad \text{on} \quad \partial g,$$

and satisfies on ∂g the following transmission condition

$$\mu_{\rm in}\frac{\partial}{\partial \boldsymbol{n}} W^{(1)}_{\rm in}(\boldsymbol{\xi}) - \mu_{\rm out}\frac{\partial}{\partial \boldsymbol{n}} W^{(1)}_{\rm out}(\boldsymbol{\xi}) = (\mu_{\rm out} - \mu_{\rm in})\boldsymbol{n} \cdot \nabla u^{(0)}(\boldsymbol{Y}) + O(\varepsilon), \quad \varepsilon \to 0, \tag{5.121}$$

where $\boldsymbol{n} = \boldsymbol{n}_{\boldsymbol{\xi}}$ is an outward unit normal on ∂g. The formulation is completed by setting the following condition at infinity

$$W^{(1)}_{\rm out} \to 0 \quad \text{as} \quad |\boldsymbol{\xi}| \to \infty. \tag{5.122}$$

The problem above has been solved by various techniques and the solution can be found, for example, in Movchan and Movchan [46].

Since we assume that the inclusion is at a finite distance from the interface between the half-planes, we shall only need the leading term of the asymptotics of the solution at infinity. This term reads as follows

$$W^{(1)}_{\rm out}(\boldsymbol{\xi}) = -\frac{1}{2\pi}\left[\nabla_{\boldsymbol{x}}\, u^{(0)}\big|_{\boldsymbol{Y}}\right]\cdot\left[\boldsymbol{\mathcal{M}}\frac{\boldsymbol{\xi}}{|\boldsymbol{\xi}|^2}\right] + O(|\boldsymbol{\xi}|^{-2}) \quad \text{as} \quad \boldsymbol{\xi}\to\infty, \tag{5.123}$$

where $\boldsymbol{\mathcal{M}}$ is a 2×2 matrix which depends on the characteristic size ℓ of the domain g and the ratio $\mu_{\rm out}/\mu_{\rm in}$; it is called the dipole matrix. For example, in the case of an elliptic inclusion with the semi-axes ℓ_a and ℓ_b making an angle α with the positive direction of the x-axis and y-axis, respectively, the matrix $\boldsymbol{\mathcal{M}}$ takes the form

$$\boldsymbol{\mathcal{M}} = -\frac{\pi}{2}\ell_a\ell_b(1{+}e)(\mu_\star{-}1)\begin{bmatrix} \dfrac{1+\cos 2\alpha}{e+\mu_\star}+\dfrac{1-\cos 2\alpha}{1+e\mu_\star} & -\dfrac{(1-e)(\mu_\star-1)\sin 2\alpha}{(e+\mu_\star)(1+e\mu_\star)} \\ -\dfrac{(1-e)(\mu_\star-1)\sin 2\alpha}{(e+\mu_\star)(1+e\mu_\star)} & \dfrac{1-\cos 2\alpha}{e+\mu_\star}+\dfrac{1+\cos 2\alpha}{1+e\mu_\star}\end{bmatrix}, \tag{5.124}$$

where $e=\ell_b/\ell_a$ and $\mu_\star=\mu_{\rm out}/\mu_{\rm in}$. We note that for a soft inclusion, $\mu_{\rm out}>\mu_{\rm in}$, the dipole matrix is negative definite, whereas for a stiff inclusion, $\mu_{\rm out}<\mu_{\rm in}$, the dipole matrix is positive definite. In the limit $\mu_{\rm in}\to\infty$, we obtain the dipole matrix for a rigid movable inclusion. In the case of an elliptic rigid inclusion, we have

$$\boldsymbol{\mathcal{M}} = \frac{\pi}{2}\ell_a\ell_b(1/e{+}1)\begin{bmatrix} 1+\cos 2\alpha+e(1-\cos 2\alpha) & (1-e)\sin 2\alpha \\ (1-e)\sin 2\alpha & 1-\cos 2\alpha+e(1+\cos 2\alpha)\end{bmatrix}. \tag{5.125}$$

The term $\varepsilon W^{(1)}(\boldsymbol{\xi})$ in a neighbourhood of the x-axis written in the $\boldsymbol{x}$ coordinates takes the form

$$\varepsilon W^{(1)}(\boldsymbol{\xi}) = \varepsilon^2 w^{(1)}(\boldsymbol{x}) + o(\varepsilon^2), \quad \varepsilon\to 0, \tag{5.126}$$

where

$$w^{(1)}(\boldsymbol{x}) = -\frac{1}{2\pi}\left[\nabla_{\boldsymbol{x}} u^{(0)}\big|_{\boldsymbol{Y}}\right]\cdot\left[\boldsymbol{\mathcal{M}}\frac{\boldsymbol{x}-\boldsymbol{Y}}{|\boldsymbol{x}-\boldsymbol{Y}|^2}\right]. \tag{5.127}$$

As a result, one can compute the average $\varepsilon^2\langle\sigma^{(1)}\rangle$ and the jump $\varepsilon^2[\![\sigma^{(1)}]\!]$ of the "effective" tractions on the crack faces induced by the elastic inclusion g_ε. Since $\partial u^{(1)}_{1,2}/\partial y = -\partial w^{(1)}/\partial y$ must hold on the crack line (to satisfy the original boundary conditions (5.4)), this gives for $x < 0$

$$\langle\sigma^{(1)}\rangle^{(-)}(x) = -\frac{1}{2}(\mu_1+\mu_2)\frac{\partial w^{(1)}}{\partial y} := P^{(-)}(x), \tag{5.128}$$

$$[\![\sigma^{(1)}]\!]^{(-)}(x) = -(\mu_1-\mu_2)\frac{\partial w^{(1)}}{\partial y} := Q^{(-)}(x), \tag{5.129}$$

where

$$\frac{\partial w^{(1)}}{\partial y} = -\frac{1}{2\pi}\left[\nabla_{\boldsymbol{x}} u^{(0)}\big|_{\boldsymbol{Y}}\right]\cdot\boldsymbol{\mathcal{M}}\frac{\boldsymbol{e}_2}{|\boldsymbol{x}-\boldsymbol{Y}|^2}+\frac{1}{\pi}\left[\nabla_{\boldsymbol{x}} u^{(0)}\big|_{\boldsymbol{Y}}\right]\cdot\boldsymbol{\mathcal{M}}\frac{(\boldsymbol{x}-\boldsymbol{Y})(y-Y)}{|\boldsymbol{x}-\boldsymbol{Y}|^4}. \tag{5.130}$$

Additionally, we can compute the transmission conditions for the functions $u^{(1)}_{1,2}$ across the interface. In order for the perturbed solution $u_{1,2}$ in (5.117) to satisfy the original transmission conditions (5.2) and (5.3), the following relations must hold for $x > 0$

$$[\![u^{(1)}]\!]^{(+)}(x) = \kappa\langle\sigma^{(1)}\rangle^{(+)}(x) + \frac{\kappa}{2}(\mu_1+\mu_2)\frac{\partial w^{(1)}}{\partial y} := \kappa\langle\sigma^{(1)}\rangle^{(+)}(x) - \kappa P^{(+)}(x), \tag{5.131}$$

$$[\![\sigma^{(1)}]\!]^{(+)}(x) = -(\mu_1-\mu_2)\frac{\partial w^{(1)}}{\partial y} := Q^{(+)}(x). \tag{5.132}$$

Note that we have defined the functions $P^{(\pm)}$ and $Q^{(\pm)}$ above. We will later need an expression for the Fourier transform of $\partial w^{(1)}/\partial y$, so we note the useful expressions for $\xi \in \mathbb{R}$

$$\int_{-\infty}^{\infty}\frac{e^{i\xi x}\mathrm{d}x}{|\boldsymbol{x}-\boldsymbol{Y}|^2} = \int_{-\infty}^{\infty}\frac{e^{i\xi x}\mathrm{d}x}{(x-X)^2+Y^2} = \frac{\pi}{Y}e^{i\xi X}e^{-Y|\xi|}, \tag{5.133}$$

and

$$\int_{-\infty}^{\infty}\frac{e^{i\xi x}\mathrm{d}x}{|\boldsymbol{x}-\boldsymbol{Y}|^4} = \int_{-\infty}^{\infty}\frac{e^{i\xi x}\mathrm{d}x}{((x-X)^2+Y^2)^2} = \frac{\pi}{2|Y|^3}e^{i\xi X}e^{-|\xi Y|}(1+|\xi Y|). \tag{5.134}$$

5.8 Model problem for the first order perturbation

The constant a_0 which describes the traction near the crack tip (see (5.9)) is expanded in the form

$$a_0 = a_0^{(0)} + \varepsilon^2 \Delta a_0 + o(\varepsilon^2), \quad \varepsilon \to 0. \tag{5.135}$$

Our objective is to find the first order variation Δa_0.

Let us consider the model problem for the first order perturbation $u^{(1)}$ and write the corresponding Betti identity in the form

$$\int_{-\infty}^{\infty} \Big\{ [\![U]\!](x'-x)\langle \sigma^{(1)} \rangle(x) + \langle U \rangle(x'-x)[\![\sigma^{(1)}]\!](x) \\ - \langle \Sigma \rangle(x'-x)[\![u^{(1)}]\!](x) \Big\} \mathrm{d}x = 0. \tag{5.136}$$

This follows immediately from (5.66) by noting that $[\![\Sigma]\!] \equiv 0$. We split the terms for stress into two parts,

$$\langle \sigma^{(1)} \rangle = \langle \sigma^{(1)} \rangle^{(+)} + P^{(-)}, \qquad [\![\sigma^{(1)}]\!] = Q^{(+)} + Q^{(-)}, \tag{5.137}$$

observing that in contrast to the zero order problem where the load is described by (5.70), the terms with superscript $^{(+)}$ are non-zero since the presence of inclusions induces stresses along the imperfect interface and should be taken into account. Equation (5.136) becomes

$$\int_{-\infty}^{\infty} \big\{ [\![U]\!](x'-x)\langle \sigma^{(1)} \rangle^{(+)}(x) - \langle \Sigma \rangle(x'-x)[\![u^{(1)}]\!](x) \big\} \, \mathrm{d}x = \\ - \int_{-\infty}^{\infty} \big\{ [\![U]\!](x'-x)P^{(-)}(x) + \langle U \rangle(x'-x)Q^{(-)}(x) + \langle U \rangle(x'-x)Q^{(+)}(x) \big\} \, \mathrm{d}x. \tag{5.138}$$

We now split $[\![U]\!]$ into the sum of $[\![U]\!]^{\pm}$ and similarly split $[\![u]\!]$ into the sum of $[\![u]\!]^{\pm}$. This gives

$$[\![U]\!]^{(+)} * \langle\sigma^{(1)}\rangle^{(+)} + [\![U]\!]^{(-)} * \langle\sigma^{(1)}\rangle^{(+)} - \langle\Sigma\rangle * [\![u^{(1)}]\!]^{(+)} - \langle\Sigma\rangle * [\![u^{(1)}]\!]^{(-)} =$$
$$-[\![U]\!] * P^{(-)} - \langle U\rangle * Q^{(-)} - \langle U\rangle * Q^{(+)}. \tag{5.139}$$

Taking the Fourier transform in x yields

$$[\![\overline{U}]\!]^{+}(\xi)\langle\overline{\sigma}^{(1)}\rangle^{+}(\xi) + [\![\overline{U}]\!]^{-}(\xi)\langle\overline{\sigma}^{(1)}\rangle^{+}(\xi) - \langle\overline{\Sigma}\rangle(\xi)[\![\overline{u}^{(1)}]\!]^{+}(\xi) - \langle\overline{\Sigma}\rangle(\xi)[\![\overline{u}^{(1)}]\!]^{-}(\xi) =$$
$$-[\![\overline{U}]\!](\xi)\overline{P}^{-}(\xi) - \langle\overline{U}\rangle(\xi)\overline{Q}^{-}(\xi) - \langle\overline{U}\rangle(\xi)\overline{Q}^{+}(\xi). \tag{5.140}$$

We now make use of the transmission conditions

$$[\![\overline{U}]\!]^{-}(\xi) = \kappa\langle\overline{\Sigma}\rangle(\xi), \qquad [\![\overline{u}^{(1)}]\!]^{+}(\xi) = \kappa\langle\overline{\sigma}^{(1)}\rangle^{+}(\xi) - \kappa\overline{P}^{+}(\xi), \tag{5.141}$$

thus obtaining

$$[\![\overline{U}]\!]^{+}(\xi)\langle\overline{\sigma}^{(1)}\rangle^{+}(\xi) - \langle\overline{\Sigma}\rangle(\xi)[\![\overline{u}^{(1)}]\!]^{-}(\xi)$$
$$= -[\![\overline{U}]\!](\xi)\overline{P}^{-}(\xi) - \langle\overline{U}\rangle(\xi)\overline{Q}^{-}(\xi) - \kappa\langle\overline{\Sigma}\rangle(\xi)\overline{P}^{+}(\xi) - \langle\overline{U}\rangle(\xi)\overline{Q}^{+}(\xi). \tag{5.142}$$

The same reasoning used in Section 5.5, allows us to derive the integral representation for Δa_0 in the form

$$\Delta a_0 = -\frac{1}{2}\sqrt{\frac{\mu_0}{\pi}}\left\{\int_{-\infty}^{\infty}\left[\xi[\![\overline{U}]\!](\xi)\overline{P}^{-}(\xi) + \xi\langle\overline{U}\rangle(\xi)\overline{Q}^{-}(\xi)\right]d\xi\right.$$
$$\left. + \int_{-\infty}^{\infty}\left[\kappa\xi\langle\overline{\Sigma}\rangle^{-}(\xi)\overline{P}^{+}(\xi) + \xi\langle\overline{U}\rangle(\xi)\overline{Q}^{+}(\xi)\right]d\xi\right\}. \tag{5.143}$$

This important constant has an immediate physical meaning. If $\Delta a_0 = 0$ then the defect configuration is neutral; its presence causes zero perturbation to the leading order of tractions at the crack tip. Otherwise, if $\Delta a_0 < 0$,

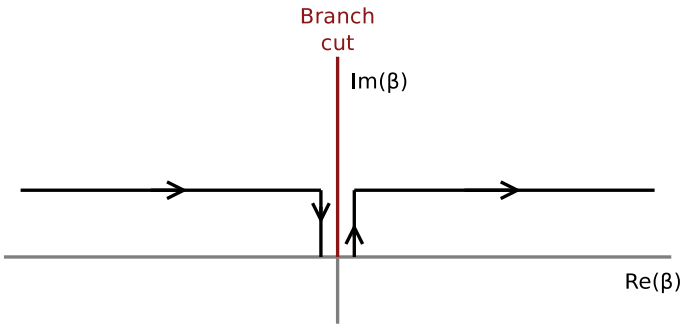

Figure 5.3: Contour of integration around the branch cut occupying $\mathrm{Re}(\beta) = 0$, $\mathrm{Im}(\beta) > 0$.

the presence of the defect causes a reduction in the crack tip traction and so shields the crack from propagating further. Finally, if $\Delta a_0 > 0$ then the defect causes an amplification effect and so can be considered to be encouraging the propagation of the main crack. This interpretation makes the vital assumption that the crack will propagate along the imperfect interface. This assumption seems reasonable since the interface is soft, but should be treated with caution when the inclusion is lying near to the interface; in such a configuration the crack may deviate from the interface line.

5.9 Computation of the solution's gradient

The remainder of this chapter is devoted to performing numerical computations of a_0 and Δa_0. We will use the balanced point loading configuration as described earlier for computations of a_0, but for computations of Δa_0 we will use smooth loadings in order to reduce the complexity of the computations. In particular, this alternative loading will cause integrands to have more favourable (i.e. faster decaying) behaviour at infinity. Nevertheless, we

stress that it is perfectly possible to perform computations for Δa_0 in the point loading case.

In the present section we discuss the computation of $\frac{\partial u_0}{\partial x}$, which is needed in the evaluation of the function $\frac{\partial w^{(1)}}{\partial y}$, as can be seen in (5.130). We here detail the computation for a point above the interface ($y > 0$). We see from equation (5.115) that for $y > 0$,

$$\bar{u}_0(\xi, y) = -\frac{1}{\mu_1|\xi|}\left\{\varphi^+(\xi) + \langle\bar{p}\rangle(\xi) + \frac{1}{2}[\![\bar{p}]\!](\xi)\right\} e^{-|\xi|y}. \tag{5.144}$$

It follows that

$$\frac{\partial u_0}{\partial x} = \frac{1}{2\pi}\int_{-\infty}^{\infty} \frac{i\xi}{\mu_1|\xi|}\left\{\varphi^+(\xi) + \langle\bar{p}\rangle(\xi) + \frac{1}{2}[\![\bar{p}]\!](\xi)\right\} e^{-|\xi|y}e^{-i\xi x}\mathrm{d}\xi. \tag{5.145}$$

We split this integral into two parts, writing $\frac{\partial u_0}{\partial x} = \frac{1}{2\pi}(I_A + I_B)$, where I_A and I_B are defined by

$$I_A = \int_{-\infty}^{\infty} \frac{i\xi}{\mu_1|\xi|}\left\{\langle\bar{p}\rangle(\xi) + \frac{1}{2}[\![\bar{p}]\!](\xi)\right\} e^{-|\xi|y}e^{-i\xi x}\mathrm{d}\xi, \tag{5.146}$$

$$I_B = \int_{-\infty}^{\infty} \frac{i\xi}{\mu_1|\xi|}\varphi^+(\xi)e^{-|\xi|y}e^{-i\xi x}\mathrm{d}\xi. \tag{5.147}$$

The integral I_A may be evaluated analytically, while I_B is to be computed numerically.

5.9.1 Imposed tractions

As described in the introduction to this section, while the procedure described is suitable for application to point loadings, we will ease the computational effort required by performing computations for specific imposed tractions on the upper and lower crack face given respectively by

$$p_+(x) = -\frac{a_1^2}{a_2^2}xe^{a_1x}, \quad p_-(x) = -xe^{a_2x}, \quad x < 0,\ a_1, a_2 > 0. \tag{5.148}$$

The Fourier transforms of the loadings are

$$\bar{p}_1(\xi) = \frac{a_1^2}{a_2^2(a_1+i\xi)^2}, \quad \bar{p}_2(\xi) = \frac{1}{(a_2+i\xi)^2}, \tag{5.149}$$

and so the transformed jump and average functions are found to be

$$[\![\bar{p}]\!](\xi) = \frac{a_1^2}{a_2^2(a_1+i\xi)^2} - \frac{1}{(a_2+i\xi)^2}, \quad \langle\bar{p}\rangle(\xi) = \frac{1}{2}\left\{\frac{a_1^2}{a_2^2(a_1+i\xi)^2} + \frac{1}{(a_2+i\xi)^2}\right\}. \tag{5.150}$$

As expected, the transformed jump disappears as $\xi \to 0$ while the average does not, with

$$[\![\bar{p}]\!](\xi) = \frac{2i(a_1-a_2)}{a_1 a_2^3}\xi + O(\xi^2), \quad \langle\bar{p}\rangle(\xi) = \frac{1}{a_2^2} + O(\xi), \quad \xi \to 0, \tag{5.151}$$

and both the jump and average decay as $O(1/\xi^2)$ as $\xi \to \infty$. This quadratic decay for large ξ makes computation easier than for point loadings, since the analogous transformed jump in the point loading case oscillates boundedly at infinity. This makes the numerical computation of $L^+(\xi)$ (as defined in (5.110)) difficult (in the sense of being very sensitive to computational error) since terms in the integrand decay only as $1/\beta$ multiplied by a bounded oscillation.

5.9.2 Computation of I_B

The integral I_A may be evaluated analytically. Let us now restrict our attention to the integral I_B. Recalling the expression for $\varphi^+(\xi)$ obtained in (5.112), we see that

$$I_B = \frac{-i}{\kappa\pi\mu_0\mu_1}\int_{-\infty}^{\infty} \frac{\xi}{|\xi|}\frac{L^+(\xi)}{B^+(\xi)} e^{-|\xi|y} e^{-i\xi x} \mathrm{d}\xi. \tag{5.152}$$

Note that the integrand is well behaved in the upper half-plane, with the exception of a branch cut along the positive imaginary axis. We write

$$I_B = \frac{-i}{\kappa\pi\mu_0\mu_1}\left\{\int_{-\infty}^{0} -\frac{L^+(\xi)}{B^+(\xi)}e^{\xi y}e^{-i\xi x}\mathrm{d}\xi + \int_{0}^{\infty}\frac{L^+(\xi)}{B^+(\xi)}e^{-\xi y}e^{-i\xi x}\mathrm{d}\xi\right\}. \quad (5.153)$$

We will evaluate I_B along a contour split into four parts (see Figure 5.3 on page 138), with the horizontal contours of integration having an imaginary part of $\tau > 0$. That is, we write the first integral in (5.153) as

$$\int_{-\infty+i\tau}^{-\varepsilon+i\tau} -\frac{L^+(\xi)}{B^+(\xi)}e^{\xi y}e^{-i\xi x}\mathrm{d}\xi - \int_{-\varepsilon+0i}^{-\varepsilon+i\tau} -\frac{L^+(\xi)}{B^+(\xi)}e^{\xi y}e^{-i\xi x}\mathrm{d}\xi, \quad (5.154)$$

and the second integral in (5.153) as

$$\int_{\varepsilon+0i}^{\varepsilon+i\tau}\frac{L^+(\xi)}{B^+(\xi)}e^{-\xi y}e^{-i\xi x}\mathrm{d}\xi + \int_{\varepsilon+i\tau}^{\infty+i\tau}\frac{L^+(\xi)}{B^+(\xi)}e^{-\xi y}e^{-i\xi x}\mathrm{d}\xi, \quad (5.155)$$

where $0 < \varepsilon \ll 1$. We can combine the integrals along the vertical contours, and find that as $\varepsilon \to 0$, these integrals become

$$\int_{-\varepsilon+0i}^{-\varepsilon+i\tau}\frac{L^+(\xi)}{B^+(\xi)}e^{\xi y}e^{-i\xi x}\mathrm{d}\xi + \int_{\varepsilon+0i}^{\varepsilon+i\tau}\frac{L^+(\xi)}{B^+(\xi)}e^{-\xi y}e^{-i\xi x}\mathrm{d}\xi = \int_{0}^{i\tau}\frac{2L^+(\alpha)}{B^+(\alpha)}e^{-ix\alpha}\cosh(\alpha y)\mathrm{d}\alpha. \quad (5.156)$$

In order to compute the integrals along the horizontal contours, we need to tabulate $L^+(\xi)/B^+(\xi)$ along the contour $\mathrm{Im}(\xi) = \tau$. After this tabulation, we will be able to follow the above procedure to find I_A and I_B, and thus $\frac{\partial u_0}{\partial x}$ for $y > 0$.

5.9.3 Computation of $L^+(\xi)$

While the function $B^+(\xi)$ can be easily computed, $L^+(\xi)$ (as defined in (5.110)) requires more effort. We write

$$L^+(\xi) = \frac{\kappa}{2\pi i}\left\{I_C(\xi) + \pi\mu_0 I_D(\xi)\right\}, \quad \mathrm{Im}(\xi) > 0, \quad (5.157)$$

where

$$I_C(\xi) = \int_{-\infty}^{\infty} \frac{\Lambda(\beta)[\![\bar{p}]\!](\beta)}{B^-(\beta)} \frac{\mathrm{d}\beta}{\beta - \xi}, \quad \mathrm{Im}(\xi) > 0, \tag{5.158}$$

and

$$I_D(\xi) = \int_{-\infty}^{\infty} B^+(\beta)\langle\bar{p}\rangle(\beta) \frac{\mathrm{d}\beta}{\beta - \xi}, \quad \mathrm{Im}(\xi) > 0. \tag{5.159}$$

Computation of I_C

Noting that we only aim to compute I_C for ξ with positive imaginary part, the integral is not singular. We further note from our asymptotic estimates for $[\![\bar{p}]\!]$ and B^- (see (5.106), (5.107) and (5.151)) that

$$\frac{\Lambda(\beta)[\![\bar{p}]\!](\beta)}{B^-(\beta)} \sim \frac{\mu_* \mu_0 i(a_2 - a_1)\sqrt{\pi}}{a_1 a_2^3} \,\mathrm{sgn}(\beta)\beta_-^{1/2}, \quad \beta \to 0, \tag{5.160}$$

and

$$\frac{\Lambda(\beta)[\![\bar{p}]\!](\beta)}{B^-(\beta)} \sim \frac{(a_2^2 - a_1^2)\sqrt{\pi\mu_0}}{2a_2^2\beta^2}, \quad \beta \to \infty, \tag{5.161}$$

and so we may straightforwardly compute the integral I_C along the real line.

Computation of I_D

We note that

$$B^+(\beta)\langle\bar{p}\rangle(\beta) = O(\beta^{-1/2}), \quad \beta \to 0. \tag{5.162}$$

In order to make the computation more simple by removing this integrable singularity, we further split the integral I_D, writing

$$I_D = \int_{-\infty}^{\infty} B^+(\beta) \left\{ \langle\bar{p}\rangle(\beta) - \frac{1}{a_2^2 - i\beta} \right\} \frac{\mathrm{d}\beta}{\beta - \xi} + \int_{-\infty}^{\infty} B^+(\beta) \frac{1}{a_2^2 - i\beta} \frac{\mathrm{d}\beta}{\beta - \xi}. \tag{5.163}$$

The term in curly braces in the first integral now behaves as $O(\beta)$ as $\beta \to 0$ (see (5.151) and (5.162)), and so this integral is easily computed. Noting

that the second integrand in (5.163) is analytic in the upper half-plane and decays faster than $1/\beta$ as $\beta \to \infty$, the residue theorem yields that

$$\int_{-\infty}^{\infty} B^+(\beta) \frac{1}{a_2^2 - i\beta} \frac{\mathrm{d}\beta}{\beta - \xi} = \frac{2\pi i B^+(\xi)}{a_2^2 - i\xi}, \tag{5.164}$$

and so I_D is now computed.

With I_C and I_D now computed, we can substitute their values into (5.157) to obtain $L^+(\xi)$ and follow the procedure described at the beginning of this section to obtain $\frac{\partial u_0}{\partial x}$.

5.10 Numerical results

5.10.1 Computations of a_0

In this section we present results of computations obtained by following the methods previously described in this chapter. All results have been computed using MATLAB.

Figure 5.4 on page 144 plots a_0 against μ_*, showing how the constant from the asymptotic expansion at the crack tip a_0 varies with differently contrasting stiffnesses of materials. Recalling that

$$\mu_* = \frac{\mu_1 - \mu_2}{\mu_1 + \mu_2}, \tag{5.165}$$

we note that when μ_* is near to -1, this corresponds to $\mu_2 \gg \mu_1$. That is, the material occupying the region below the crack is far stiffer than the material above the crack. As this limit is approached, the precise locations of the point loadings on the lower face of the crack decrease in importance, since the material becomes sufficiently stiff for the material to act as an almost rigid body; this explains the meeting of the two lines at $\mu_* = -1$.

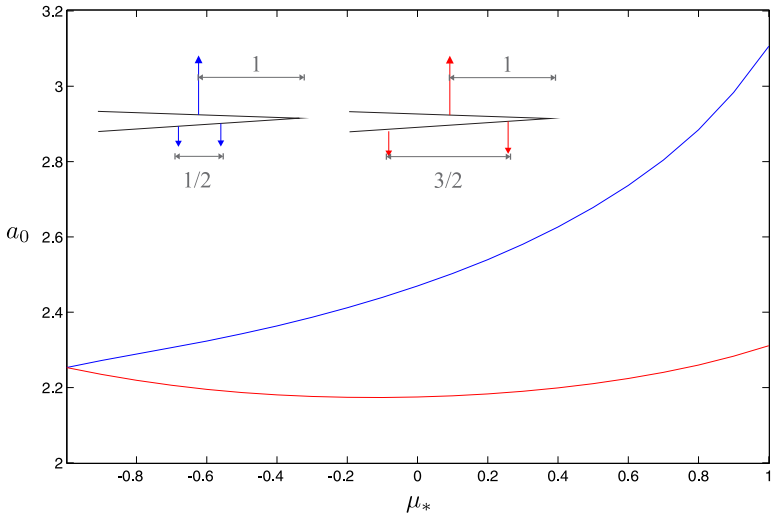

Figure 5.4: Plot of a_0 against μ_*. Both cases plotted here use the parameters $\kappa_* = 1$ and $a = 1$, but with different values for b, which controls the separation between the point loadings. The red plot has $b = 3/4$ while the blue plot uses $b = 1/4$.

In Figure 5.5 we present a log-log plot of a_0 against κ_*, the dimensionsless parameter of interface imperfection defined as $\kappa_* = \kappa(\mu_1 + \mu_2)$. This has been computed for different values of μ_* (describing the contrast in material stiffnesses) and also for different values of b (describing the separation distance between the point loadings) while keeping a fixed ($a = 1$). The solid lines correspond to $b = \frac{3}{4}$ while dotted lines represent $b = \frac{1}{4}$ and different colours correspond to different values of μ_*: green corresponds to $\mu_* = -0.8$, blue to $\mu_* = 0$ and red to $\mu_* = +0.8$.

Bearing in mind our remarks regarding Figure 5.4, we would expect that changing the value of b would have the greatest impact for values of μ_* near $+1$. This is indeed the case in Figure 5.5.

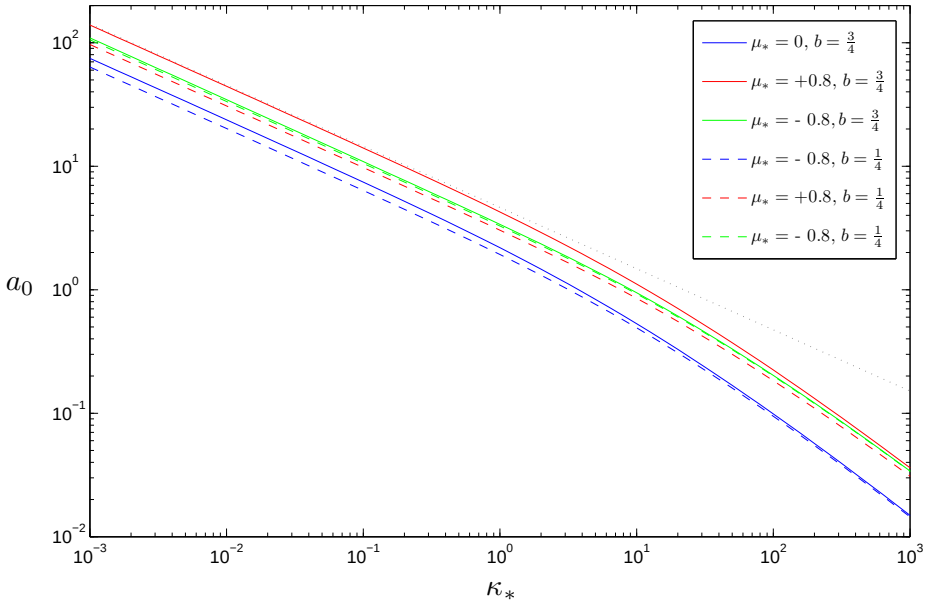

Figure 5.5: Log-log plot of a_0 against κ_* for differently contrasting materials.

Also plotted in Figure 5.5 is a grey dotted line that is tangent to the curves (which run parallel) as $\kappa_* \to 0$; this tangent has slope $-\frac{1}{2}$, indicating that $a_0 = O(\kappa_*^{-1/2})$ as $\kappa_* \to 0$. As $\kappa_* \to 0$, the interface becomes almost perfect, and so the square-root behaviour associated with fields near crack tips in the perfect interface setting is not unexpected. This is consistent for instance with the estimate given for the case in the strip in equation (3.210) on page 75. Moreover, as $\kappa \to +\infty$, the curves on the log-log plot have slope -1, implying that $a_0 = O(\kappa_*^{-1})$ as $\kappa_* \to +\infty$.

5.10.2 Comparison of a_0 with stress intensity factors from the perfect interface case

In this subsection we discuss an approach which enables a comparison to be made between imperfect and perfect interface situations.

Comparing the fields directly is not a simple task since in the perfect interface case the stresses become unbounded at the crack tip, exhibiting asymptotic behaviour of the form $\sigma_{yz} \sim O(r^{-1/2})$, $r \to 0$. In the imperfect setting, we have derived the leading order of stresses at the crack tip, a_0, which is independent of r. Moreover, different normalisations may make comparisons difficult.

However, given two particular pairs of materials with constrast parameters $(\mu_*)_1$ and $(\mu_*)_2$ say, we might expect the dimensionless ratios of stress intensity factors $(K_{III}^{(0)})_1/(K_{III}^{(0)})_2$ (from the perfect interface case) and $(a_0)_1/(a_0)_2$ (imperfect case) to be similar for small κ_*.

This approach of comparing ratios of a_0 with stress intensity factors can be justified by considering the paper of Mishuris *et al.* [43] which examines the use of the crack tip opening displacement in fracture criteria by considering a crack within a thin soft layer of shear modulus μ_{int} and thickness H between two larger, stiffer bodies. Lemma 5.3 in that paper demonstrates that the Mode-III stress intensity factor for the crack in the soft medium is given by

$$K_{III}^{\text{int}} = \frac{\mu_{\text{int}}}{\sqrt{H}} [\![u]\!](0^+), \tag{5.166}$$

where $[\![u]\!](0^+)$ is computed from the model problem in which the thin layer is replaced by soft imperfect interface transmission conditions; in the presently considered problem recall that $[\![u]\!](0^+) = \kappa a_0$ and $\kappa = H/\mu_{\text{int}}$. Thus the stress intensity factor for the crack inside the thin layer is related to a_0 by

the expression

$$K_{III}^{\text{int}} = \sqrt{H} a_0. \tag{5.167}$$

Thus given two pairs of material parameters for a fixed extent of interfacial imperfection ($\kappa, H, \mu_{\text{int}}$ fixed), the ratio of the respective $(a_0)_1$ and $(a_0)_2$ values is related to the ratios of the stress intensity factors $(K_{III}^{\text{int}})_1$ and $(K_{III}^{\text{int}})_2$ via

$$\frac{(a_0)_1}{(a_0)_2} = \frac{(K_{III}^{\text{int}})_1}{(K_{III}^{\text{int}})_2}. \tag{5.168}$$

Note that while H does not explicitly appear in equation (5.168), all parameters in the equation depend on the thickness of the interfacial layer H. If we fix μ_{int} and let $H \to 0$ then the perfect interface case is approached.

In the perfect interface case, the stress intensity factor (derived in [54]) is given by

$$K_{III}^{(0)} = -\sqrt{\frac{2}{\pi}} \int_0^\infty \left\{ \langle p \rangle(-r) + \frac{\mu_0}{2} [\![p]\!](-r) \right\} r^{-1/2} \mathrm{d}r. \tag{5.169}$$

As derived earlier in this thesis in Section 5.5, the leading order of tractions near the crack tip in the imperfect interface case is given by

$$a_0(\kappa_*) = \frac{1}{2} \sqrt{\frac{\mu_0}{\pi}} \int_{-\infty}^\infty \xi \left([\![\bar{U}]\!](\xi) \langle \bar{p} \rangle(\xi) + \langle \bar{U} \rangle(\xi) [\![\bar{p}]\!](\xi) \right) \mathrm{d}\xi. \tag{5.170}$$

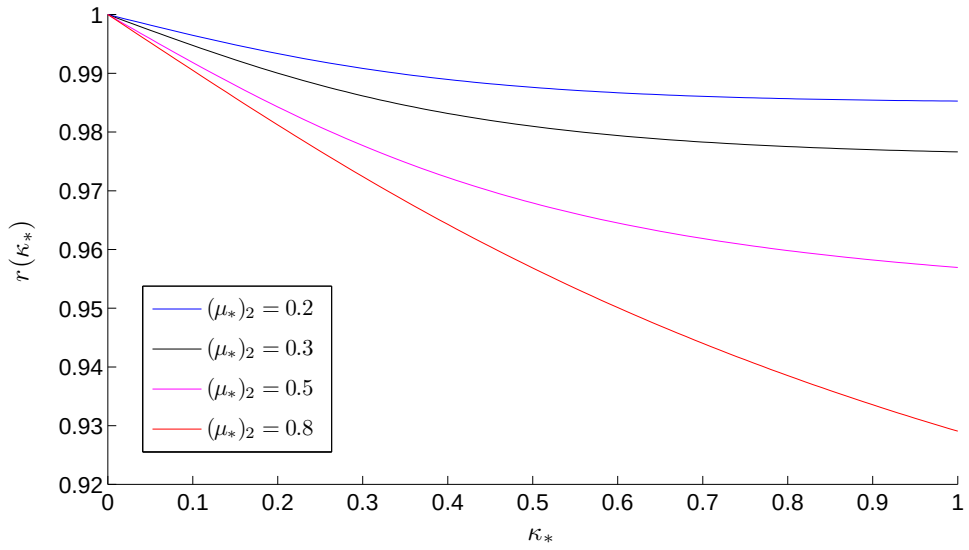

Figure 5.6: Plot of the ratio r as defined in (5.171) for four different values of $(\mu_*)_2$.

Figure 5.6 plots the ratio

$$r(\kappa_*) = \frac{(a_0(\kappa_*))_1/(a_0(\kappa_*))_2}{(K_{III}^{(0)})_1/(K_{III}^{(0)})_2} \tag{5.171}$$

for $0 < \kappa_* < 1$ with $(\mu_*)_1 = 0$ fixed and for four different values of $(\mu_*)_2$. The loadings used are balanced; a point loading on the upper crack face at $x = -1$ is balanced by two equal loadings at $x = -1.25$ and $x = -0.75$.

We see from the plot that as $\kappa_* \to 0$, $r(\kappa_*) \to 1$. This provides some verification of the accuracy of our computations and demonstrates that the comparison of ratios approach for small κ again the perfect interface case is useful.

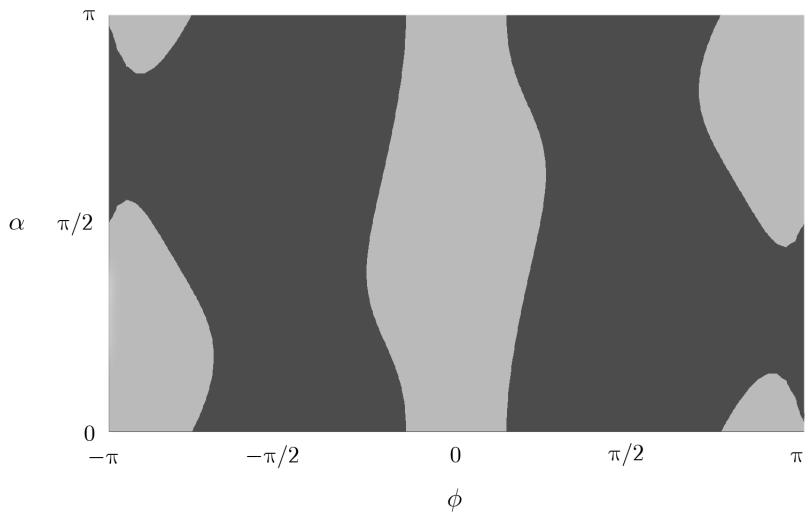

Figure 5.7: Plot of the sign of Δa_0 for varying α and ϕ which describe the defect's location and orientation (see Figure 5.1). The darker shaded areas are those (ϕ, α) for which $\Delta a_0 > 0$ while paler regions have $\Delta a_0 < 0$.

5.10.3 Computation of Δa_0

We now present numerical results for the perturbed problem computed using MATLAB. Figure 5.7 shows the sign of Δa_0 for a specific configuration. The tractions on the upper and lower crack faces are of the form described earlier in equation (5.148) with $a_1 = 2$ and $a_2 = 3$ and the imperfect interface has $\kappa_* = 1$. The inclusion is stiff, with the contrast between the internal and external materials of the inclusion given by $\mu_\star = 5$.

The figure clearly shows the regions for which crack growth is encouraged or discouraged for this configuration. When the stiff inclusion is located near the interface (that is, ϕ is close to zero), the orientation angle α appears to have little influence on the sign of Δa_0; in this case the propagation of the crack is discouraged (that is, $\Delta a_0 < 0$). However, we should be particularly

cautious when interpreting results when ϕ is particularly close to zero since this corresponds to the crack being placed near the imperfect interface which makes our model invalid as we commented before equation (5.123). Moreover, if the inclusion is close to the interface then the assumption that the crack propagates along the interface line may become invalid, since the inclusion's presence may deflect the line of propagation.

The other regions of the graph illustrate that both the angle of orientation and location of the defect play a more complicated role in determining whether the main crack's propagation is encouraged or discouraged, as was also seen in the analysis of the perfect interface analogue to the problem presented in [54], albeit for different types of loading.

5.11 Conclusion

To conclude this chapter, the imperfect interface weight function techniques presented allow for the leading order out-of-plane component of stress and the displacement discontinuity near the crack tip to be quantified. The displacement discontinuity can serve as an important parameter in fracture criteria for imperfect interface problems; we demonstrated that, in the limiting case as the extent of imperfection tends towards zero, the criterion is consistent with classical criteria based on the notion of the stress intensity factor. Perturbation analysis further enables us to correct the solution to account for the presence of a small inclusion.

Chapter 6

Summary of main results and indications of possible further work

6.1 Summary of main results

In this thesis we have adapted the weight function technique to solve problems in solids containing cracks and imperfect interfaces.

We first considered a weight function problem in a strip for a semi-infinite crack sitting on an imperfect interface and derived a new weight function with significantly different behaviour to previously derived weight functions for analogous perfect interface problems. We then applied this weight function to find expressions for physical fields near the crack tips in a periodic structures consisting of an array of cracks sitting on an imperfect interface in a thin bimaterial strip. This analysis not only yielded constants describing the distribution of stresses near the crack tip in terms of the solution to an easily

solved low dimensional model, but allowed us to estimate eigenfrequencies for the thin structures.

In both the imperfect interface case and a previously studied analogous perfect interface problem, the asymptotic approach displayed a discrepancy against finite element simulations in the prediction of standing wave eigenfrequencies; other eigenfrequencies displayed excellent accuracy. We amended the model by improving the asymptotic algorithm, considering the frequency as an asymptotic quantity. While it is not clear *a priori* that this would make a significant difference, we found that in most cases the accuracy of the standing wave eigenfrequency improves by around an order of magnitude while the eigenfrequencies for propagating waves retain their already excellent accuracy. The correction made by this improved model is most uniform in materials with similar wave speeds, although still gives useful information for bimaterial strips consisting of more contrasting materials. Different analysis should be sought if the interface is *very* highly imperfect however, since this causes slow decay of boundary layers and thus the model's assumption of independent boundary layers may become unjustified.

We then considered a different weight function problem, defined for a bi-material structure sitting in the whole plane rather than a strip, with a semi-infinite crack sitting on an imperfect interface. Betti's formula in a new imperfect interface setting allowed us to find asymptotic expressions for the physical behaviour near the crack tip for prescribed loadings applied to the crack faces. We conducted perturbation analysis to determine how the leading order coefficient of stress near the crack tip is affected by the presence of small linear defects such as elliptic inclusions in the materials. Depending on whether this increased or decreased the coefficient, this is interpreted as

the inclusion having a shielding or amplifying effect on the propagation of the main crack.

6.2 Further work

There are many different possible directions in which the research presented here could be extended. Among these would be the extension of the problem formulated in the strip containing imperfect interfaces to the full 2D case to include consideration of shear longitudinal waves. This problem would involve some additional technical difficulties but the approach would be fundamentally similar. The work in Chapter 5 could be extended to provide integral identities which would aid in the solution of many further imperfect interface problems. Further, a range of delamination problems for sandwich-type structures is another area for possible research.

6.2.1 Wider areas for further work

The cases examined in this thesis have all concerned *isotropic* materials; there are many interesting and important applications relating to *anistropic* materials in which modelling could be performed, including the addition of imperfect interfaces. An example of such a case is the modelling of piezoelectric structures.

Piezoelectricity is the charge that accumulates in certain solids (including many ceramics) in response to applied mechanical stress. Similarly, such a material undergoes stress and thus deformation when a current is passed through it. Actuators are components that are constructed from multilayered structures whose layers are typically thinner than 100μm; thin metal

electrode films are embedded in a piezo-ceramic material. The modelling of these structures can make use of asymptotic approaches for the thin layers and it may be interesting to investigate how the presence of manufacturing defects affects such components.

Another potential application of imperfect interface techniques is in the modelling of hydraulic fracture for enhanced oil and gas extraction, the process by which fractures propagate through a brittle rock layer due to pressurized fluid. Problems related to this application are computationally challenging; many physical mechanisms are simultaneously in play, including fracture mechnics, fluid flow in the fracture, fluid leak-off into the rock and deformation of the rock due to the fluid pressure. These coupled mechanisms introduce a number of challenges including strong non-linearity.

Bibliography

[1] Antipov, Y.A., Avila-Pozos, O., Kolaczkowski, S.T. and Movchan, A.B., 2001, Mathematical model of delamination cracks on imperfect interfaces. *International Journal of Solids and Structures*, **38**, 6665–6697.

[2] Asplund, S.O., 1966, Structural mechanics: classical and matrix methods. *Prentice-Hall.*

[3] Atkinson, C., Eshelby, J.D., 1968, The flow of energy into the tip of a moving crack. *International Journal of Fracture Mechanics*, **4**, 3–8.

[4] Atkinson, C., 1977, On stress singularities and interfaces in linear elastic fracture mechanics. *Int. J. Fracture*, **13**, 807–820.

[5] Avila-Pozos, O. and Movchan, A.B., 2003, Slow decay of end effects in layered structures with an imperfect interface. *J. Engrg. Math.*, **45**, 155–168.

[6] Baik, J.-M., Thompson, R.B., 1984, Ultrasonic scattering from imperfect interfaces — A quasi-static model. *Journal of Nondestructive Evaluation*, **4**, 177–196.

[7] Barenblatt, G.I., 1959, The formation of equilibrium cracks during brittle fracture: general ideas and hypotheses, axially-symmetric cracks. *J. Appl. Math. Meth.*, **23**, 622-636.

[8] Benveniste, J.R., 2006, A general interface model for a three-dimensional curved thin anisotropic interphase between two anisotropic media. *J. Mech. Phys. Solids*, **54(4)**, 708–734.

[9] Benveniste, Y. and Miloh, T., 2001, Imperfect soft and stiff interfaces in two-dimensional elasticity. *Mech. Materials*, **33**, 309–323.

[10] Boström, A., Golub, M., 2009, Elastic SH wave propagation in a layered anisotropic plate with interface damage modelled by spring boundary conditions. *Q. J. Mechanics Appl. Math.*, **62**, 39–52.

[11] Bueckner, H.F., 1970, A novel principle for the computation of stress intensity factors. *Zeit. Angew. Math. Mech.*, **50**, 529–546.

[12] Bueckner, H.F., 1985. Weight functions and fundamental fields for the penny-shaped and the half-plane crack in three-space. *International Journal of Solids and Structures* **23**, 57–93.

[13] Cherepanov, G.P., 1967, The propagation of cracks in a continuous medium. *Journal of Applied Mathematics and Mechanics*, **31(3)**, 503–512.

[14] Comninou, M., 1977, The interface crack. *J. Appl. Mech.*, **44**, 631–636.

[15] Cottrell, A. H., 1962, Theoretical aspects of radiation damage and brittle fracture in steel pressure vessels. *Iron Steel Institute Special Report* **69**, 281–296.

[16] Dugdale, D.S., 1960, Yielding of steel sheets containing slits. *J. Mech. Phys. Solids.* **8**, 100–104.

[17] Euler, L., 1744, Methodus inveniendi lineas curvas maximi minimive proprietate gaudentes, sive solutio problematis isoperimitrici latissimo sensu accepti. *Lausanne: Bousquet*.

[18] Evans, D.V., Linton, C.M. and Ursell, F., 1993, Trapped mode frequencies embedded in the continuous spectrum. *Quarterly Journal of Mechanics and Applied Mathematics*, **46**, 253–274.

[19] Gifford, L.N., Hilton, P.D., 1978, Stress intensity factors by enriched finite elements. *Engineering Fracture Mechanics*, **10(3)**, 485–496.

[20] Golub, V., Boström, A., 2011, Interface damage modeled by spring boundary conditions for in-plane elastic waves. *Wave Motion*, **48(2)**, 105–115.

[21] Golub, M., Zhang, C., Wang, Y.S., 2011, SH-wave propagation and resonance phenomena in a periodically layered composite structure with a crack. *Journal of Sound and Vibration*, **330**, 3141–3154.

[22] Griffith, A.A., 1920, The phenomenon of rupture and flow in solids. *Philosophical Transactions of the Royal Society (London)*, **221**, 163–198.

[23] Hashin, Z., 2001, Thin interphase/imperfect interface in conduction. *J. Appl. Phys.*, **89**, 2261–2267.

[24] Hutchinson, J.W., Mear, M.E. and Rice, J.R., 1987, Crack paralleling an interface between dissimilar materials. *ASME J. Appl. Mech.*, **54**, 828–832.

[25] Inglis, C.E., 1913, Stresses in a plate due to the presence of cracks and sharp corners. *Transactions of the institute of naval architects*, **55**, 219–241.

[26] Irwin, G.R., 1957, Analysis of stresses and strains near the end of a crack traversing a plate. *Journal of Applied Mechanics*, **24**, 361–364.

[27] Kanninen, M.F., Rybicki, E.F., Stonesifer, R.B., Broek, D., Rosenfiels, A.R., Marschall, C.W., Hahn, G.T., 1979, Elastic-Plastic fracture mechanics for two-dimensional stable crack growth and instability problems. *Elastic-Plastic fracture ASTM STP 668*, 121–150.

[28] Kaplunov, J.D., Kossovitch, L., Nolde, E.V., 1998, Dynamics of Thin Walled Elastic Bodies, *N.-Y.: Academic Press.*

[29] Kaplunov, J.D., Krynkin, A., 2006, Resonance vibrations of an elastic interfacial layer. *Journal of Sound and Vibration*, **294**, 663–677.

[30] Kassir, M.K., Sih, G.C., 1973, Application of Papkovich-Neuber potentials to a crack problem. *Int. J. Solids Struct.* **9**, 643–654.

[31] Klarbring, A., Movchan, A.B., 1998, Asymptotic modelling of adhesive joints. *Mechanics of Materials*, **28**, 137–145.

[32] Kozlov, V., Maz'ya, V.G., Movchan, A.B., 1999, Asymptotic analysis of fields in multi-structures. *Oxford University Press.*

[33] Lazarus, V., Leblond, J.B., 1998, Three-dimensional crack-face weight functions for the semi-infinite interface crack–I: variation of the stress intensity factors due to some small perturbation of the crack front. *J. Mech. Phys. Solids*, **46**, 489–511.

[34] Leunpichcharoen, S., Wijeyewickrema, A.C., 2003, Dispersion effects of extensional waves in pre-stressed imperfectly bonded incompressible elastic layered composites. *Wave Motion*, **38(4)**, 311–325.

[35] Linton, C.M. and McIver, M., 2002, Periodic structures in waveguides. *Proceedings of the Royal Society A*, **458**, 3003–3021.

[36] Lipton R., 2001, Effect of interfacial bonding on Fiber reinforced shafts subject to antiplane shear. *Int. J. Solids Struct.*, **38**, 369–387.

[37] Maz'ya, V.G., Nazarov, S.A., Plamenevskii, V.A., 1983, Evaluation of the asymptotic form of the 'intensity coefficients' on approaching corner or conical points. *USSR Computational Mathematics and Mathematical Physics*, **23(2)**, 50–58.

[38] McIver, M., Linton, C.M., McIver, P., Zhang, J. and Porter, R., 2001, Embedded trapped modes for obstacles in two-dimensional waveguides. *Quarterly Journal of Mechanics and Applied Mathematics*, **54**, 273–293.

[39] Mikata, Y., Achenbach, J.D., 1988, Interaction of harmonic waves with a periodic array of inclined cracks. *Wave Motion*, **10**, 59–72.

[40] Mishuris, G.S., 2001, Interface crack and nonideal interface concept (Mode III). *International Journal of Fracture*, **107**, 279–296.

[41] Mishuris, G., Kuhn, G., 2001, Asymptotic behaviour of the elastic solution near the tip of a crack situated at a nonideal interface. *Zeitschrift f ur Angewandte Mathematik und Mechanik*, **81(12)**, 811–826.

[42] Mishuris, G.S., 2003, Mode III interface crack lying at thin nonhomogeneous anisotropic interface. Asymptotics near the crack tip. *IUTAM Symposium on Asymptotics, Singularities and Homogenisation in Problems of Mechanics*, Kluwer Academic Publishers, 251–260.

[43] Mishuris, G., Movchan, N.V., Movchan, A.B., 2006, Steady-state motion of a Mode-III crack on imperfect interfaces, *Quart. J. Mech. Appl. Math.*, **59(4)**, 487–516.

[44] Mishuris, G.S., Movchan, A.B. and Bercial, J.P., 2007, Asymptotic analysis of Bloch-Floquet waves in a thin bi-material strip with a periodic array of finite-length cracks. *Waves in Random and Complex Media*, **17**, 511–533.

[45] Mishuris, G., Movchan, A., Movchan, N. and Piccolroaz, A., 2011, Interaction of an interfacial crack with linear small defects under out-of-plane shear loading. *Computational Materials Science*, in press, arXiv:1010.6223v4.

[46] Movchan, A.B., Movchan, N.V., 1995, Mathematical modeling of solids with nonregular boundaries. CRC-Press.

[47] Murakami, Y., 1987, Stress Intensity Factors Handbook Volume 2. *Pergamon Press.*

[48] Neuber, H., 1937, Kerbspannungslehre. Springer, Berlin.

[49] Novozhilov, V.V., 1969, On necessary and sufficient criterion of brittle strength. *Appl. Math. Mech. (PMM)*, **33**, 212–222.

[50] Noble, B., 1988, Methods based on the Wiener-Hopf technique for the solution of partial differential equations. Chelsea Publishing Company, New York.

[51] Piccolroaz, A., Mishuris, G., Movchan, A.B., 2009, Evaluation of the Lazarus-Leblond constants in the asymptotic model of the interfacial wavy crack. *J. Mech. Phys. Solids*, **55(8)**, 1575–1600.

[52] Piccolroaz, A., Mishuris, G., Movchan, A.B., 2009, Symmetric and skew-symmetric weight functions in 2D perturbation models for semi-infinite interfacial cracks. *J. Mech. Phys. Solids*, **57(9)**, 1657–1682.

[53] Piccolroaz, A., Mishuris, G., Movchan, A.B., Perturbation of mode III interfacial cracks. *Int J Frac*, **166**, 41–51.

[54] Piccolroaz, A., Mishuris, G., Movchan, A., Movchan, N., 2012, Perturbation analysis of Mode III interfacial cracks advancing in a dilute heterogeneous material. *International Journal of Solids and Structures*, **49**, 244–255.

[55] Rice, J.R., Sih, G.C., 1965. Plane problems of cracks in dissimilar media. *ASME J. Appl. Mech.*, **32**, 418–423.

[56] Rice, J.R., 1967, Some remarks on elastic crack tip stress fields. *Int. J. Solids Struct.*, **8**, 751–758.

[57] Rice, J.R., 1968, A path independent integral and the approximate analysis of strain concentrations by notches and cracks. *Journal of Applied Mechanics*, **35**, 379–386.

[58] Rice, J.R., Sorensen, E.P., 1978, Continuing crack tip deformation and fracture for plane strain crack growth in elastic-plastic solids. *J. Mech. and Phys. of Solids* **26**, 163–186.

[59] Rice, J.R., 1988, Elastic fracture mechanics concepts for interfacial cracks. *J. Appl. Mech.*, **55**, 98–103.

[60] Rice, J.R., 1989, Weight function theory for three-dimensional crack analysis. *Fracture Mechanics: Perspective and Directions*, Special Technical Publication 1020, 29–57. ASTM, Philadelphia.

[61] Shih, C.F., de Lorenzi, H.G., Andrews, W.R., 1979, Studies on crack initiation and stable crack growth. *Elastic-Plastic Fracture ASTM STP 668*, 65–120.

[62] Vellender, A., Mishuris, G.S., Movchan, A.B., 2011, Weight function in a bimaterial strip containing an interfacial crack and an imperfect interface. Application to Bloch-Floquet analysis in a thin inhomogeneous structure with cracks. *Multiscale Model. Simul.*, **9**, 1327–1349.

[63] Vellender A., Mishuris, G.S., 2012, Eigenfrequency correction of Bloch-Floquet waves in a thin periodic bi-material strip with cracks lying on perfect and imperfect interfaces. *Wave Motion*, **49**, 258–270.

[64] Vellender A., Mishuris G.S., Piccolroaz, A., 2013, Perturbation analysis for an imperfect interface crack problem using weight function techniques, *Submitted, Int. J. Solids Struct.*

[65] Wells, A. A., 1961, Unstable crack propagation in metals: Cleavage and fracture. *Proceedings of the crack propagation symposium, Cranfield*, 210–230.

[66] Williams, M.L., 1959, The stresses around a fault or crack in dissimilar media. *Bul. Seismol. Soc. Am.*, **49**, 199–204.

[67] Willis, J.R., 1967, A comparison of the fracture criteria of Griffith and Barenblatt, *Journal of the Mechanics and Physics of Solids*, **15 (3)**, 151–162.

[68] Willis, J.R., 1971, Fracture mechanics of interfacial cracks. *J. Mech. Phys. Solids*, **19**, 353–368.

[69] Willis, J.R., 1971, Interfacial stresses induced by arbitrary loading of dissimilar elastic half-spaces joined over a circular region. *J. Inst. Math. Appl.*, **7**, 179–197.

[70] Willis, J.R., 1972, The penny-shaped crack on an interface. *Quart. J. Mech. Appl. Math.*, **25**, 367–385.

[71] Willis, J.R., Movchan, A.B., 1995, Dynamic weight functions for a moving crack. I. Mode I loading *J. Mech. Phys. Solids*, **43(3)**, 319–341.

[72] Zheng, X.J., Glinka, G., Dubey, R.N., 1996, Stress intensity factors and weight functions for a corner crack in a finite thickness plate. *Eng. Frac. Mech.*, **54(1)**, 49–61.